INAUGURAL-DISSERTATION

zur

Erlangung der Doktorwürde

der

Naturwissenschaftlich-Mathematischen Gesamtfakultät

der

Ruprecht-Karls-Universität

Heidelberg

vorgelegt von

Diplom-Biologe Pier Giorgio Pacifici

Tag der mündlichen Prüfung: ....

CHARACTERIZATION OF A MOUSE MODEL LACKING ACETYLCHOLINE RECEPTOR ACTIVITY DURING EMBRYONIC DEVELOPMENT

Gutachter: Prof. Dr. Christoph Schuster

                  Prof. Dr. Veit Witzemann

To my family.

*It is a good morning exercise for a research scientist
to discard a pet hypothesis every day before breakfast.
It keeps him young.*

- ***Konrad Lorenz (1903 – 1989)***

ACKNOWLEDGEMENTS

each year. Thanks in particular to Steffen Jährling and Martin Novak for the great evenings, Florian Freudenberg for the friendship and Sophie Knobloch for, well, being herself.

Even with the support provided by all these people, this thesis would never have been completed without my friends – Sandro Altamura, Simone Astori, Anne Charlotte and Chris Balduf, Daniele Campa, Davide Cerone, Paolo Del Rocino, Valentina Della Gatta, Maria Teresa Di Mascio, Samuele Marro, Paolo Mele, Petra Örsy, Cosmeri Rizzato, Gabriele Rizzo, Jakub and Dagmara Swiercz, as well as all those whom I may have forgotten to thank here.

My greatest thanks, however, go to my family, who always believed in me and without whom I could never have finished. To my grandmother Anna for being here, to my grandfather Sante because he would have liked to see this day, to my grandmother Velia and my grandfather Sisto whom I also wish were here today. To my relatives (especially the little ones) for always being interested in how my thesis was going and for always being supportive.
Most of all to my parents, for their patience, love and understanding (not to mention enduring my discussions on how interesting the experiments were, even though they would not understand a word), and to my brother Daniele for always being there… in his own unique way.

And finally, I would like to thank all those whom I did not mention, but who were very helpful during the thesis period.

Heidelberg, 9/11/2008   *Pier Giorgio*

1. ABSTRACT AND ZUSAMMENFASSUNG

1.1   Abstract

During embryonic development, acetylcholine (ACh) and the acetylcholine receptor (AChR) play a pivotal role in the establishment, maturation and maintenance of the neuromuscular junction (NMJ). In humans, genetic mutations affecting AChR-mediated signal transduction give rise to a variety of phenotypes mainly defined by muscle weakness, and known as congenital myasthenic syndromes (CMS), demonstrating the importance of AChR for the correct development of nerve/muscle contacts. However, thus far it has been impossible to determine the specific role played by AChR-mediated postsynaptic activity in NMJs during embryonic development.

In this work, the effects caused by lack of postsynaptic activity in the NMJ were studied on a reporter mouse line generated by homologous recombination and expressing a structurally intact but functionally silent GFP-tagged AChR. In these animals, the γ subunit of the AChR, normally expressed during embryonic development, carries a point mutation (P121L) which causes fast-channel CMS in human patients. Homozygous γ/ε-fc animals die at birth, and a wide variety of severe physiological abnormalities appears during embryonic development, caused by the silencing of AChR-mediated postsynaptic potentials. The size, shape and density of the NMJ were profoundly altered by lack of postsynaptic activity, although the overall number of receptors did not seem to change. A vastly increased outgrowth of motor axons could also be detected, and this alteration is associated with the absence of motoneuron death at late embryonic stages. Further alterations could be found in the disorganization of muscle fiber architecture, and the presence of multiple innervation sites on single muscle fibers. These results clarify the role of AChR-mediated postsynaptic activity in the proper development and maturation of nerve/muscle contacts, and support the possibility that presynaptic development is influenced by putative reciprocal signaling between nerve and muscle. The reporter mice provide a new tool to distinguish in an as-yet unknown resolution between activity-dependent and putative structurally-dependent pathways during NMJ maturation, leading to important implications in the study of synapse formation and maintenance, as well as in the field of receptor studies.

1.2   Zusammenfassung

Während der Embryonalentwicklung, spielen Acetylcholin (ACh) und der Acetylcholinrezeptor (AChR) eine entscheidende Rolle bei der Etablierung, Entwicklung und Stabilisierung der neuromuskulären Synapse (NMJ). Genetische Mutationen, die die AChR-vermittelte Signaltransduktion beeinträchtigen, verursachen in Menschen Krankheiten, die vor allem durch Muskelschwäche definiert, und als Congenitale Myasthenische Syndrome (CMS) bekannt sind. Dies demonstriert wie wichtig der AChR für die korrekte Entwicklung der Nerv/Muskel-Kontakte ist. Allerdings war es bislang unmöglich, die spezifische Rolle der AChR-vermittelten postsynaptischen Aktivität in NMJ während der Embryonalentwicklung zu bestimmen.

In dieser Arbeit wurde untersucht, wie sich das Fehlen von postsynaptischen Aktivitäten in NMJ auswirkt. Dazu wurde mittels homologer Rekombination eine Reportermauslinie generiert, die strukturell intakte aber funktionell stumme mit GFP-markierte AChR exprimierte. In diesen Tieren trägt die γ Untereinheit des AChR, die normalerweise während der Embryonalentwicklung exprimiert wird, eine Punktmutation (P121L), welche „fast-channel" CMS in Humanpatienten verursacht. Homozygote γ/ε-fc Tiere sterben bei der Geburt. Die Analyse zeigt schwerwiegenden, physiologischen Abnormalitäten während der Embryonalentwicklung. Die Größe, Form und AChR Dichte der NMJ wird durch der Mangel an synaptischer Aktivität tiefgreifend verändert, obwohl die Gesamtzahl der Rezeptoren scheinbar unverändert ist. Außerdem ist das Wachstum des motorischen Axons stark erhöht und das entwicklungsabhängige Sterben von Motorneuronen finden nicht statt. Weitere Veränderungen können hinsichtlich der Desorganisation von Muskelfaserarchitektur und der Anwesenheit von multiplen Innervierungsstellen an einzelnen Muskelfasern festgestellt werden. Diese Ergebnisse verdeutlichen die zentrale Rolle von AChR-vermittelter postsynaptischer Aktivität für die korrekte Entwicklung und Reifung der Nerv/Muskel-Kontakte, und deuten darauf hin, dass präsynaptische Entwicklung durch ein putatives reziprokes Signal zwischen Nerv und Muskel beeinflusst wird. Die Reportermäuse stellen ein neues Werkzeug dar, um in bisher unerreichter Auflösung zwischen „aktivitätsabhängigen" und bzw. „strukturabhängigen" Signalen während der Entwicklung der NMJ zu unterscheiden. Sie tragen entscheidend zur Erforschung der Bildung und Stabilisierung von Synapsen und der regulatorischen Funktion der Neurotransmitterrezeptoren bei.

2. TABLE OF CONTENTS

9

11

3. LIST OF ABBREVIATIONS

A

A488-bgtx — Alexa488-coupled bungarotoxin
abs. — absolute
ACh — acetylcholine
AChE — acetylcholinesterase
AChR — nicotinic acetylcholine receptor
AChRγ — fetal-type acetylcholine receptor incorporating subunit γ
AChRγ/ε-fc — fetal-type acetylcholine receptor incorporating transgenic subunit γ/ε-fc
AChRε — adult-type acetylcholine receptor incorporating subunit ε

B

Bgtx — α bungarotoxin
bp — base pair
BSA — bovine serum albumin

C

C57Bl/6 — mouse line C57 Black/6
Ca — calcium
ChAT — cholin-acetyltransferase
ChAT$^{-/-}$ — knock-out mouse line lacking expression of ChAT
Cl — chlorine
CMS — congenital myasthenic syndrome

D

d — day
DEPC — diethylpyrocarbonate
dNTP — desoxynucleotide triphosphate
Dok7 — downstream of tyrosine kinase 7
DTT — dithiotreitol

E

E# — embryonic day #

F

FCCMS — fast-channel congenital myasthenic syndrome
FITC — fluorescein isothiocyanate
FITC-bgtx — FITC-coupled bungarotoxin

G

g — gram
GAPDH — glyceraldehyde-3-phosphate dehydrogenase
GFP — green fluorescent protein

H

h — hour

K

kb — kilobase pair
kD — kilodalton
K-S Test — Kolmogorov-Smirnov test

L

l — liter
LMC — brachial lateral motor column
Lrp4 — low-density lipoprotein receptor protein 4

M

M — transmembrane domain
M — molar
mA — milliampere
Mg — magnesium
mg — milligram
min — minute
ml — milliliter
mM — millimol
Mol — mol
ms — millisecond
MuSK — muscle-specific kinase
mV — millivolt

N

Na — sodium
Neo — neomycinphospho-transferase, neomycin resistance

12

ng   nanogram
nl   nanoliter
NMJ   neuromuscular junction

O
o.n.   overnight

P
P   phosphorus
P#   postnatal day #
PBS   phosphate-buffered saline
PCR   polymerase chain reaction

R
Rh-bgtx.   rhodamin-labeled α
            bungarotoxin
RT   room temperature
RT-   reverse transcription
            reaction

S
s   second

S
Tris   N-Trishydroxymethyl-
            aminomethane

U
U   unit

W
WT   wild type

3,4-DAP   3,4-diaminopyridine
μg   microgram
μl   microliter
γ-GFP   transgenic construct
            containing a GFP sequence
            within the long cytoplasmic
            loop of the γ subunit.
γ/ε-fc   transgenic construct
            replacing most of the γ
            subumit with the ε subunit
            and bearing the P121L
            mutation

4. INTRODUCTION

4.1 The Neuromuscular Junction

Animals coordinate cellular activities, process and respond to stimuli through the activity of highly specialized nerve cells. Neurons signal to target cells through specific sites of contact, called synapses, through the release of different chemicals known as neurotransmitters. Target cells are usually other neurons, but they can also be endocrine cells or, in the case of motor neurons, skeletal muscle fibers. The synapse between a motor neuron and a muscle fiber is called a neuromuscular junction (NMJ).

The NMJ is the best studied chemical synapse in vertebrates, due to a number of advantages: NMJs are readily accessible because of their peripheral location, and they are over one hundred times larger than the typical brain synapse. Furthermore, NMJs are relatively simple, and because each muscle fiber is normally innervated by only one nerve terminal, they produce a very simple innervation pattern. Finally, chemical signaling at the NMJ involves the opening of a single type of ion channel in the postsynaptic membrane. These features make the NMJ an ideal site to study synapse development, synapse maintenance and chemical signaling, and to explore the role of individual molecules in these processes.

4.1.1 Structure of the NMJ

The vertebrate NMJ is a chemical synapse, composed by the presynaptic nerve ending, the postsynaptic muscle membrane, called endplate, the basal lamina, and the terminal Schwann cell. The axon of the motor neuron innervates the specialized endplate region of the muscle fiber, and is separated from the muscle membrane by a 100 nm synaptic cleft. The number and positioning of the NMJs on a muscle fiber, their shape and complexity vary not only from species to species, but also from muscle to muscle within individual organisms. In vertebrates, the NMJ responds to the neurotransmitter acetylcholine (ACh).

The presynaptic nerve ending contains synaptic vesicles filled with ACh, and voltage-gated Ca^{2+} channels which allow Ca^{2+} entry within the nerve terminal with each action potential, triggering the fusion of synaptic vesicles to the presynaptic membrane, and the release of ACh into the synaptic cleft.

The endplate muscle membrane is organized into a series of postjunctional folds; nicotinic AChRs (AChR) are densely clustered on the crests of these postjunctional folds. The membrane within the postjunctional folds is instead rich in voltage-gated $Na_v1.4$ channels. The basal lamina is located within the synaptic cleft, and is composed of collagen and other extracellular matrix proteins, including acetylcholinesterase (AChE) which is anchored to the basal lamina through collagenase Q (ColQ) and rapidly hydrolises released ACh.
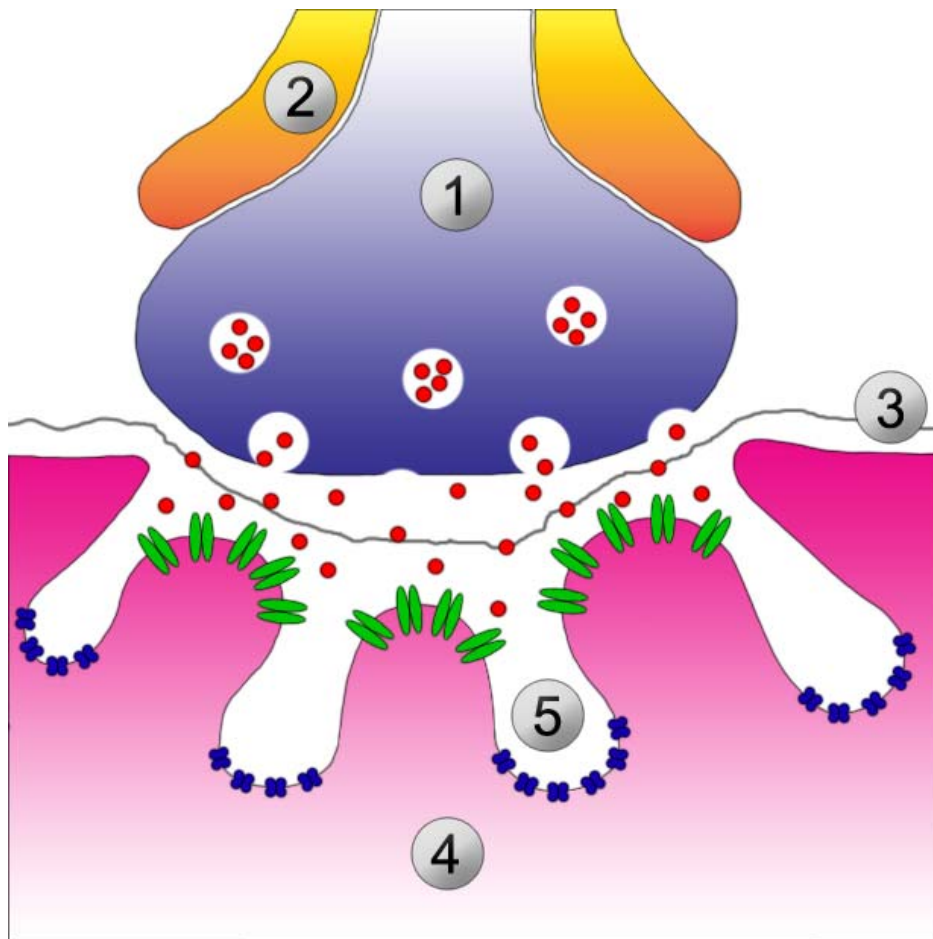
Fig. 1: Structure of the NMJ.

The NMJ is composed of the presynaptic nerve terminal (1), the Schwann cell (2), the basal lamina (3) and the postsynaptic endplate (4). ACh (red) is contained within synaptic vesicles. The postsynaptic membrane is arranged into postjunctional folds

(5) rich in voltage-gated $Na_v1.4$ channels (blue), and whose crests are densely packed with AChRs (green). Upon the arrival of an action potential, ACh is released into the synaptic cleft and binds to the AChRs, evoking an endplate potential.

4.1.2   Activity of the NMJ

Under normal circumstances, the resting potential of a muscle fiber is about -90 mV (Fatt and Katz, 1951). When an action potential propagates along the axon and reaches the presynaptic nerve terminal, it triggers the opening of voltage-gated Ca^{2+} channels in the neuronal cell membrane, leading to the entry of Ca^{2+} ions into the presynaptic nerve terminal according to the electrochemical gradient. The increase in Ca^{2+} concentration within the presynaptic nerve terminal in turn triggers the fusion of synaptic vesicles into the presynaptic nerve membrane, and the release of the ACh contained within them into the synaptic cleft. Released ACh freely diffuses into the cleft, and binds to the nicotinic AChRs on the postjunctional crests, opening their ion channels. The short activation of the AChRs on the postsynaptic membrane (approximately a few ms) allows entry of a large number of Na^+ ions as well as a small number of Ca^{2+} ions, and to the release of K^+ ions, leading to a rapid depolarization. This excitatory postsynaptic potential is called the endplate potential (EPP). The electrical current generated by the channel opening event is called endplate current (EPC) (Fatt and Katz, 1951).

If the endplate potential reaches threshold voltage (approximately -50 mV), it triggers the activation of voltage-gated $Na_v1.4$ channels in the postjunctional folds, converting the endplate potential into an action potential that propagates in both directions along the muscle fiber, causing its contraction. In the meantime, the concentration of ACh in the synaptic cleft is quickly reduced due to diffusion outside the cleft and to rapid hydrolysis on the part of the enzyme acetylcholinesterase into acetate and choline. This leads to the deactivation of AChRs, and to the repolarization of the muscle fiber in the absence of further stimuli. Choline is then reabsorbed by the nerve terminal and recycled into new molecules of ACh through the action of choline acetyltransferase (ChAT). AChRs on the postsynaptic muscle membrane therefore play a critical role in the correct functioning of the NMJ.

4.2   The Acetylcholine Receptor

4.2.1   Structure of the Acetylcholine Receptor

The muscle-specific nicotinic AChR is a glycoproteic pentameric ligand-gated ion channel (Raftery et al., 1980), located in the crests of the postjunctional folds of the NMJ (Sanes and Lichtman, 2001). It is composed of two α subunits, one β subunit, one δ subunit, and either a γ subunit during embryonic development (AChRγ) or an ϵ subunit in mature synapses (AChRϵ) (Mishina et al., 1986).

Each subunit contains between 450 to 520 amino acids, with a long N-terminal extracellular region, four transmembrane domains (labeled M1 to M4), a large cytoplasmic loop between M3 and M4 (Karlin and Akabas, 1995), and a short C-terminal extracellular region. The M2 transmembrane domain of each subunit forms the channel pore of the AChR and is responsible for cation selectivity (Imoto et al., 1988; Miyazawa et al., 1999; Miyazawa et al., 2003), while the cytoplasmic loop is involved in the clustering of receptors in the NMJ (Maimone and Enigk, 1999).

A

B
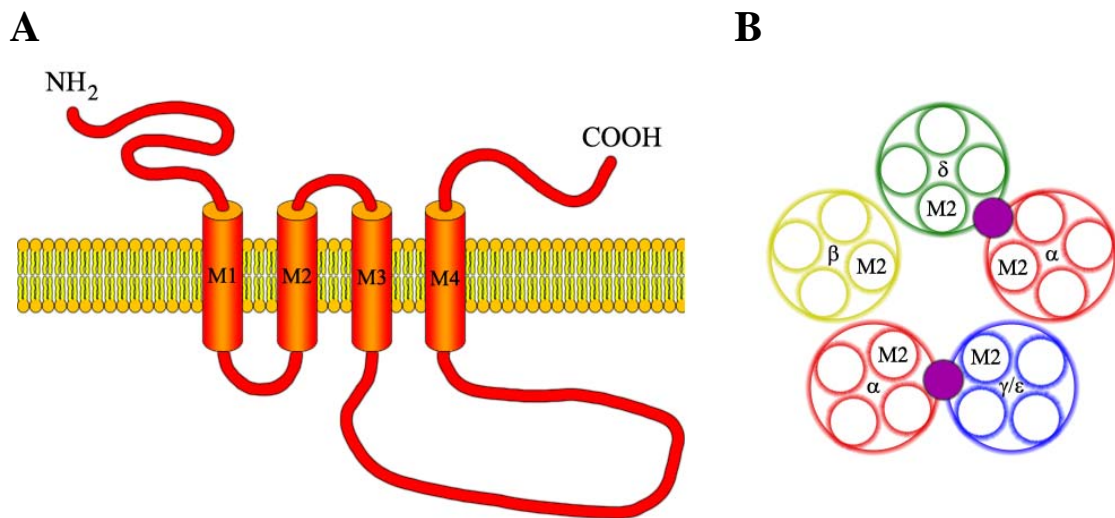
Fig. 2: Structure of the AChR.

(A) Schematic drawing of the structure of an AChR subunit. Each subunit contains four transmembrane domains (M1 to M4), a long N-terminal region, and a large cytoplasmic loop between transmembrane domains M3 and M4, which plays a role in the aggregation of subunits. (B) Schematic drawing of the complete pentameric AChR receptor. Each subunit (large circles) is drawn along with the arrangement of

the four transmembrane domains (small white circles). The two ACh binding sites, located between the α and δ subunit, and the α and γ (or ε) subunit are shown as dark circles. The M2 transmembrane domains of the five subunits make up the inner surface of the ion channel.

The AChR is present in the adult NMJ with a density of about 10^4 AChRs per μm^2, concentrated on the postjunctional crests, whereas its density in the rest of the muscle fiber is 10 molecules per μm^2 (Colledge and Froehner, 1998). This heterogeneity is established during the embryonic development of the NMJ.

4.3   Development of the NMJ

4.3.1   Embryonic Development of the Muscle

Myoblasts are generated from the somites of the embryonic paraxial mesoderm, located on both sides of the neural tube and the notochord. These cells migrate together and fuse into syncytia, forming myotubes which eventually grow into skeletal muscle fibers.

4.3.2   Prenatal Nerve-Muscle Interactions

Further development of the myotubes occurs through muscle-specific gene transcription under the control of myogenic differentiation factors (MDFs). Among them are the members of the "basic helix-loop-helix" protein family, such as MyoD, myogenin, myf5 and MRF4. In their activated form, MDFs dimerize with the so-called E-proteins and bind to specific promoter elements, the E-box (CANNTG consensus sequence). Since E-box promoter elements are prevalently found in muscle-specific genes, the binding of MDFs increases transcriptional activity for these genes in the context of myogenic differentiation (Lassar et al., 1991).

The establishment of synaptic contact between nerve and muscle cells occurs after the beginning of myotube development; this leads to further differentiation of the two cell types through coordinated neuromuscular interaction (Witzemann, 2006).

Investigations of the relationship between innervation and control of gene transcription identified neural factors influencing the expression of structural proteins and receptors in muscle cells (McMahan, 1990; Misgeld et al., 2002). Similarly, putative retrograde muscle-derived signals capable of affecting the differentiation of the presynaptic nerve were reported (Caroni, 1993; Godfrey and Schwarte, 2003). Signal transmission, which initiates and modulates these processes, can be found almost exclusively in the vicinity of the NMJ.

It is not yet clear how the differentiation of pre- and postsynaptic elements might be coordinated, and how precise patterning and location of synaptic activity might be achieved. Glial cells in the immediate vicinity of the synapse might provide additional signals (Goda and Davis, 2003).

During prenatal development, the NMJ undergoes far-reaching changes. The AChRs form clusters in key areas of skeletal muscle fibers, which will later differentiate into functioning NMJ; subsynaptic nuclei increase the transcription levels of AChR subunits, and the muscle fiber membrane forms characteristic postjunctional folds. Synaptic contacts are established and, later, partially eliminated. Uninnervated clusters disgregate.

4.3.3 The γ / ε Subunit Switch

During embryonic development, fetal-type AChRs are assembled from two α subunits, one β subunit, one δ subunit and one γ subunit. The composition of the receptor, however, changes during perinatal development, when the fetal γ subunit is replaced by the adult-type ε subunit (Sakmann and Brenner, 1978; Witzemann et al., 1987; Witzemann et al., 1989; Witzemann et al., 1991; Kues et al., 1995a; Kues et al., 1995b).

The subunit switch leads to a change in the electrophysiological properties of the AChR (Mishina et al., 1986), such as conductivity, permeability to Ca^{2+} ions, and channel opening times (Villarroel and Sakmann, 1996). In mice, the γ/ε subunit switch occurs within the first week after birth.

4.3.4 Pre-patterning of the NMJ

In the diaphragm muscle, NMJs are normally localized in the center of the muscle fibers, forming a region known as the synaptic band. This highly ordered organization of NMJs is formed during embryogenesis through a process known as pre-patterning, in which small aggregates of AChRs form in the muscle membrane. The process is continued and stabilized by the nerve terminal through the action of nerve-derived factors (Yang et al., 2001). The fetal subunit of the AChR plays a role in the proper distribution of these aggregates as well. The molecular mechanisms of synaptic band positioning are not yet well understood.

4.3.5 The Agrin Signal Cascade

Several nerve-derived factors have been shown to play a role in the further differentiation of the postsynaptic muscle fiber, in the stabilization of AChR aggregates, and in the development of a mature NMJ. *In vivo* and *in vitro* studies have identified several components of the molecular machinery driving this process, and their functions in the developing NMJ (Sanes and Lichtman, 2001). With the increase in the number of transgenic mouse lines and the development of conditional knockout lines, the model for the embryonic development of the NMJ has recently undergone several changes (Kummer et al., 2006).

The current model, which is primarily based on studies of transgenic mouse lines, describes the nerve-independent formation of small clusters of AChRs which are attracted and incorporated in the nascent synapse (Flanagan-Steet et al., 2005), and which in turn stabilize nerve-muscle interactions, and attract new filopodia towards the contacted region. Further AChR clustering requires the action of agrin (McMahan et al., 1990; Gautam et al., 1996), a large heparin sulphate proteoglycan whose nerve-derived isoform, called z^+ agrin, has been demonstrated to function as an aggregation factor for AChRs (McMahan, 1990; Burgess et al., 1999). Z^+ agrin is transported down motor neurons and released from the nerve terminal, where it stably associates with the basal lamina of the synaptic cleft.

Secretion of z+ agrin on the part of the nerve terminal activates a muscle-specific transmembrane receptor tyrosine kinase called MuSK (DeChiara et al., 1996; Glass et

al., 1996). Because no experiments have yet conclusively proved direct binding of agrin to MuSK, it is currently suggested that z^+ agrin interacts with MuSK through the low-density lipoprotein receptor protein, Lrp4 (Kim et al., 2008; Zhang et al., 2008), which is believed to form dimers or oligomers in the absence of agrin and associates with MuSK. Once activated, Lrp4-MuSK complexes are reorganized, MuSK is dimerized and phosphorylates itself; the newly discovered protein Dok7 has been suggested to play a role in the self-phosphorylation of MuSK (Okada et al., 2006). *In vitro* experiments have shown that z^+ agrin – MuSK interaction can activate tyrosine kinases of the SRC family, such as cdc42, Rac and PAK (Weston et al., 2000; Luo et al., 2002). The activation of these kinases in turn phosphorylates the β subunit of the AChRγ. (Mohamed et al., 2001).
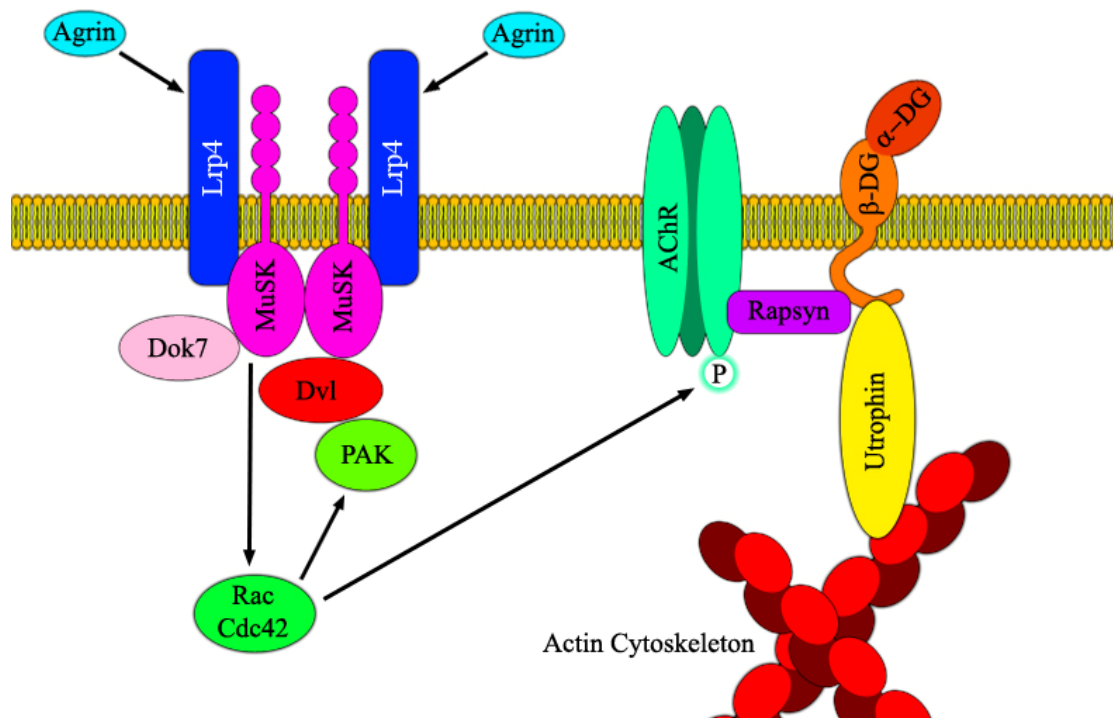
Fig. 3: Possible Signal Cascade involved in AChR Clustering.
Schematic drawing of the possible signal cascade involved in AChR clustering during embryonic development. The motor axon secretes z^+ agrin, which interacts with MuSK through a receptor protein (Lrp4). MuSK-Lrp4 complexes are reorganized and MuSK dimers interact with kinase Dok7, leading to MuSK self-phosphorylation, which activates SRC-family kinases such as PAK, Rac and Cdc42. These kinases phosphorylate the β subunit of the AChR, possibly leading to docking of the receptor to the β unit of the dystroglycan complex (DG) through the action of

rapsyn (Gautam et al., 1995). The dystroglycan complex is bound to utrophin, which tethers it to the actin cytoskeleton.

Clustering of the AChRs requires the presence of rapsyn, a 43-kDA membrane-associated cytoplasmic protein which is equimolar with the AChR, and is tightly associated with it (Noakes et al., 1993; LaRochelle et al., 1986); *in vivo* and *in vitro* studies have demonstrated that in the absence of rapsyn, no AChR clustering can occur (Gautam et al., 1995).

Rapsyn might tether the AChR to the actin cytoskeleton through dystroglycan, playing an important role in receptor clustering. However, although rapsyn in non-muscle cells can cluster in response to agrin with or without AChRs, absence of AChRs in muscle cells prevents clustering of rapsyn, showing that AChRs contribute actively to the clustering process (Grow and Gordon, 2000; Missias et al., 1997). In fact, AChR-mediated activity leads to the inhibition of AChR transcription in extra-synaptic nuclei, and to the transcriptional specialization of subsynaptic nuclei.

In vivo studies on knock-out mice have further elucidated aspects of the signal cascade. Among other things, the discovery of AChR clusters in agrin-deficient or aneural muscles (Gautam et al., 1996; Yang et al., 2001), as well as the characterization of agrin- and AChR-deficient double KO mice (Misgeld et al., 2005), demonstrated that agrin counteracts the dispersal effect of a second nerve-derived factor; *in vitro* experiments have identified ACh as a dispersal factor. Although the mechanism remains unclear, it is known to require kinase Cdk5, and to presumably involve endocytosis (Lin et al., 2005).

4.3.6   Regulation of Transcription of AChR Subunits

Under the current paradigm of NMJ formation, little is known about the regulation of transcription of the various AChR subunits. While it was once thought that neuregulin, a nerve-derived factor, stimulated subsynaptic nucleus specialization and the synthesis of AChRs, studies of transgenic mouse lines have painted a more complicated picture. While neuregulin might have a modulatory role in regards to the synthesis of AChR subunits, AChRs are synthetized even in its absence (Escher et al., 2005). Furthermore, transcriptional specialization has been demonstrated to occur

even in the absence of innervation (Lin et al., 2001; Yang et al., 2001), although its maintenance appears to require both agrin and MuSK (DeChiara et al., 1996; Lin et al., 2000; Escher et al, 2005). The ETS transcription factor Erm, whose expression is limited to subsynaptic nuclei, has also been shown through transgenic mouse models to play a role as an upstream regulator of a transcriptional program which includes genes for several postsynaptic proteins, such as MuSK and the ε subunit of the AChR receptor (Hippenmeyer et al., 2007). Although other molecules have been implicated in the process, the exact mechanisms of transcription regulation of the AChRs is still unclear.

4.3.7   Differentiation of Motor Axons

Innervating axons undergo several changes during the development of the NMJ. Axons innervate muscle fibers at the synaptic band, and then halt their growth; it is speculated that a yet unknown retrograde signal from muscle to nerve may be implicated in the process. In embryonic development, each endplate is innervated by several axons; during perinatal and early postnatal development, each neuromuscular synapse undergoes elimination of the majority of its innervating axons, until each NMJ is innervated by only one axon. The mechanism by which this selection occurs is still unclear, although activity has been proposed as one of the factors involved (Wyatt and Balice-Gordon, 2003). In the meantime, the surviving axon also undergoes further development, and its nerve terminal is enriched with ACh vesicles, which can be released in response to an action potential.

4.3.8   Maturation of the NMJ

The NMJ undergoes maturation during the perinatal and early postnatal period, in conjunction with the onset of the γ/ε switch (4.3.3). The NMJ dramatically increases in size, and changes shape from ovoid to a more elaborate, "pretzel-like" structure. At the same time, postjunctional folds become more prominent, increasing the overall area of the synapse, until the NMJ reaches its adult configuration (Marques et al., 2000). During this process, AChRs cluster on the postjunctional crests, the closest

position to the presynaptic terminal, while the $Na_v1.4$ channels accumulate at the bottom of the postjunctional folds (Figure 2). Although little is known about the mechanisms that drive NMJ maturation, *in vitro* studies have demonstrated that cultured myotubes can form complex structures, very similar to mature NMJs, even in absence of innervation (Kummer et al., 2004). However, it is still unknown how muscle-derived and nerve-derived factors may interact to produce a mature endplate *in vivo*.

4.4   Congenital Myasthenic Syndromes

Inherited defects in genes involved in the development and maintenance of the NMJ produce a heterogeneous group of disorders collectively known as congenital myasthenic syndromes (CMSs), associated with abnormal muscle weakness and fatigability on exertion (Engel et al., 2003a). The genetic defects involved in CMSs may impair neuromuscular transmission either directly, or by causing alterations of the NMJ structure which eventually compromise its safety margin.

Different types of CMSs are caused by mutations in different genes, or sometimes in different exons of the same gene (Table 1).

Table 1. Classification of congenital myasthenic syndromes

Presynaptic defects
  ChAT deficiency
  Paucity of synaptic vesicles/reduced quantal release
Synaptic – Basal lamina-associated defects
  Endplate AChE deficiency
      AChE deficiency
      ColQ deficiency
Postsynaptic defects
  Kinetic abnormalities of AChR (with or without AChR deficiency)
      Slow-channel syndrome
      Fast-channel syndrome
      High-conductance fast channel syndrome
  Impaired AChR clustering
  Rapsyn deficiency
  MuSK deficiency
  Dok7 deficiency
  Kinetic defects in $Na_v1.4$

Mutations involving choline acetyltransferase (ChAT), acetylcholinesterase (AChE), rapsyn, ColQ (a form of collagenase tethering AChE to the basal lamina) or subunits of the AChRs have all been identified in CMS patients (Müller et al., 2007). The current CMS classification is based on the recognized site of the defect, i.e. presynaptic, synaptic or postsynaptic.

The diagnosis of congenital myasthenic syndromes is based on the presence of myasthenic symptoms since birth or early childhood, such as a high-arched palate, weakness in the ocular muscles, cranial muscles and/or limbs, a history of similarly affected relatives, and abnormal electromyographic measurements. They may also include respiratory symptoms, delayed motor milestones, and negative tests for AChR antibodies (Engel and Franzini-Armstrong, 1994). Although many different types of CMSs have been identified and classified, the causes behind others remain elusive.

Most of the genetic defects associated with CMSs are caused by recessive, loss-of-function mutations, except for slow-channel syndrome which is associated with a dominant gain-of-function mutation (Engel et al., 2003b).

Congenital myasthenic syndrome mutations have been identified in various domains of all AChR subunits; depending on their effect, they produce kinetic abnormalities which can be grouped into two categories: slow-channel and fast-channel syndromes (Table 2).

Table 2. Kinetic abnormalities of AChR (adapted from Engel et al., 2003b)

	Slow-channel	**Fast-channel**
Endplate currents	Slow decay	Fast decay
Channel-opening events	Prolonged	Brief
Open states	Stabilized	Destabilized
Closed states	Destabilized	Stabilized
Mechanisms	Increased affinity	Decreased affinity
	Increased β	Decreased β
	Decreased α	Increased α
Pathology	Endplate myopathy	No anatomic footprint
Genetic Background	Dominant gain-of-function	Recessive loss-of-function

Abbreviations: β, channel-opening rate; α, channel-closing rate.

4.4.1   Fast-Channel Congenital Myasthenic Syndrome

Fast-channel congenital myasthenic syndromes (FCCMS) are characterized by an abnormally short channel-opening time, giving rise to a fast decay of the synaptic response. Depending on the mutation, AChR expression might or might not be reduced, quantal release by nerve impulse remains normal, but very small MEPPs are observed (Uchitel et al., 1993). Mutations giving rise to fast-channel congenital myasthenic syndrome have been identified in subunits α, δ and ε of the AChR (Wang et al., 1999; Brownlow et al., 2001; Ohno et al., 1996), which form the ligand binding sites for ACh (Fig. 2). Depending on their location in the protein sequence, these mutations impair normal AChR function in different ways (Fig. 4)
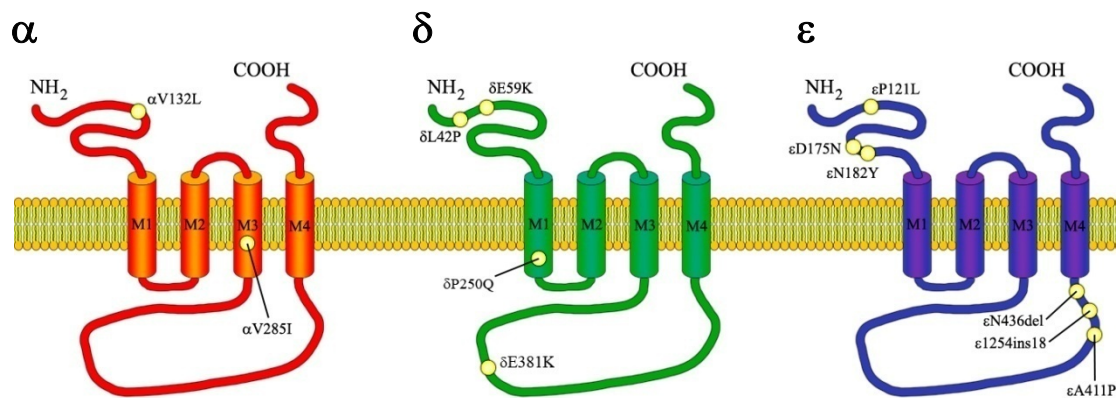
Fig. 4: Mutations Involved in Fast-Channel Congenital Myasthenic Syndromes.
Fast-channel congenital myasthenic syndromes can be caused by mutations in the α, δ and ε subunit. Mutations in the extracellular domain diminish receptor affinity for ACh; mutations in the transmembrane domains impair gating efficiency; mutations in the long cytoplasmic loop affect channel kinetics. Genetic defects producing FCCMS are recessive, loss-of-function mutations.

Common to all fast-channel congenital myasthenic syndromes is reduced postsynaptic activity in response to ACh, due to reduced probability of channel-opening events. However, mutations in different loci produce this effect in different ways. In the case of mutations located in the extracellular domain, this effect is due to a dramatic decrease in frequency and duration of bursts of ACh-induced openings (Ohno et al., 1996; Wang et al., 1999). Mutations in the cytoplasmic loop disrupt the normal kinetics of the receptor, either causing switches in gating from efficient to

inefficient within individual activation episodes, or producing a broad range of open probabilities (Milone et al., 1998; Wang et al., 2000). Therapy in humans involves the use of 3,4-diaminopyridine and pyridostigmine, a potassium channel blocker and an acetylcholinesterase inhibitor, respectively (Engel et al., 2003b; Parr and Jayawant, 2007), to increase the concentration of ACh in the synaptic cleft and increase the probability of channel-opening events.

4.5   Transgenic Mouse Models

The creation of transgenic mouse models is a powerful tool to analyze the specific functions of individual molecules in an *in vivo* model, as well as to mimic human-specific pathologies.

Classical transgenic mouse models can be created by pronucleus injection (Gordon et al., 1980) or homologous recombination. The latter method, developed thanks to technological advances in stem cell culture, has several advantages over pronucleus injection, and is currently regarded as the method of choice for the creation of classical transgenic mouse lines (Evans and Kaufman, 1981; Capecchi, 1989; Thompson et al., 1989).

Embryonic stem cells from early embryos are genetically altered through *in vitro* homologous recombination, and injected into blastocysts which are implanted into pseudopregnant animals, producing chimeric offspring. Breeding chimeric offspring expressing the mutation in their germinal cell lines eventually leads to the production of a stable transgenic mouse line.

Homologous recombination is a flexible method which allows both deletion of existing genetic material (knock-out) or its replacement with artificial genetic material (knock-in). Reporter genes can also be added in order to label cells expressing the mutation.

5. Objectives

5.1   Overview

Despite the fact that the NMJ has been considered for many years as the main model system for synaptogenesis, many questions still remain unanswered, and the mechanisms which regulate nerve-muscle contacts, synapse development and differentiation are still not fully known. The development of transgenic mouse models in the last few years has allowed us to discover the answers to some of these questions, offering new insights into the roles of various molecules involved in synaptic development and maturation, and forcing us to re-evaluate the previously established paradigm describing neuromuscular synapse formation (Kummer et al., 2006; Witzemann, 2006).

The role played by the AChR during the formation, development and maturation of the NMJ cannot be underestimated. The activity of MuSK, rapsyn and possibly Dok7 leads to the clustering and pre-patterning of the receptors in skeletal muscle fibers, even in the absence of nerve terminals or nerve-derived factors (Yang et al., 2001). Agrin stabilizes nerve-muscle contacts and contributes to the further development of the nascent NMJ (McMahan et al., 1992). But the analysis of transgenic mouse lines reveals that when the presence or functionality of the AChR is compromised (Misgeld et al., 2005; Brandon et al., 2003; Heeroma et al., 2003), or when motor neurons fail to innervate skeletal muscle fibers (Yang et al., 2001; Lin et al., 2001), further NMJ development is impaired and no functional synapses form, implying that both the release of ACh from the nerve terminal, and the activity of the AChR play a fundamental part in the development of the NMJ. Even so, the retrograde mechanisms through which synaptic activity regulates its own further maturation are still unknown. Previous studies aimed at analyzing the role of AChR in the development of the NMJ using knock-out mouse lines, however, could not differentiate between effects caused by disruption of AChR functionality alone, and effects caused by the absence of the AChR receptor as a whole.

Previous work in our lab included the generation of a knock-in mouse model expressing structurally intact but functionally silent AChR during embryonic development (Peter et al., 2005; Koenen et al., 2005). The goal of this thesis is to

characterize this mouse line, analyzing in detail the consequences caused by lack of AChR activity during the embryonic development and differentiation of the NMJ, and identifying the resulting morphological changes.

5.1.1   The γ/ε-fc Mouse Model

Two different forms of AChR play a role in the development and maturation of the NMJ (Mishina et al., 1986). The physiological reason for the presence of two different types of AChR is still unclear, but it is known that they have different electrophysiological properties, and that activity of the AChR is a critical factor during the development of the NMJ: it has been shown that transgenic mice lacking expression of the fetal γ subunit die shortly after birth (Takahashi et al., 2002), while transgenic animals in which expression of the γ subunit has been replaced by expression of the adult-type ε subunit during embryonic development show no obvious phenotype, and minor morphological changes (Koenen et al., 2005).

A mouse model generated in our lab permits the study of the effects of AChR activity reduction during embryonic development *in vivo*: while the overall structure of the AChR in these mice remains intact, a point mutation originally found in patients suffering from a fast-channel congenital myasthenic syndrome was inserted in a hybrid γ/ε subunit, drastically reducing the affinity of the receptor for ACh. The choice of inserting the mutation into a hybrid subunit, as opposed to the wild-type γ subunit, was made following the results of electrophysiological studies performed in *Xenopus laevis* oocytes (Peter et al., 2005), ensuring that receptor activity would be almost entirely silenced. Using this model, this thesis aims to answer questions such as, what effects are specifically caused by lack of receptor activity during embryonic development? Which molecular mechanisms are affected by the silencing of fetal-type AChRs, and what physiological changes do they lead to? What is the minimum level of activity which ensures functionality of the junction, or in other words how much redundancy is present in wild-type NMJs?

6. RESULTS

6.1   The γ/ε-fc Mouse Line

In 1996, a point mutation was identified in the ε subunit of patients suffering from a type of postsynaptic congenital myasthenic syndrome (Ohno et al., 1996). The mutation replaced the proline located in position 121 with a leucine (εP121L). Previous work in our lab used this mutation as the basis to generate a mouse line expressing a modified γ subunit with highly reduced activity (Peter C., dissertation 2003), in order to study the effects caused by lack of activity during the development of the neuromuscular junction.

6.1.1   Generation of the γ/ε-fc Mouse Line

Because the P121L mutation had maximum effect when expressed in the ε subunit as compared to the γ subunit (Peter et al., 2005), the targeting strategy used a γ/ε fusion gene, in which ε cDNA replaces the wild-type γ sequence from exon 4 onwards. The original vector, γ/ε-p1002, was generated and graciously offered by Dr. Michael Koenen. It also contained a GFP cDNA sequence inserted between the transmembrane domains M3 and M4, in the long cytoplasmatic loop of the ε cDNA. The P121L point mutation was inserted in the ε cDNA using modified primers (Fig. 5A-C).

The functional properties of the channel were tested by injecting γ/ε-fc cRNA in *Xenopus laevis* oocytes (Peter et al., 2005). Homologous recombination was confirmed through PCR and Southern Blot after ES cell transfection (Fig. 5D-E) (Peter C., dissertation 2003). The mRNA expression in muscle cells was verified through RT-PCR on muscles of WT and homozygous animals (Fig. 5F-G).
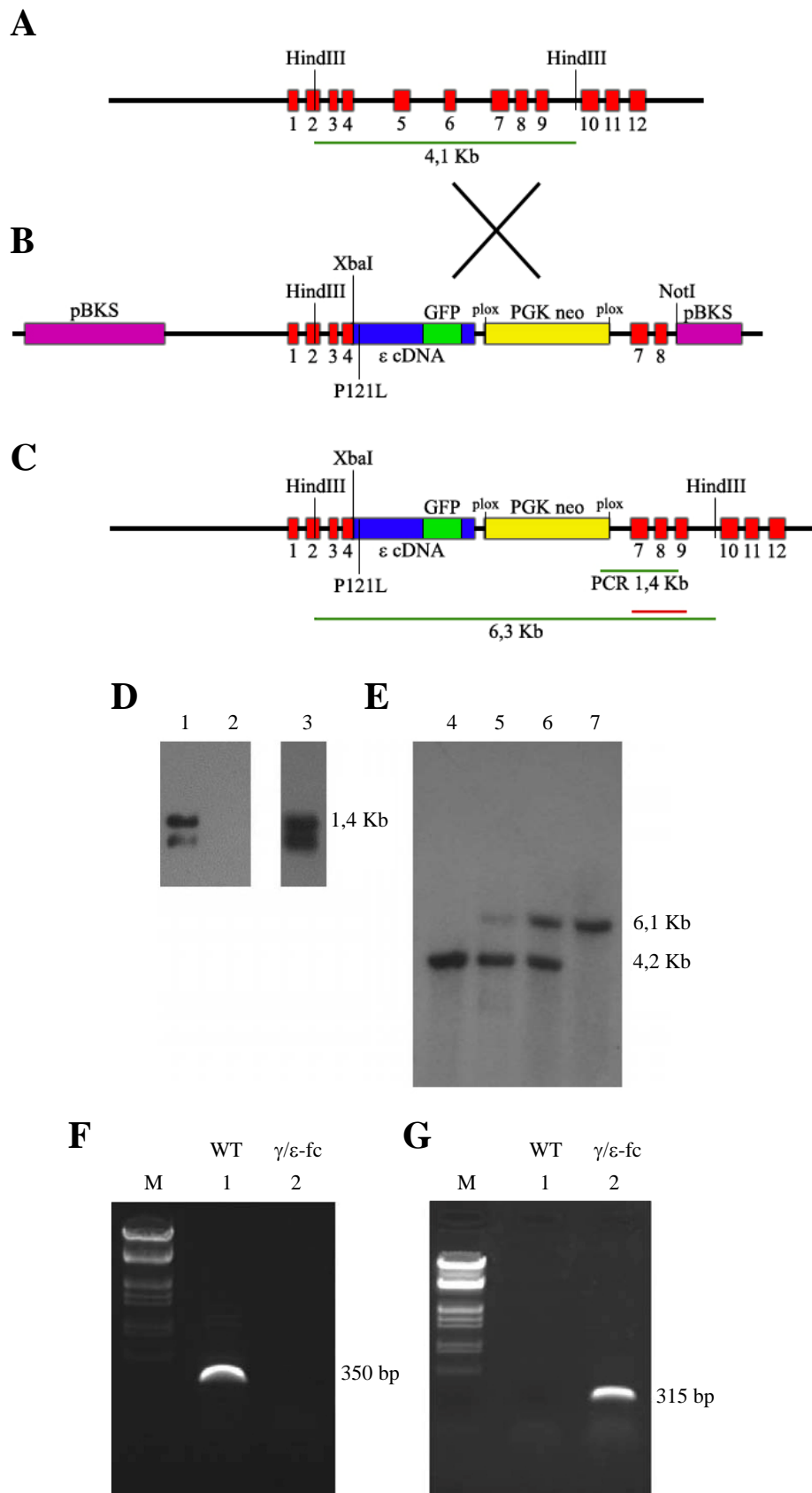
Fig. 5: Generation and Structure of the γ/ε - fc Gene.

(A) Diagram of the wild-type γ subunit. Exons 1 to 12 are represented by red boxes.
The scheme also shows the position of HindIII restriction sites used to produce the

4,1 Kb-long fragment for Southern blot analysis. (B) Schematic representation of the targeting vector γ/εP121L-GFP-p1002. The purple boxes represent the pBKS vector. The ε cDNA (blue box) was inserted in the genomic cDNA sequence using the XbaI restriction enzyme. The cDNA contained the P121L mutation, the stop codon and the polyA sequence. The PGK Neo selection cassette is represented by a yellow box and flanked by two loxP sequences. (C) Schematic representation of the mutated γ/ε gene, obtained through homologous recombination. The fragment located between the HindIII restriction sites, used for Southern blot analysis, is 6,3 Kb long. The fragment was analyzed using synthetized Probe 7 (in red). The fragment used for PCR analysis of homologous recombination is 1,4 Kb long. (D) PCR analysis of genomic ES cell DNA. Lane 1: PCR analysis of recombined ES cells; Lane 2: PCR analysis of wild-type ES cells. (E) Southern Blot of wild-type mouse (lane 4), positive ES cell clone (lane 5), heterozygous mouse (lane 6) and homozygous animal (lane 7). The wild type γ subunit is represented by a 4,2 Kb fragment while the γ/ε-fc subunit is represented by a 6,1 Kb fragment. (F) RT-PCR on muscle cDNA using a g subunit-specific primer (mg F 187, mg R 536). The 350 bp fragment is present only in muscles of WT animals. (G) RT-PCR on muscle cDNA using a γ/ε subunit-specific primer (g/e 241 for, mg/e 555 rev). The 315 bp DNA fragment is present only in the muscles of homozygous γ/ε-fc animals (M: λ/EcoRI, HindIII marker).

6.1.2   Expression of the γ/ε-fc Subunit in the Endplate

The correct expression and localization of the γ/ε-fc subunit can be verified thanks to the GFP sequence integrated in the transgene. Diaphragm muscles of homozygous mice showing GFP fluorescence were stained with rhodamine-labeled bungarotoxin (Rh-bgtx) and analyzed by confocal microscopy (Fig. 6).

The results showed that the green fluorescence produced by the integrated GFP co-localized with Rh-bgtx staining the endplate AChRs. Green fluorescence was absent in the wild type, as expected. The presence of GFP fluorescence in the endplate of the γ/ε-fc animals also confirmed that the γ/ε-fc subunit is assembled into the AChRγ complexes that were concentrated at the specific "endplate-like" sites in the developing muscle fibers.

| | **A** GFP | **B** Rh-bgtx | **C** Merge |

γ/ε-fc hom

WT
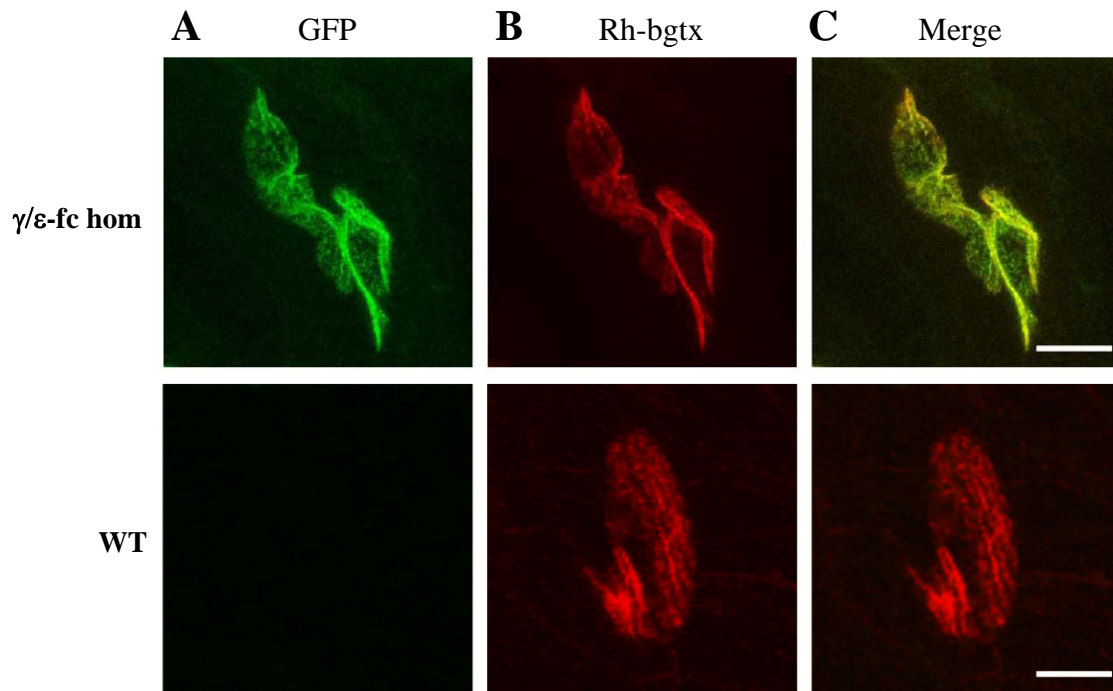
Fig. 6: Expression of GFP-tagged γ/ε-fc in a Diaphragm Endplate of E18 Embryos.

(A) confocal image of the endplate of a γ/ε-fc homozygous mouse shows GFP fluorescence, which is absent in the endplate of a WT animal; (B) Rh-bgtx staining of the γ/ε-fc and WT endplates. (C) Merged image showing the co-localization of GFP and the Rh-bgtx staining in the γ/ε-fc endplate, and the lack of green fluorescence in the WT endplate. Scale bar: 10 μm.

6.2   General Anatomy

6.2.1   Phenotype of the γ/ε-fc Heterozygous Mice

Heterozygous γ/ε-fc mice are viable, showing no differences in phenotype when compared to wild-type littermates. Males and females develop normally, are fertile, and their lifespan is not affected by the presence of one γ/ε-fc allele.

6.2.2 Phenotype of the γ/ε-fc Homozygous Mice

Homozygous γ/ε-fc mice display no movement and no muscle tension during embryonic development, and they die at birth, presumably from respiratory failure. Differences in appearance can be consistently identified between γ/ε-fc homozygous mice and their wild-type littermates (Fig. 7), although their severity varies in different embryos even within the same litter.

Differences in phenotype in γ/ε-fc embryos include the presence of a subcutaneous cavity on the dorsal side of the animal, most prominently between the head and the upper half of the embryo's torso, lack of muscle tension, as well as seemingly atrophied limbs, a curled-up posture, and lack of movement. Embryos may display skin color abnormalities as well.
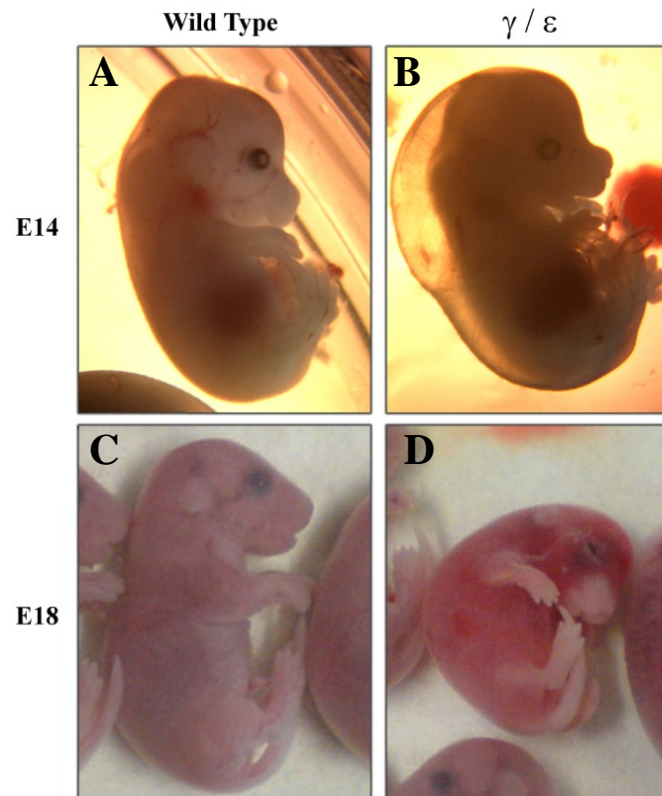
Fig. 7: Phenotypic Differences between Wild Type and Homozygous Embryos.
(A, B) Wild type (A) and homozygous (B) E14 embryos. The γ/ε-fc embryo displays a slight limb atrophy, and a very prominent subcutaneous cavity on the dorsal side, especially noticeable between the head and the upper half of the torso. (C, D) Wild type (C) and homozygous (D) E18 embryos. Differences in phenotype include abnormal skin pigmentation of the homozygous animal, as well as limb atrophy,

curled-up posture, smaller size, lack of muscle tension and movement. The subcutaneous cavity is still present, although it is reduced in size.

6.2.3   Diaphragm

The diaphragm muscle is a good model to analyze the morphological phenotype of γ/ε-fc mutants (Greer et al., 1999). Its relative simplicity, the orderly distribution of endplates along the central endplate band, and the innervation pattern which involves only the phrenic nerve (and not a mixed population of motoneurons), as well as the ease of accessibility and analysis, contribute to the advantages offered by this muscle.
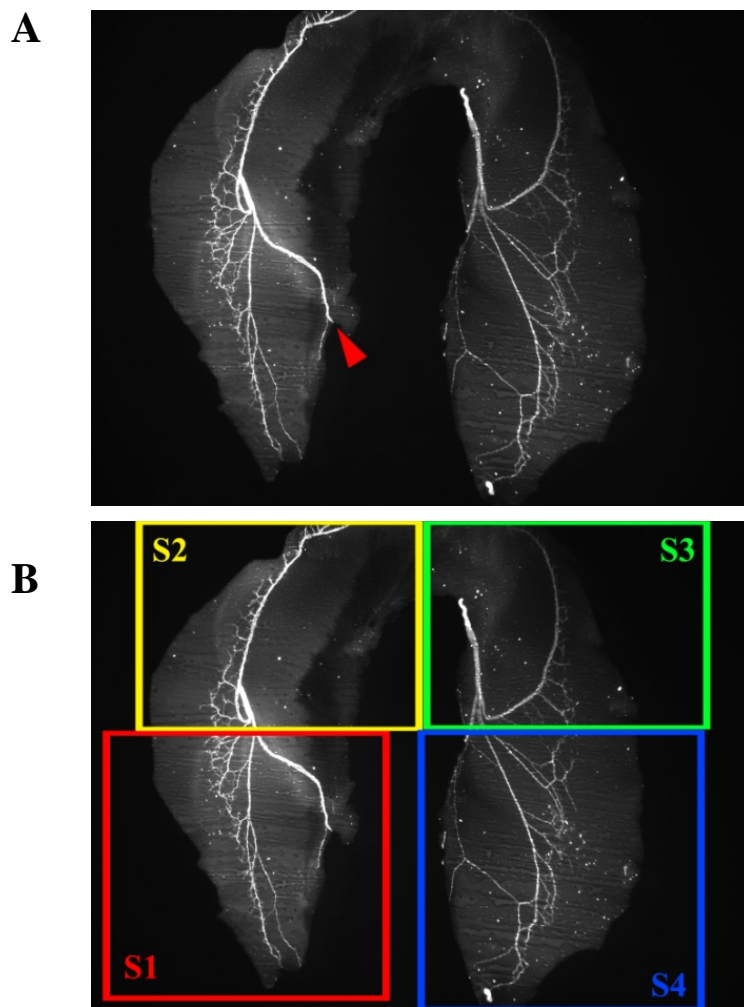
Fig. 8: Anatomy of the Diaphragm.

(A) Innervation pattern of the wild type mouse diaphragm muscle (age E18). Top: sternum; bottom: lumbar area. The red arrow represents where the phrenic nerve enters the left hemidiaphragm. Branches departing from the phrenic nerve innervate

the NMJs located in the central endplate band (not shown). (B) Localization of four different anatomical sectors in the mouse diaphragm muscle. S1: left lumbar area; S2: left sternal area; S3: right sternal area; S4: right lumbar area. The location where the phrenic nerve enters and exits the diaphragm (on the left and right hemidiaphragm, respectively) is treated as the border between lumbar and sternal sectors.

The diaphragm muscle is innervated by the left phrenic nerve, and can be divided into two morphologically different hemidiaphragms according to muscle fiber innervation pattern (Fig. 8A). Furthermore, because the phrenic nerve splits into two main branches upon entering the diaphragm, we decided to further increase the level of detail in our analysis by dividing the left and right hemidiaphragms into lumbar and sternal regions as well (Fig. 8B).

6.3 Anatomy of the NMJ

6.3.1 AChR Clusters

The receptor density in NMJs of wild-type and homozygous γ/ε-fc animals aged E16 and E18 was analyzed through confocal microscopy, in order to study whether clustering of the AChRs and endplate formation were significantly affected by the reduction of AChR activity. In order to magnify the GFP fluorescence of γ/ε-fc subunits, AChRs were stained with FITC- or Alexa488-labeled α-bgtx.
Fig. 9A and C are confocal images taken from an E16 WT embryo, while Fig. 9B and D are confocal images taken from E16 homozygous γ/ε-fc embryo. AChRs cluster both in the WT and the homozygous embryo, however, endplates present a round shape in WT embryos and a more elongated, irregular shape in the γ/ε-fc. Close-up images (Fig. 9C, 9D) reveal slight morphological differences between WT and homozygous endplates: the shape of γ/ε-fc endplates is irregular in comparison to that of WT endplates, and receptors appear to be clustered unevenly along the surface of the endplate, creating areas within the endplate where no receptor fluorescence can be detected.

At E18, differences in size and shape appeared even more pronounced; endplates in the g/e-fc embryo are much larger and irregularly shaped than WT endplates, and AChRs are abnormally clustered within discrete punctae in the endplate area, giving the endplate a distinct, speckled appearance. Fig. 10A and C are images taken from an E18 WT embryo, while Fig. 10B and D are images taken from an E18 γ/ε-fc embryo. Endplates persist in both animals, but the structure of γ/ε-fc endplates appears altered in comparison to WT (Fig. 10C, 10D).

WT γ/ε-fc
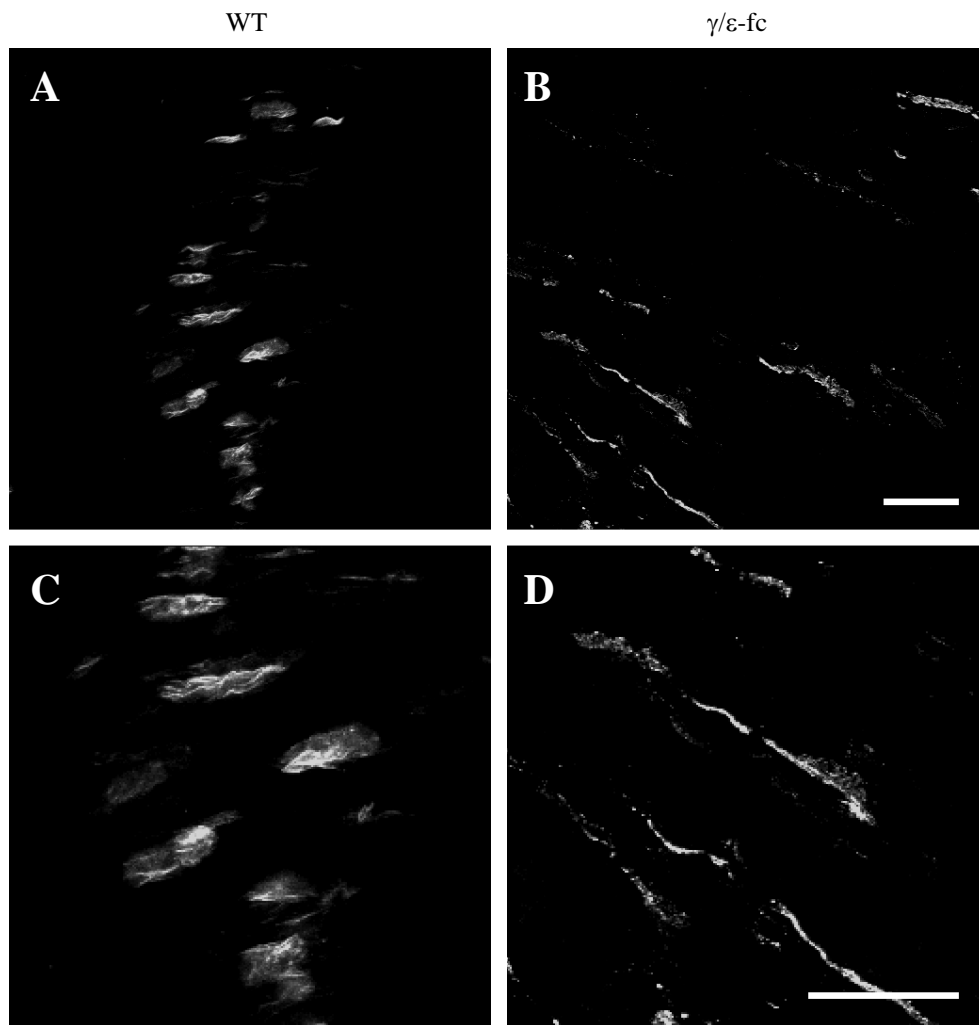
Fig. 9: Bungarotoxin Staining of Diaphragm Endplates from E16 Embryos.
(A) Overview of endplate distribution in the E16 WT diaphragm. Endplates are patterned in the central region of muscle fibers, forming a characteristic central endplate band along the diaphragm. (B) Overview of endplate distribution in the E16 γ/ε-fc diaphragm. Endplates are not concentrated in the central region of muscle fibers, but they are patterned randomly across the whole diaphragm. (C) and (D) Close-ups of endplates from an E16 WT and γ/ε-fc diaphragm, respectively. Individual endplates in the γ/ε-fc embryo are irregularly shaped in comparison to the

round WT endplates, and their loss of prepatterning is clearly visible. Both WT and γ/ε-fc AChRs are stained with FITC-labeled α-bungarotoxin. Scale bars = 25 μm.

WT   γ/ε-fc
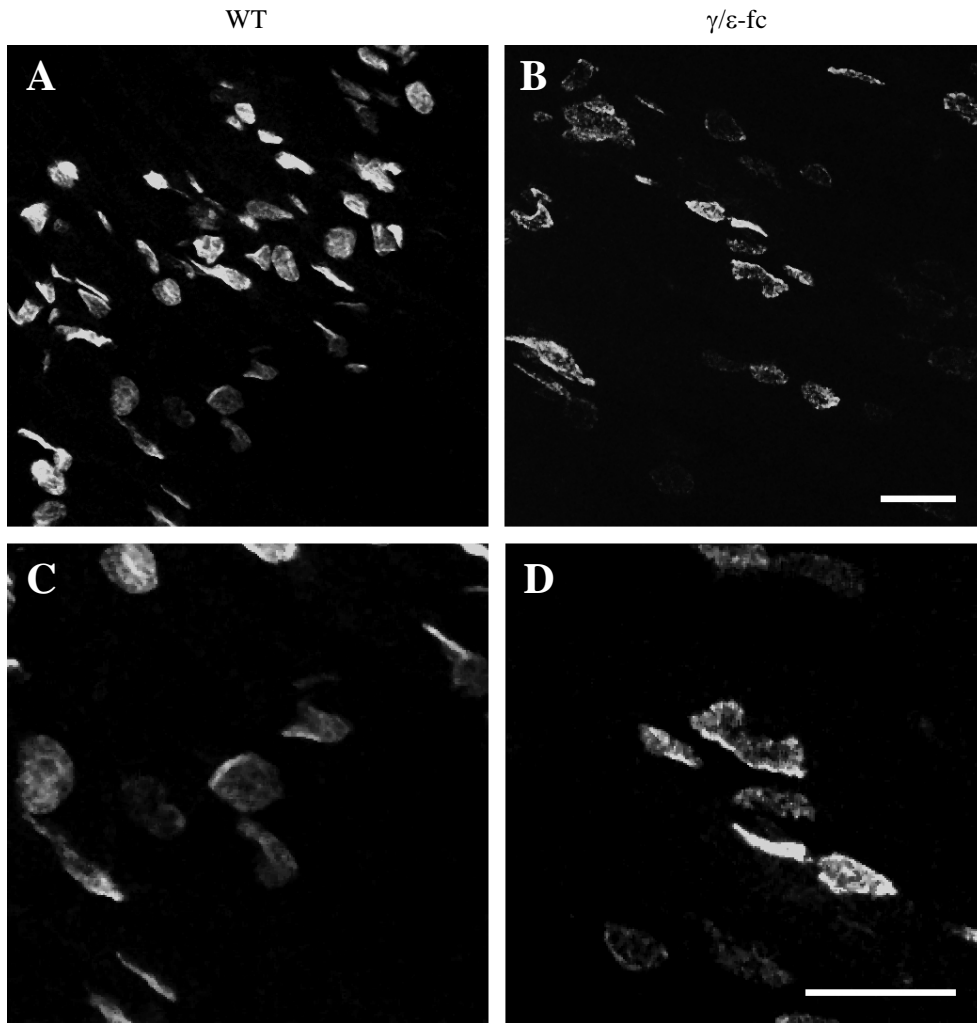
Fig. 10: Bungarotoxin Staining of Diaphragm Endplates from E18 Embryos.
(A) Overview of endplate distribution in the E18 WT diaphragm. Endplates clustered in the central muscle region (see Fig. 9A). (B) Overview of endplate distribution in the E18 γ/ε-fc diaphragm. Endplates, scattered across the diaphragm (see Fig. 9B). (C) and (D) Close-ups of endplates from an E18 WT and γ/ε-fc diaphragm, respectively. Endplate appearance shows morphological differences between the WT and γ/ε-fc animal; WT endplates display a homogeneous round shape, whereas γ/ε-fc endplates display a more heterogeneous, speckled appearance. Both WT and γ/ε-fc AChRs are stained with FITC-labeled α-bungarotoxin. Scale bars = 25 μm.

The different morphology of E16 and E18 endplates from WT and γ/ε-fc embryos is exemplified in Fig. 11A. The density of AChRs in E16 and E18 endplates was

quantitatively evaluated by measuring fluorescence intensities from different regions of the WT and γ/ε-fc diaphragms (Fig. 11B). The average receptor density in the endplates of E16 γ/ε-fc embryos does not appear to be significantly different from that of their WT littermates. In the WT endplates, receptor density remains constant between E16 and E18, but a change can be detected in the γ/ε-fc endplates and possibly correlates in part with the increase in endplate size. In the endplates of E18 embryos, a significant reduction of AChR density (about 40%) can be observed when compared to the endplates of E18 WT diaphragms. Furthermore, due to the presence of the GFP insertion in the γ/ε-fc subunit and the fluorescence increase due to FITC-labeled α-bgtx, average density in the homozygous embryos might be overestimated, and the actual AChR density in γ/ε-fc embryos might be lower than the presented results.
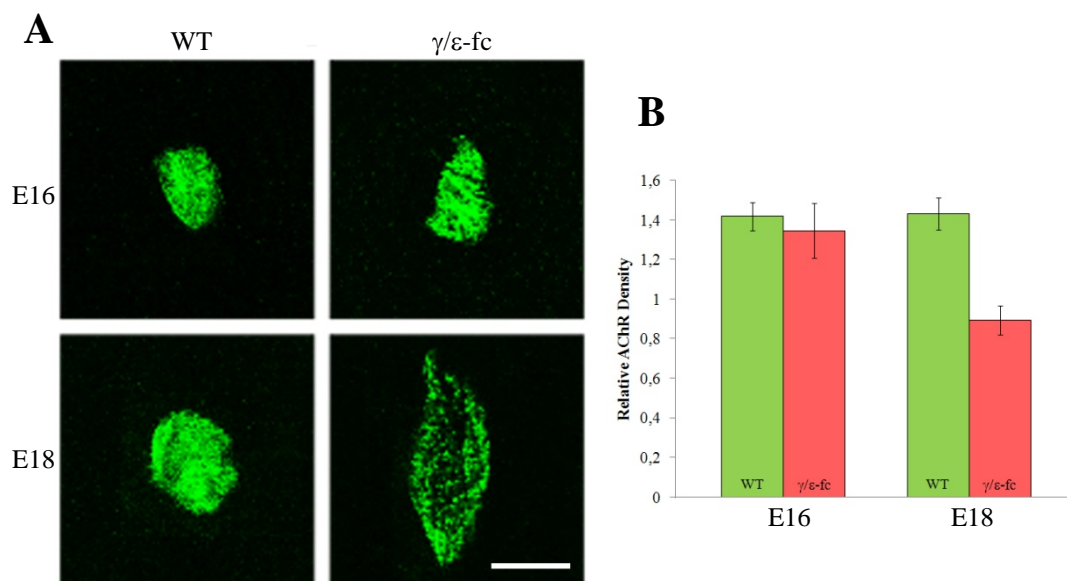
Fig. 11: Endplate Appearance and Receptor Density in E16 and E18 Embryos.
(A) Comparison of endplates of WT and γ/ε-fc animals at embryonic days E16 and E18. While there are only minor morphological differences between E16 endplates, the E18 endplates of γ/ε-fc animals are larger and display a more speckled distribution of receptor clusters than in the WT littermates. Scale bar = 10 μm. (B) Receptor density measurements in E16 and E18 endplates, performed through fluorescence intensity analysis (n = 40, 3 embryos per point). Green: WT embryo; red: γ/ε-fc homozygous embryo. At embryonic day E16, no significant difference can be detected between AChR density in the γ/ε-fc as compared to their WT

littermates. At embryonic day E18, however, a significant (p = 0,0006) decrease in receptor density can be detected in the γ/ε-fc, in comparison to their WT littermates.

Reduced AChR activity in the γ/ε-fc embryos caused not only a reduction in AChR density within the putative endplates, but also affected shape and size, as shown in Fig. 12 and 13. Fig. 12 shows average areas for endplates in E16 and E18 WT and γ/ε-fc embryos. As shown in Fig. 12A, overall the average endplate area does not show any significant changes between WT and γ/ε-fc embryos at E16. Between E16 and E18, endplate areas in the WT embryos increases slightly, but γ/ε-fc endplates undergo a much more pronounced increase, and at E18, a significant difference emerges, with γ/ε-fc endplates being on average 20% larger than the endplates of WT littermates. However, the severity of these changes appears to vary in different regions of the diaphragm; Fig. 12B shows a comparison of the average endplate areas for WT and γ/ε-fc embryos in the lumbar or sternal region of the diaphragm, both at E16 and E18. At E16, there are no significant differences between endplate areas in either the lumbar or the sternal region of γ/ε-fc embryos in comparison to WT littermates. At E18, endplate area in the lumbar region of γ/ε-fc embryos does not differ significantly from WT littermates, but the average endplate area in the sternal region is instead significantly increased by about 25%.
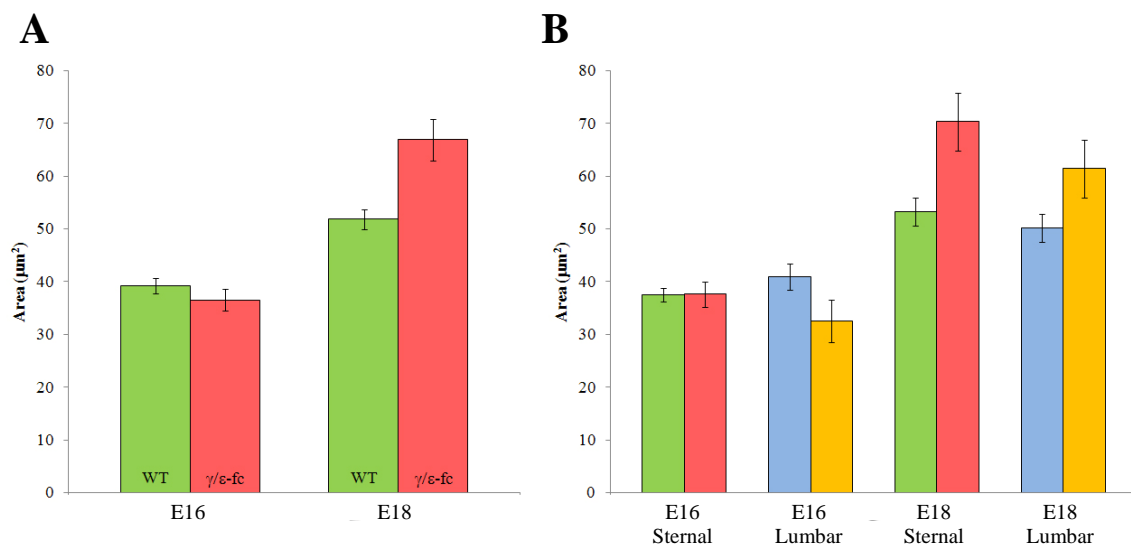
Fig. 12: Endplate Area in E16 and E18 Embryos.

(A) Comparison of average endplate areas in E16 and E18 WT and γ/ε-fc homozygous embryos (n = 60 endplates among 3 embryos). Endplates appear to be significantly larger in E18 γ/ε-fc homozygous animals than in their WT littermates (p

= 0,0009). (B) Comparison of average endplate areas in the sternal and lumbar regions of the diaphragms of E16 and E18 embryos. Green: WT sternal region; red: γ/ε-fc sternal region; blue: WT lumbar region; orange: γ/ε-fc lumbar region. No significant differences can be detected in the areas of sternal endplates in E16 embryos (p = 0,77) as well as in the areas lumbar endplates, both in E16 and E18 embryos (p = 0,09 and 0,07, respectively). However, the average endplate area in the sternal region of E18 embryos is significantly increased in comparison to wild type (p = 0,007).

Fig. 13 shows the average circularity of endplates in E16 and E18 WT and γ/ε-fc embryos as a quantitative measurement of their shape. Circularity is a measurement indicating regularity of object shapes. It is calculated according to the formula *circularity = 4π (area / perimeter^2)*. A value of 1,0 indicates a perfect circle, while a value of 0,0 indicates a completely irregular polygon. Fig. 13A compares the average circularities of endplates at ages E16 and E18; the data clearly indicate that the average endplate shape in γ/ε-fc animals is significantly more irregular than in WT littermates, both at E16 and E18.
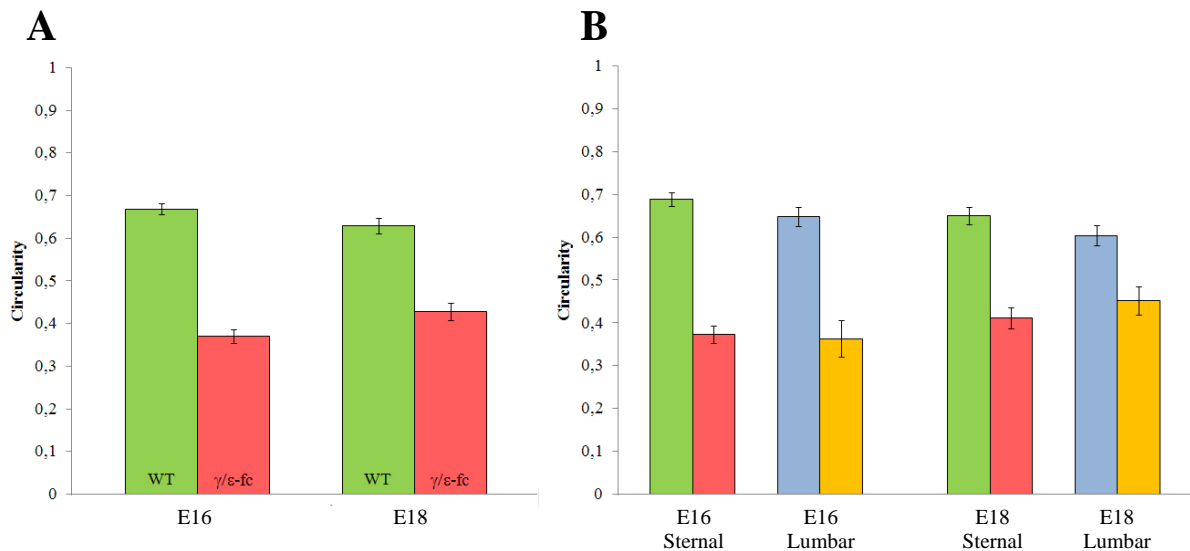
Fig. 13: Shape (Circularity) in E16 and E18 Embryos.

(A) Comparison of average endplate circularities in E16 and E18 WT and γ/ε-fc homozygous embryos (n = 20, 3 embryos per point). In both cases, endplates are significantly more irregular in shape than the endplates of WT embryos (p < 0,0001 both in E16 and E18 embryos). (B) Comparison of average endplate circularities in the sternal and lumbar regions of the diaphragms of E16 and E18 embryos. Green:

WT sternal region; red: γ/ε-fc sternal region; blue: WT lumbar region; orange: γ/ε-fc lumbar region. At both embryonic ages, endplate shape is significantly affected in all regions of the diaphragm, although the difference between WT and γ/ε-fc homozygous animals appears be reduced at E18 (p < 0,0001 for both sternal and lumbar regions at E16; p < 0,0001 for sternal region at E18, p = 0,0003 for lumbar region t E18).

However, there appears to be a slight tendency towards a reduction in the difference between WT and γ/ε-fc embryos between E16 and E18. Fig. 13B compares average circularities in the lumbar and sternal regions of WT and γ/ε-fc embryos: significant differences in shape are apparent in both regions when comparing homozygous endplates with WT endplates. However, the tendency described above appears to be stronger in the E18 lumbar region than in the E18 sternal region, though no statistical significance can be ascribed to it.

6.3.2 Distribution of Endplates

AChE present in diaphragm endplates was stained using the Koelle method, and pictures were taken using conventional light microscopy (Fig. 14).

The distribution of endplates in the diaphragms of E16 and E18 γ/ε-fc embryos is largely different from the normal distribution found in WT embryos. The central endplate band, clearly visible in WT diaphragms, is severely affected by reduced AChR activity and endplates are far more widely dispersed along the diaphragm width (Fig. 14A). This phenotype is especially noticeable in the lumbar region of the diaphragm, due to the larger average length of muscle fibers.

The quantification of average endplate distribution width in the sternal (Fig. 14C) and lumbar (Fig. 14D) regions of WT and γ/ε-fc E16 and E18 diaphragms confirms that endplates in embryos with reduced AChR activity are distributed on a much broader area, at least twice as wide as the area covered by the endplate band of WT embryos. However, while the endplate band appears to be almost completely disrupted in the lumbar regions, it is clearly still present in the sternal regions, although greatly widened in comparison to the WT endplate band. This difference is statistically significant in both sternal and lumbar regions, both at E16 and E18. Fig. 14E

compares the total endplate distribution widths of embryos within the same group (WT or γ/ε-fc) between ages E16 and E18. Whereas in the WT diaphragm the width of the endplate band (expressed as percentage of total diaphragm width) is significantly reduced between E16 and E18 due to the growth pattern of myotubes, which grow by incorporating myoblasts at the distal ends, there is no significant difference between the width of the endplate band in γ/ε-fc embryos between E16 and E18, suggesting that muscle fiber growth is impaired, and/or that new endplates continue being formed at more distal regions of myotubes even at late pregnancy stages.
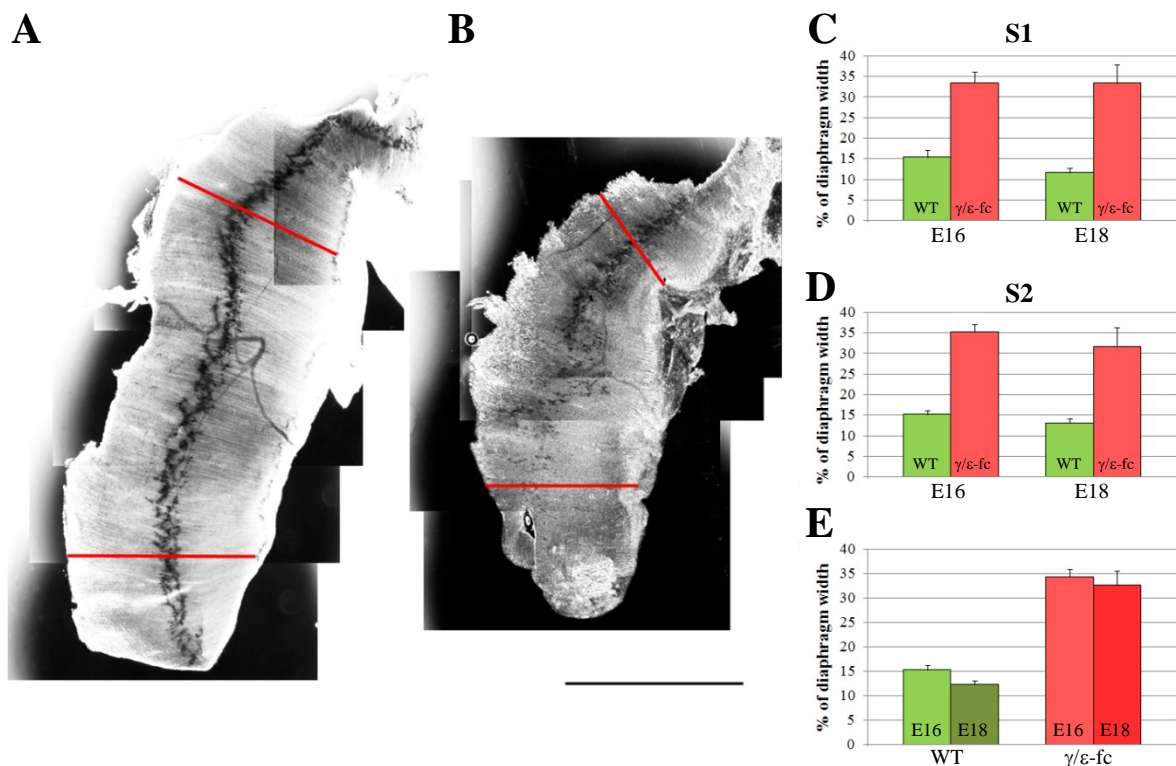
Fig. 14: Endplate Distribution in WT and γ/ε-fc Embryos.

(A, B) Composite pictures of E18 left hemidiaphragms from WT and γ/ε-fc homozygous embryos. In the WT diaphragm (A), the central endplate band is clearly recognizable and no endplates can be found in the inner or outer regions of the diaphragm. In the γ/ε-fc homozygous diaphragm (B), endplate distribution is much broader, and the central endplate band has almost completely disappeared in the lumbar regions; endplates are scattered on a much wider area. Endplate distribution width measurements were taken by selecting lines across diaphragm regions (in red) and measuring the total width of the diaphragm, and the distance between the first and last discernable endplate along the line. Scale bar = 1 mm. (C) Comparison of endplate distribution widths between WT (green) and γ/ε-fc (red) embryos in the

43

sternal region S2 at ages E16 and E18 (E16 p < 0,0001; E18 p = 0,008). Widths are expressed as percentages of total diaphragm width. (D) Comparison of endplate distribution widths between WT (green) and γ/ε-fc (red) embryos in the lumbar region S1 at ages E16 and E18 (E16 p = 0,0003; E18 p = 0,004). Widths are expressed as percentages of total diaphragm width. (E) Comparison of total endplate distribution widths between embryos with the same group (green: WT; red: γ/ε-fc) at ages E16 and E18 (WT p = 0,022; γ/ε-fc p = 0,6). Widths are expressed as percentages of total diaphragm width. n = 9, 2 embryos per point.

6.3.3   General Innervation Pattern

Motor axons were stained using anti-neurofilament primary antibodies and rhodamine-labeled secondary antibodies. Pictures were taken using confocal microscopy.

The analysis of diaphragms aged E16 and E18 reveals gross physiological aberrations in the innervation patterns of γ/ε-fc embryos (Fig. 15A-C). The growth of secondary neurites in WT diaphragms is restricted to the medial diaphragm where they innervate NMJs and does not extend any further, whereas neurites in the g/e-fc diaphragms continue growing, reaching the edge of the diaphragm and showing no detectable retraction even at E18. In WT embryos, neurites extend from the phrenic nerve in an orderly fashion, while γ/ε-fc neurites display a nearly complete loss of directionality, growing randomly and branching wildly. The total number of neurites in the diaphragm of γ/ε-fc embryos and their average length are also significantly increased when compared to WT littermates (Fig. 15D-G).

In order to accurately quantify the average number of neurites and their average length, composite pictures of the left (S1-2) and right (S3-4) hemidiaphragms were analyzed separately. As shown in Fig. 15D, while there is no significant difference in the number of neurites between hemidiaphragms of the same embryos at embryonic day E16, the average number of neurites in either hemidiaphragm of γ/ε-fc embryos is significantly increased in comparison to the same hemidiaphragm in WT embryos (p = 0,009 for S1-2 and p = 0,0008 for S3-4). The same analysis performed at age E18 (Fig. 15E) shows that aberrant neurite growth is not inhibited in the γ/ε-fc embryos, and the average number of neurites in either hemidiaphragm appears to further increase.
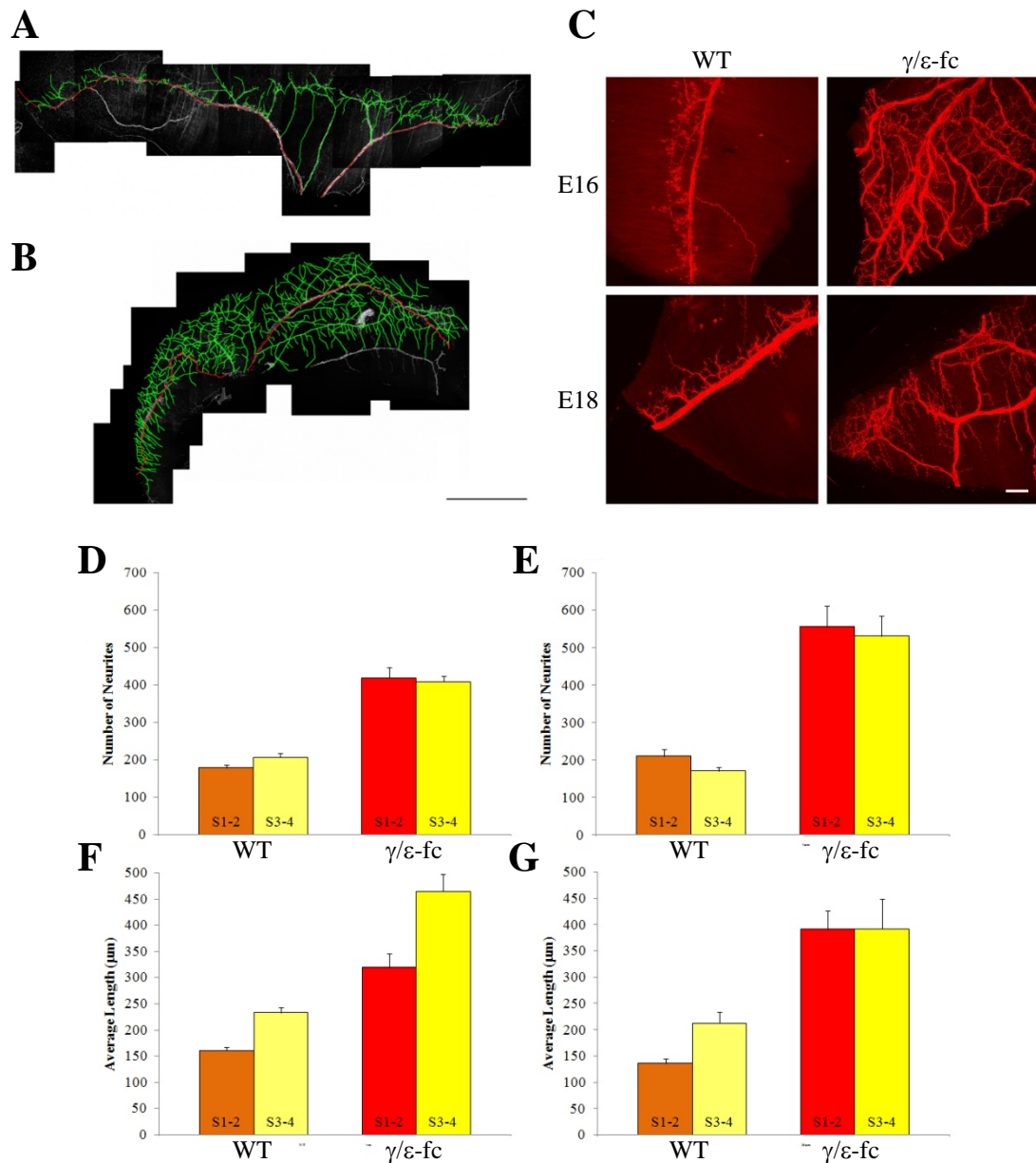
Fig. 15: Differences in the Innervation Pattern of WT and γ/ε-fc Embryos.

(A, B) Composite pictures of E18 diaphragms from WT and γ/ε-fc homozygous embryos. Neurites have been traced with the NeuronJ plug-in for ImageJ in order to follow their branching pattern. In the WT diaphragm (A), secondary neurites (green) branch from the phrenic nerve (red) and reach the central region of the diaphragm, where they innervate the NMJs of the central endplate band. In the γ/ε-fc homozygous diaphragm (B), neurite growth does not follow any discernible pattern, it is not restricted to the central endplate band, nerves reach the edge of the diaphragm without retracting, and directionality of growth is completely abolished. Branching is also highly increased. Scale bar = 1 mm. (C) Close-up pictures of the S1 region in WT and γ/ε-fc embryos aged E16 and E18. The increase in neurite

number and length is clearly visible. Scale bar = 100 μm. (D) Average number of neurites in the left (S1-2) and right (S3-4) hemidiaphragm of WT and γ/ε-fc embryos at E16. (E) Average number of neurites in the left (S1-2) and right (S3-4) hemidiaphragm of WT and γ/ε-fc embryos at E18.

(F) Average length of neurites in the left (S1-2) and right (S3-4) hemidiaphragm of WT and γ/ε-fc embryos at E16. (G) Average length of neurites in the left (S1-2) and right (S3-4) hemidiaphragm of WT and γ/ε-fc embryos at E18. n = 3 embryos per point.

The average length of neurites is also affected by reduced AChR activity (Fig. 15F and G). Fig. 15F represents the average length of neurites from the left and right hemidiaphragm of E16 WT and γ/ε-fc embryos. Minor differences between the left and right hemidiaphragms in the same embryos can be attributed to the asymmetry of the innervation pattern (as shown in Fig. 8). The average neurite length is significantly increased in both hemidiaphragms of the γ/ε-fc embryo in comparison to the WT littermate (p = 0,02 for S1-2 and p = 0,005 for S3-4); this difference loses its significance at E18 (Fig. 15G) due to the high variability of the average neurite length in different γ/ε-fc embryos (p = 0,07 for both left and right hemidiaphragms).

The analysis of neurite individual length details finer differences between WT and γ/ε-fc embryos at E16 and E18.

Fig. 16A-D display the percentage of total neurites in the left (A, C) and right (B, D) hemidiaphragms of WT and γ/ε-fc animals aged E16, arranged by length (in μm). In the WT diaphragm, the largest percentage of neurites is between 40 and 160 μm long, while the γ/ε-fc diaphragm displays a more homogeneous distribution of neurites across the spectrum of lengths. Organizing these data as a cumulative probability distribution (Fig. 16E-F), the K-S test demonstrated that the shift in neurite distribution along length categories is statistically significant (p = 0,03 for S1-2, p = 0,009 for S3-4).
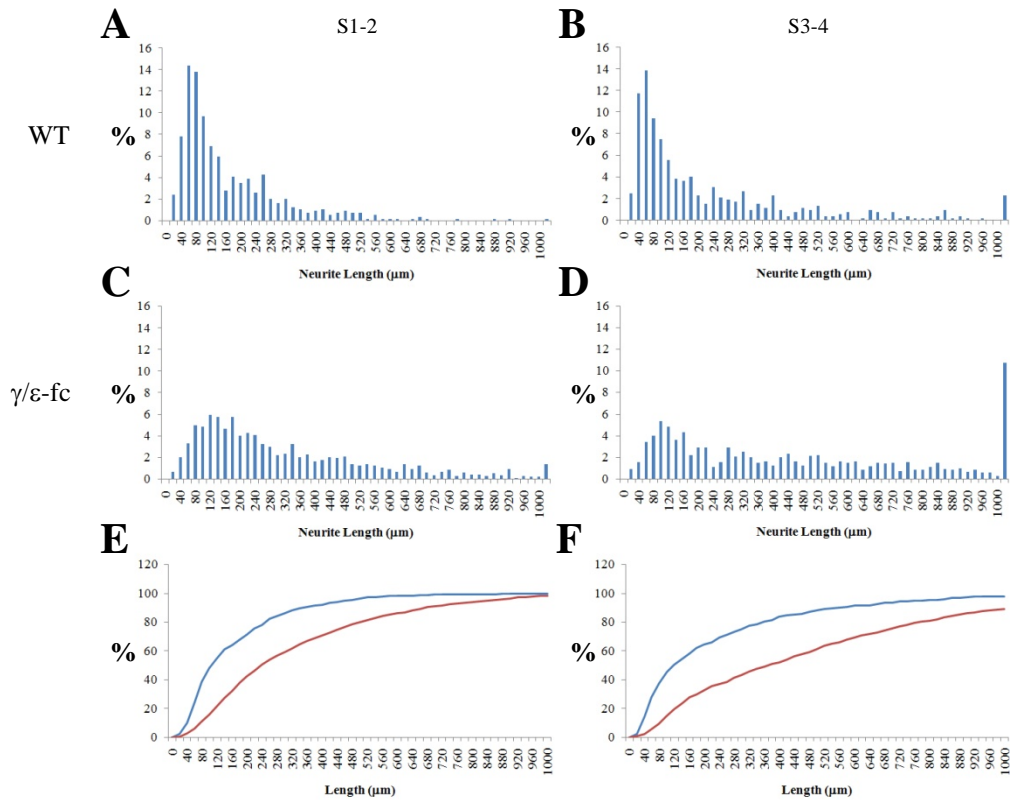
Fig. 16: Percentages of Total Neurites by Length in Diaphragms of E16 Embryos.
(A, C) S1-2 hemidiaphragms of WT and γ/ε-fc embryo, respectively; while most WT neurites are between 40 and 160 μm long, γ/ε-fc neurites are more homogeneously distributed along the spectrum of lengths. The same can be noticed comparing the S3-4 hemidiaphragms of WT and γ/ε-fc embryos (B, D). (E, F) Comparison of cumulative probability distributions of neurite lengths in S1-2 hemidiaphragms (E) and S3-4 hemidiaphragms (F) of WT (blue) and γ/ε-fc (red) embryos. In both cases, γ/ε-fc neurites are distributed along a wider spectrum of lengths, as described above. n = 3 embryos per point.

The same analysis was also performed on E18 embryos (Fig. 17A-D), showing no change in the situation in comparison to E16, with γ/ε-fc neurites remaining distributed along a significantly wider spectrum of lengths than neurites in the WT littermate (Fig. 17E-F; p = 0,002 for S1-2, p < 0,0001 for S3-4).

47
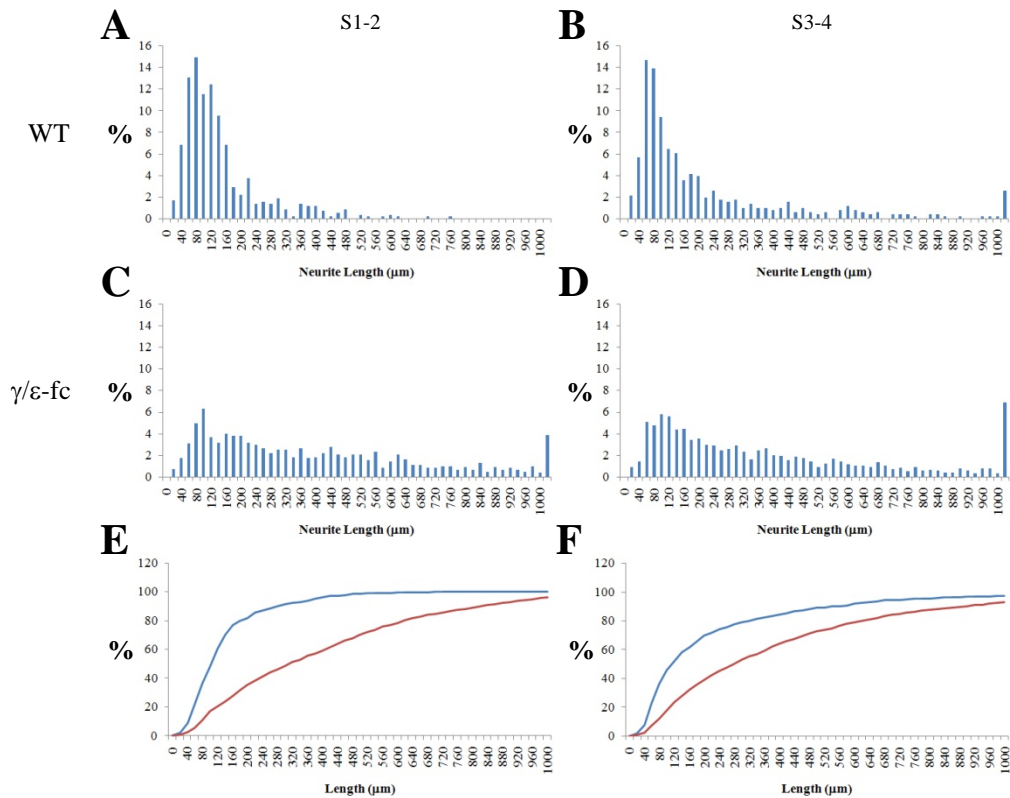
Fig. 17: Percentages of Total Neurites by Length in Diaphragms of E18 Embryos.
(A, C) S1-2 hemidiaphragms of WT and γ/ε-fc embryo, respectively; as already demonstrated in E16 embryos, most neurites in the WT diaphragm are between 40 and 160 μm long, while the γ/ε-fc diaphragm shows a much wider distribution. The same can be noticed comparing the S3-4 hemidiaphragms of WT and γ/ε-fc embryos (B, D). (E, F) Comparison of cumulative probability distributions of neurite lengths in S1-2 hemidiaphragms (E) and S3-4 hemidiaphragms (F) of WT (blue) and γ/ε-fc (red) embryos. The data suggest that no improvement occurs in the length distribution of γ/ε-fc embryos at late pregnancy stages. n = 3 embryos per point.

6.3.4   Endplate Innervation

Nerve terminals in E18 diaphragms were stained with rabbit anti-synaptophysin primary antibodies and rhodamine-labeled anti-rabbit secondary antibodies, in order to study the presence of innervation in individual endplates.

Due to the disorganization of the innervation pattern and the lack of endplate pre-patterning along the central region of the muscle fibers in the diaphragm (Fig. 18A-B), stained nerve terminals in the γ/ε-fc homozygous embryo are not restricted to the

central endplate band, but are spread over the whole diaphragm; all visible endplates in the γ/ε-fc homozygous mouse are innervated (Fig. 18C-D).

A

WT   γ/ε-fc

B

WT   γ/ε-fc

C

α-Bgtx   Rh-Synaptophysin   Merge

WT

γ/ε-fc

D   **E**
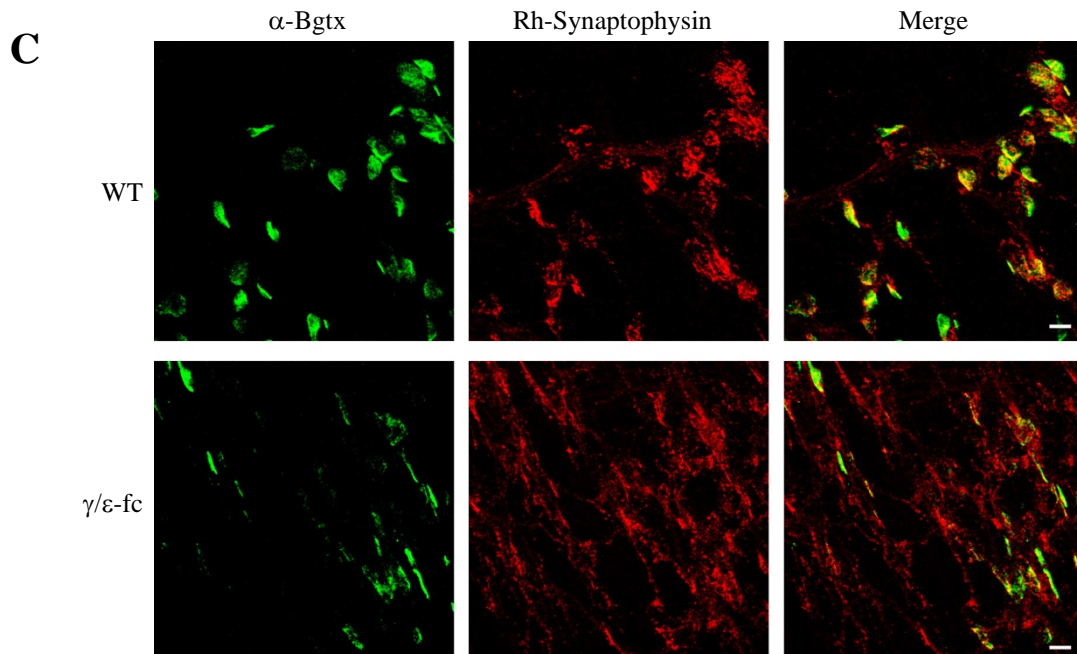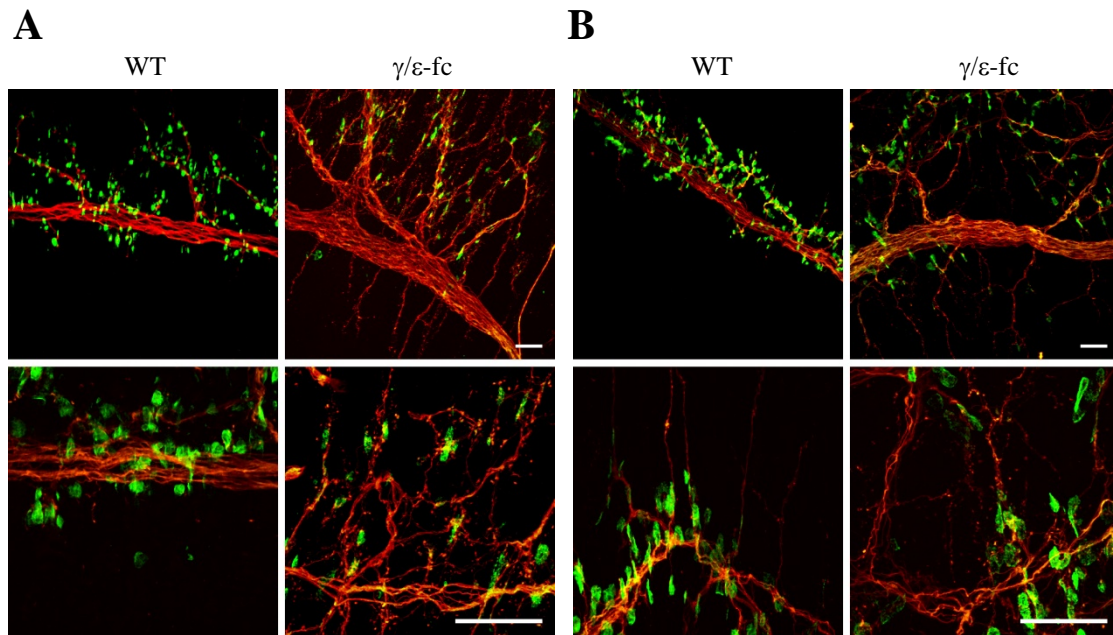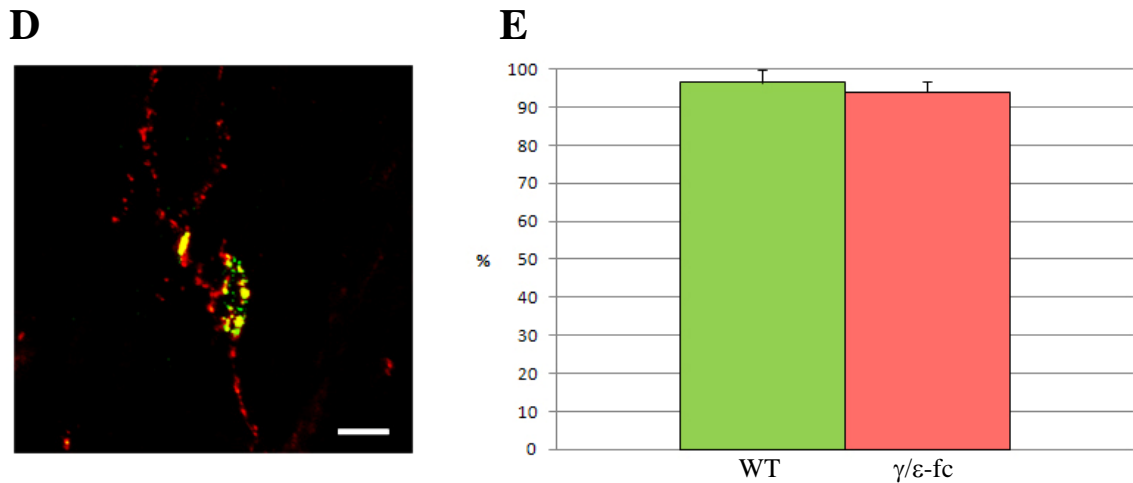
Fig. 18: Innervation of Individual Endplates.

(A, B) Overviews and close-ups of E16 (A) and E18 (B) diaphragms, stained with anti-neurofilament antibody (red) and FITC-labeled a-bgtx (green). The chaotic meshwork of neurites in the γ/ε-fc embryos appears to reach most endplates. Scale bars = 50 μm. (C) Close-up of E18 WT and γ/ε-fc homozygous diaphragms. Green: α-Bgtx-labeled endplates; red: anti-synaptophysin antibody. Although nerve terminals in the γ/ε-fc homozygous embryo are entirely disorganized, all visible endplates are innervated. Scale bar: 10 μm. (D) zoomed-in view of a γ/ε-fc endplate, showing the nerve terminal (red) which colocalizes with the green fluorescence of the AChRs. Scale bar: 10 μm. (E) Percentage of innervated endplates in WT and γ/ε-fc embryos. No significant difference can be detected ($p > 0,05$, $n = 2$).

Unlike nerve terminals in WT embryos, neurites in γ/ε-fc homozygous embryos do not stop their growth upon innervating an endplate, but continue growing and branching past the innervation point (Fig. 18D). As shown in Fig. 18E, almost all detectable endplates are innervated, both in WT and γ/ε-fc embryos.

6.3.5   Presence of Multiple Synapses

In order to study the possible presence of multiple synapses on muscle fibers, slow muscle fibers were stained with anti-slow skeletal myosin antibody; endplates were stained with FITC-labeled α-bungarotoxin; and neurofilaments were stained with α-neurofilament antibody. Pictures were taken through confocal microscopy, and analyzed by optically following several muscle fibers across the diaphragm in order to pinpoint the location of their endplates.

Fig. 19A shows close-up pictures of E16 diaphragm muscle fibers, while Fig. 19B and C show the results of the analysis. On average, there is a significant presence of multiple endplates on the same muscle fiber in γ/ε-fc embryos, with an average of 1,8 endplates per muscle fiber (Fig. 19B). The analysis of the percentage of muscle fibers displaying multiple endplates (Fig. 19C) reveals that roughly one-third of all muscle fibers in the E16 γ/ε-fc embryo contain one endplate, while the remaining muscle fibers present multiple synapses in a variable number, usually between two and three, with a very small number of fibers displaying up to five different endplates.

A

B **C**
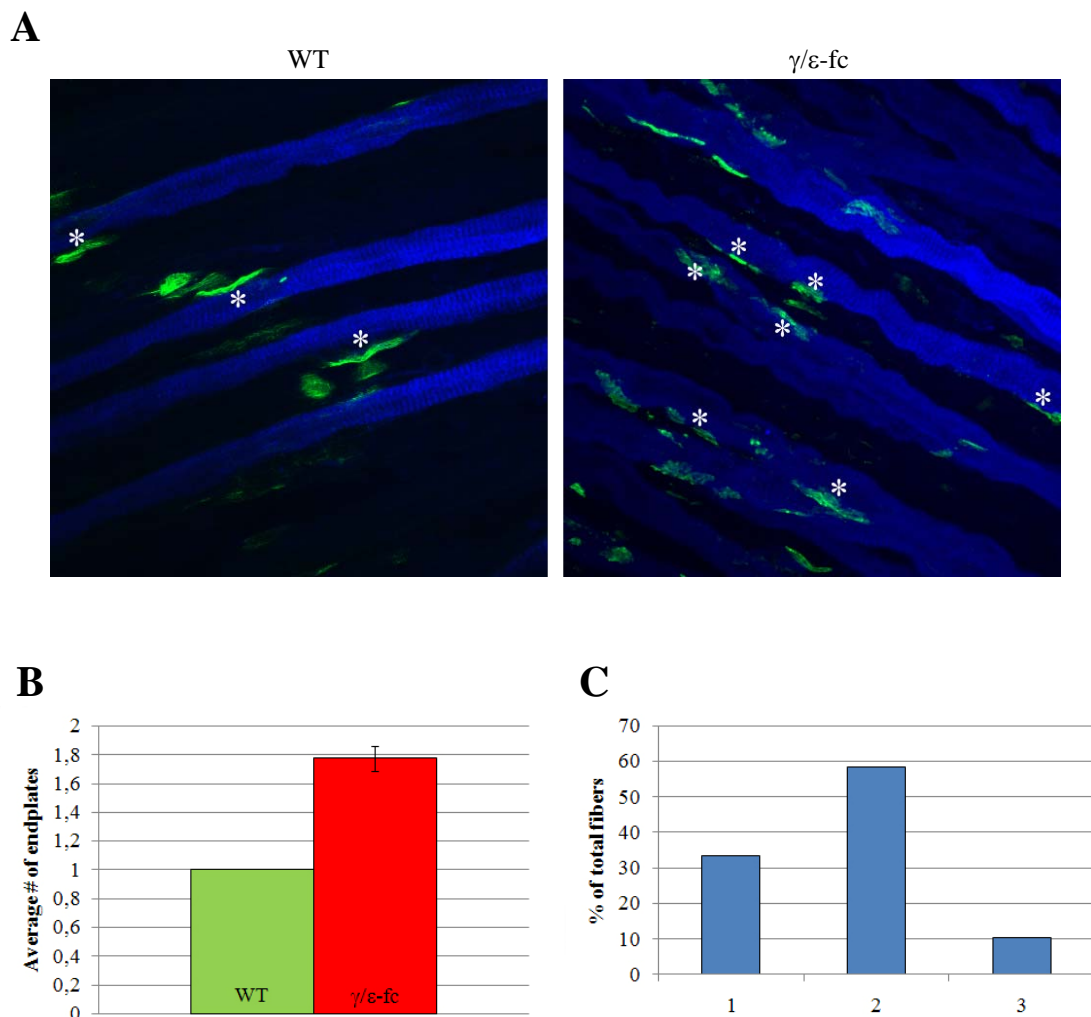
Fig. 19: Presence of Multiple Endplates in E16 Embryos.

n = 50 muscle fibers. (A) Close-ups of diaphragm muscle fibers in WT and γ/ε-fc E16 embryos. The asterisks mark the location of endplates on individual muscle fibers. While muscle fibers in the WT embryo display only one endplate each, muscle fibers in the g/e-fc embryo often display multiple endplates. (B) Average number of endplates on the muscle fibers of WT (green) and γ/ε-fc (red) E16 embryos. The number is significantly increased in the γ/ε-fc embryos (p < 0,0001).

(C) γ/ε-fc muscle fiber percentages grouped by number of endplates on the individual fiber. About one-third of all slow muscle fibers present one endplate, whereas most slow muscle fibers present multiple endplates. Values are underestimated due to the difficulty of analysis in the γ/ε-fc embryo.

6.3.6   Motoneuron Survival

Motoneurons in the brachial lateral motor column (LMC) of the spinal cord were immunostained with goat anti-ChAT primary antibodies coupled with biotinylated anti-goat secondary antibodies. Pictures were taken using a light microscope, and analyzed through ImageJ (Fig. 20A), in order to analyze the retraction of excess motoneuron projections from the diaphragm in late embryonic stages.
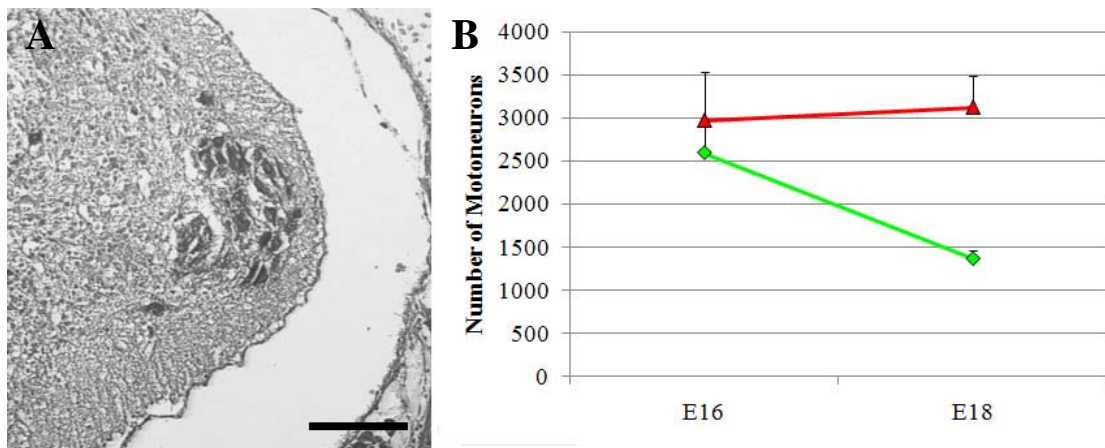
Fig. 20: ChAT Staining of Motoneurons in the LMC.
(A) Close-up of ChAT staining in whole-mount paraffin section in the cervical region of a wild-type E18 animal. Motoneurons are marked by dark staining in the lateral motor column. Scale bar = 200 μm. (B) Comparison of motoneuron numbers in WT (green) and γ/ε-fc (red) embryos at age E16 and E18. Values were collected from single animals, and mean total motoneuron numbers are shown.

Based on the comparison of total motoneuron numbers (Fig. 20B), there is little or no difference in the average number of total motoneurons in the LMCs of γ/ε-fc embryos when compared to WT littermates (p = 0,6), whereas there is a significant difference at late embryonic stages (p = 0,03). The number of motoneurons in WT embryos

decreases dramatically as a consequence of motoneuron death, whereas the number of motoneurons in the γ/ε-fc embryos remains stable.

6.3.7 Muscle Fiber Growth

Muscle fibers were stained with mouse anti-slow skeletal myosin primary antibodies coupled with AMCA-labeled anti-mouse secondary antibodies, and analyzed through confocal microscopy (Fig. 21A, B).

The organization of slow muscle fibers is partially disrupted by reduced activity of the AChRs; this disruption appears to be localized in the lumbar regions of the γ/ε-fc homozygous diaphragm, as well as the central boundary between sternal and lumbar regions, whereas the slow muscle fibers in the sternal regions remain relatively unaffected by the γ/ε-fc mutation. In the affected regions, slow muscle fibers partially lose their directionality, and form a loose meshwork of fibers woven through the unaffected muscle fibers.

B

C
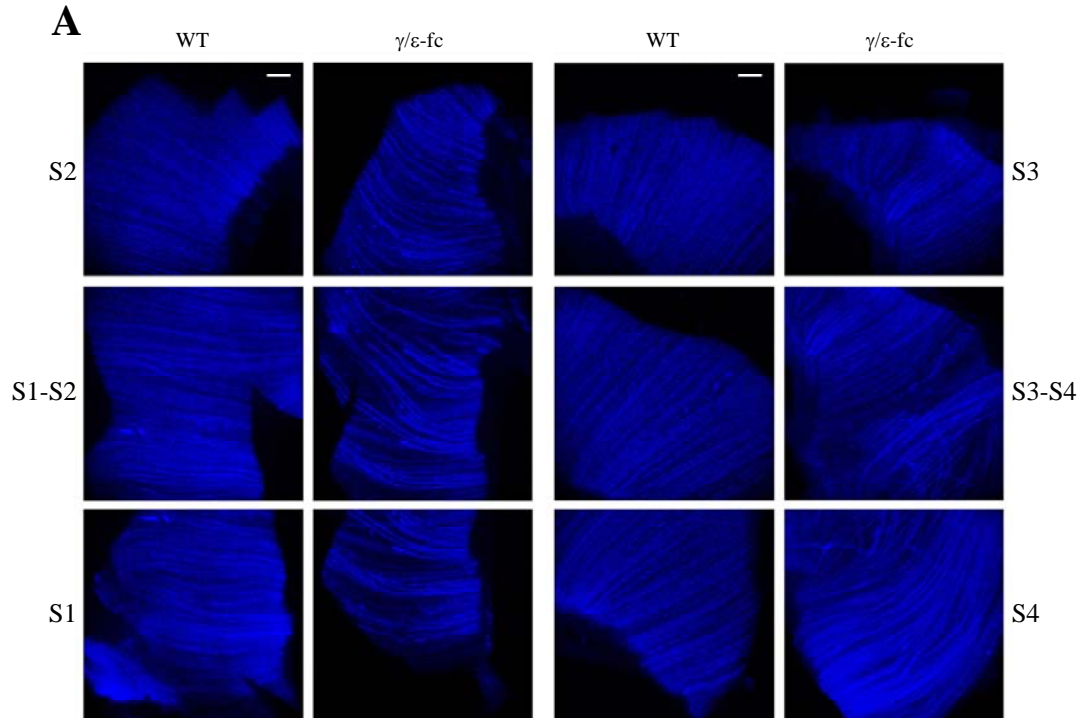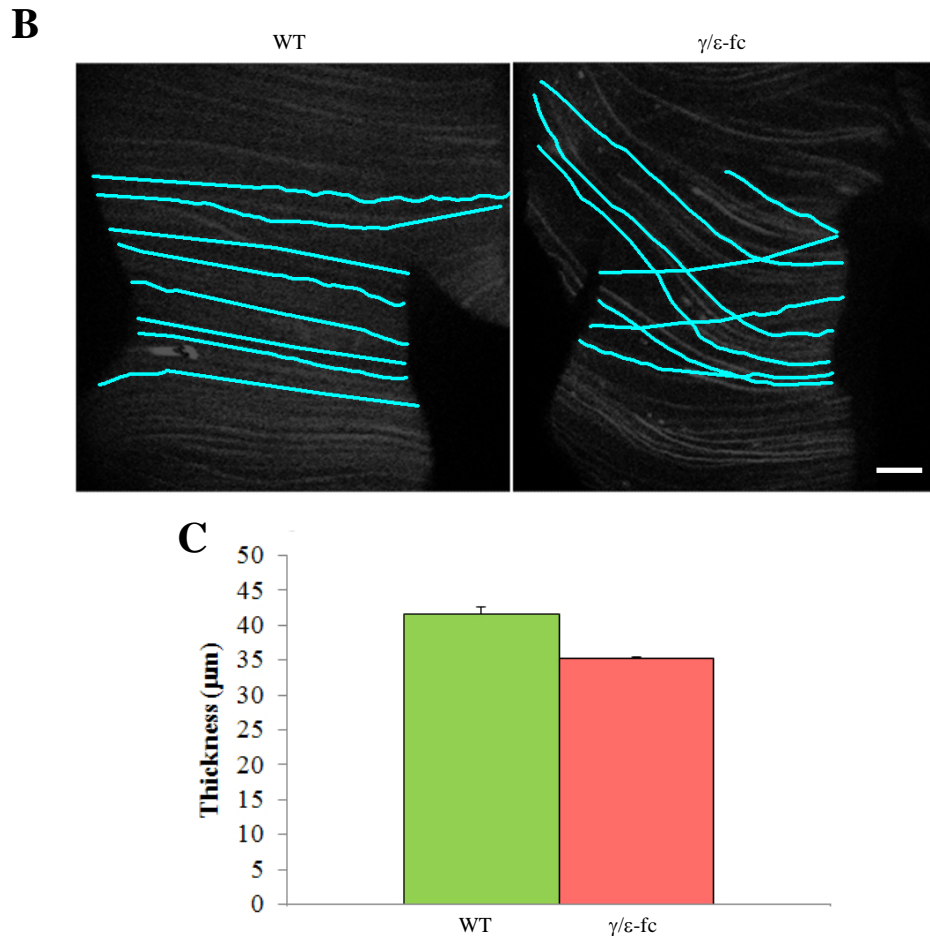
Fig. 21: Slow Muscle Fiber Organization.

(A) Comparison between the slow muscle fiber organization in a γ/ε-fc homozygous embryo aged E16 and in a WT littermate. The organization of slow muscle fibers is partially disrupted by lack of activity on the part of the AChRs; this disorganization is more evident in the lumbar regions (S1 and S4) of the diaphragm, whereas it is much less noticeable in the sternal regions (S2 and S3). (B) Close-up of region S1-S2 of the WT and γ/ε-fc diaphragm; the paths of several muscle fibers are traced in order to highlight the aberrant muscle fiber organization in the γ/ε-fc embryo, including the abnormal length, directionalitry and crisscrossing of muscle fibers. Scale bar = 100 μm. (C) Comparison between the average diaphragm thickness in a γ/ε-fc homozygous embryo aged E16 and in a WT littermate. The ~15% decrease in thickness appears to be significant ($p < 0.05$).

Diaphragm thickness in E16 γ/ε-fc embryos appears to be significantly reduced by ~15% in comparison to their WT littermates (Fig. 21C).

6.3.8 Muscle Fiber Diameter

Stained slow muscle fibers were analyzed through confocal microscopy, and data were collected through ImageJ and Leica LAS AF software (Fig. 22A, B).

Fig. 22B shows that the diameter of γ/ε-fc slow muscle fibers is not significantly different from the diameter of WT slow muscle fibers, suggesting that lack of AChR-mediated activity has little or no effect on the development and differentiation of individual muscle fibers, despite its effects on the overall diaphragm architecture.
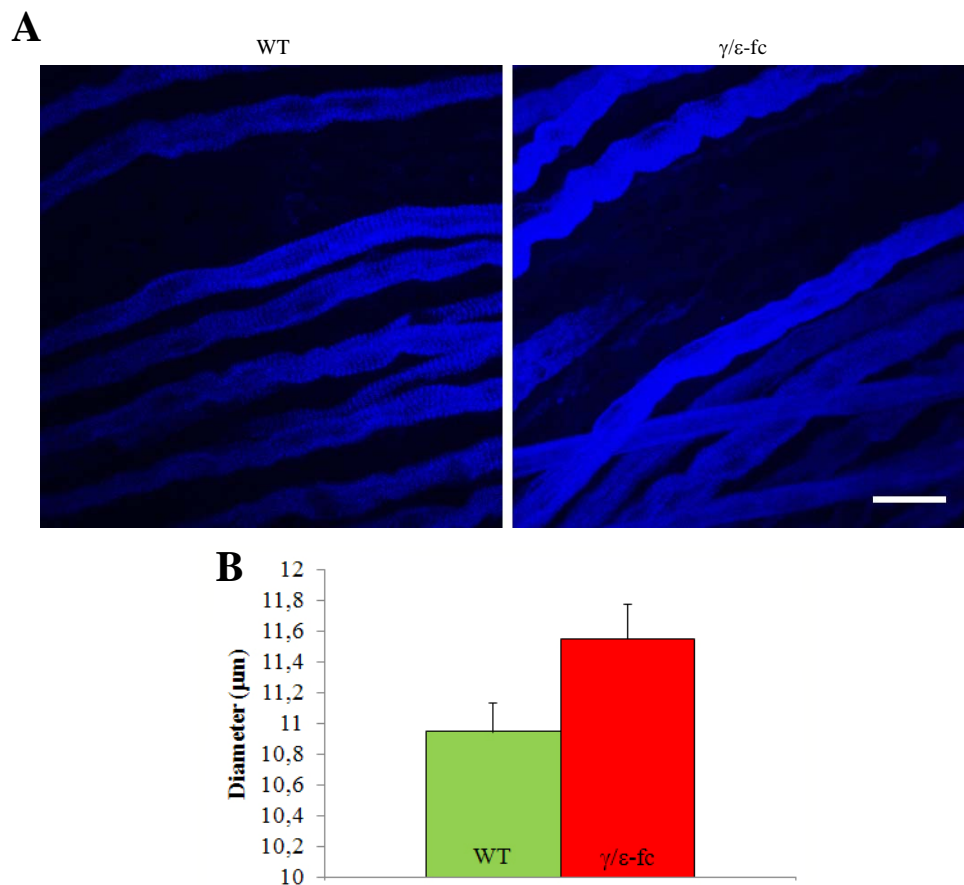
Fig. 22: Slow Muscle Fiber Diameter.

(A) Close-up of slow muscle fibers in the S1-S2 region of WT and γ/ε-fc homozygous E16 embryos. Although fiber organization in the homozygous embryos is partially disrupted in comparison to WT embryos, no appreciable difference can be noticed between the sizes of the individual muscle fibers. Scale bar = 25 μm. (B) Comparison of muscle fiber diameters between WT and γ/ε-fc homozygous E16 embryos. No significant difference can be detected ($p = 0.05$, n = 12 muscle fibers in each animal, one animal per experimental point).

6.4   Gene Profiling

6.4.1   mRNA Gene Profiling

Leg muscles from WT and γ/ε-fc homozygous embryos aged E16 and E18 were used to extract mRNA. The samples were converted to cDNA and the mRNA expression levels of different proteins were calculated through Real-Time PCR both for E16 embryos (Fig. 23A, C) and E18 embryos (Fig. 23B, D).

Data from γ/ε-fc heterozygous and homozygous embryos were quantified either relative to the mRNA expression levels in WT embryos (Fig. 23A, B) or to the mRNA expression levels of the housekeeping protein glyceraldehyde-3-phosphate dehydrogenase, GAPDH (Fig. 23C, D).

Two different probes were used to analyze the total expression levels of the WT γ subunit and the transgenic γ/ε-fc subunit. The first probe recognized a region coded by exons 2 and 3 of the γ subunit cDNA sequence, and would recognize both WT γ and transgenic γ/e-fc. The data obtained from this probe represented the total expression levels of the γ plus γ/ε-fc subunits. In homozygous γ/ε-fc embryos, the data obtained from this probe represented the total expression level of the γ/ε-fc subunit alone.

A second probe recognized a region coded by exons 6 and 7 of the γ subunit cDNA sequence, and would recognize the WT γ subunit but not the γ/e-fc subunit; this probe was used to determine the reduction of the expression levels of WT γ subunit in heterozygous embryos, or its absence in homozygous embryos.

Further probes were used to analyze the expression levels of various mRNAs codifying for the α and ε subunits, as well as MuSK.

Fig. 23A and B show results relatively to the WT expression levels. No significant change in the levels of the α or ε subunits can be detected, and the expression of MuSK is not significantly affected either, although at E16 there appears to be a tendency for MuSK expression levels to increase in the heterozygous and homozygous embryos, and for the ε subunit to increase in the E16 homozygous embryo. The total expression levels of the γ and γ/ε-fc subunits decreases slightly in the heterozygous embryo, as expected; since in the homozygous embryo, this data actually describes the total mRNAs of the two γ/ε-fc alleles, it implies that each γ/ε-fc allele maintains an expression level equal to roughly 40% that of the γ subunit allele in the WT embryo.

The data also confirm that expression of γ subunit mRNA is completely abolished in the γ/ε-fc homozygous embryos.
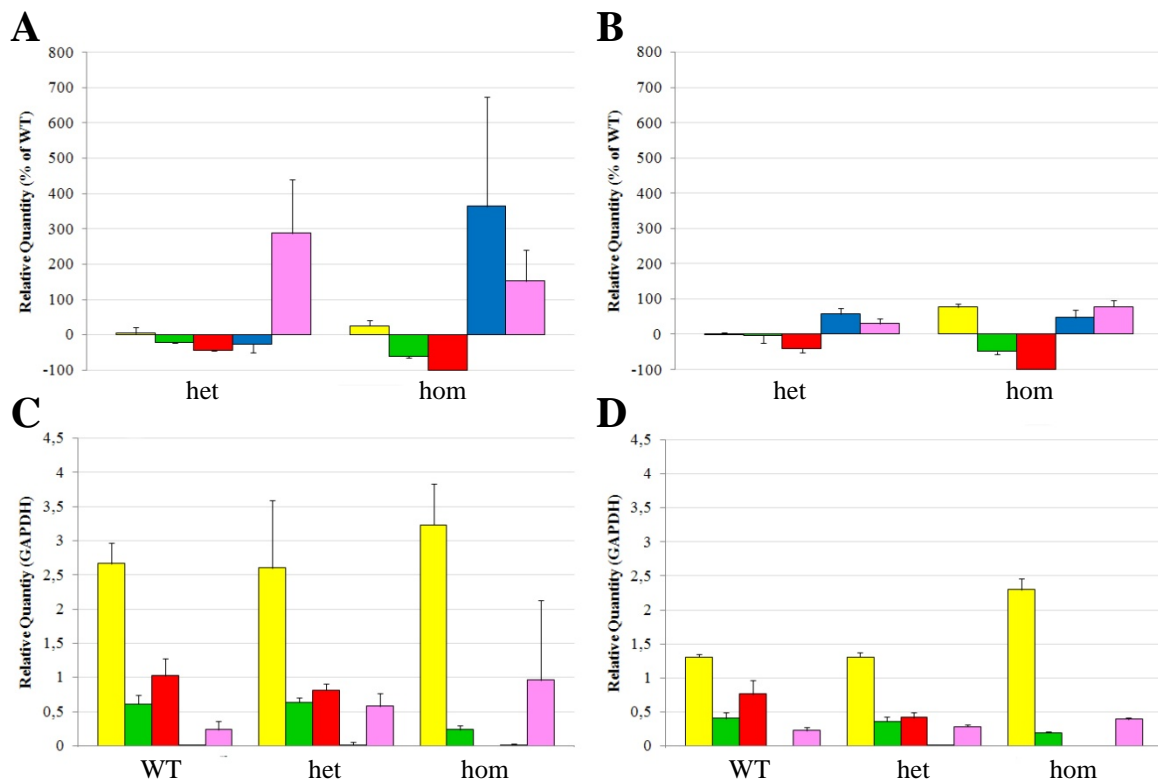
Fig. 23: Gene Profiling in E16 and E18 Embryos.

Yellow: α subunit; green: exons 2-3 of γ subunit (total expression levels of γ plus γ/ε-fc subunits); red: exons 6-7 of γ subunit (expression levels of WT γ subunit); blue: ε subunit; purple: MuSK. n = 3 embryos per point. (A) Quantification of expression levels in E16 embryos, relative to WT. (B) Quantification of expression levels in E18 embryos, relative to WT. (C) Quantification of expression levels in E16 embryos, relative to dehydrogenase GAPDH. (D) Quantification of expression levels in E18 embryos, relative to dehydrogenase GAPDH.

Fig. 23C and D present the same data relatively to the expression levels of the housekeeping dehydrogenase GAPDH, which is used as a standard in order to more directly compare WT expression levels with those of the heterozygous and homozygous γ/ε-fc embryos. The data confirm the relatively high expression levels of the γ/ε-fc alleles, which are similar to WT in the heterozygous animals, and ~50% of WT in γ/ε-fc homozygous embryos. The slight differences in MuSK, α subunit and ε subunit expression levels between WT, heterozygous and γ/ε-fc homozygous embryos,

57

on the other hand, appear not to be statistically significant. The results further clarify that the replacement of the functional γ subunit with the reduced-affinity γ/ε-fc subunit does not lead to overexpression of other AChR subunits in an attempt to rescue functionality, nor does it significantly affect the regulation of upstream members of the agrin signal cascade such as MuSK.

6.5 Phenotype Rescue

Attempts to rescue the phenotype of the γ/ε-fc mouse line are based upon the assumption that, because AChRs containing the γ/ε-fc subunit have reduced affinity for ACh, transiently increasing the quantity of released ACh in the embryonic and early postnatal NMJs may activate the AChRs and allow the pups to survive after birth. Because the γ/ε subunit switch occurs shortly afterwards, the γ/ε-fc subunit would be gradually replaced by the ε subunit, and subsequently reducing the quantity of released ACh to physiological levels should not lead to death.

6.5.1   3,4-Diaminopyridine

3,4-diaminopyridine (3,4-DAP, Fig. 24A) is an organic compound with the formula $C_5H_3N(NH_2)_2$, which is derived from pyridine through substitution of the 3 and 4 positions with an amino group. It facilitates synaptic transmission by prolonging the open time of voltage-gated K^+ channels, greatly increasing the release of ACh quanta in the NMJ (Katz and Miledi, 1979). It is mostly used as an experimental drug for the treatment of Lambert-Eaton CMS, a presynaptic FCCMS displaying impaired ACh release (Sanders, 1998), where it is moderately to largely effective in the majority of patients, with very little side effects. The beneficial effects of one dose last for 3 to 8 hours after administration and it is lost after 24 hours if the drug is withdrawn. In humans very little is known about possible side effects of 3,4-DAP during pregnancy, though one study suggests they are negligible (Pelufo-Pellicer et al., 2006). In mice, the LD_{50} of 3,4-DAP is 13 mg/Kg after intravenous injection and 35 mg/kg after subcutaneous administration; death in mice is due to uncontrolled convulsions.

58

6.5.2 Rescue Strategy

Because of several factors, such as the short effectiveness of 3,4-DAP, the need for constant administration for about two weeks starting from E12, the poor absorption rate of orally administered 3,4-DAP and the unfeasibility of administration through multiple daily intravenous injections or catheter implantation in mice, the current rescue strategy focuses on the subcutaneous implantation of osmotic pumps capable of constantly delivering a known amount of drug for the whole duration of treatment.

The results of preliminary tests performed on WT animals about the feasibility of this approach, in regard to the amount of 3,4-DAP crossing the placenta and entering the embryo's bloodstream, as well as the amount of drug absorbed by pups through the mother's milk during postnatal life are shown in Fig. 24B.
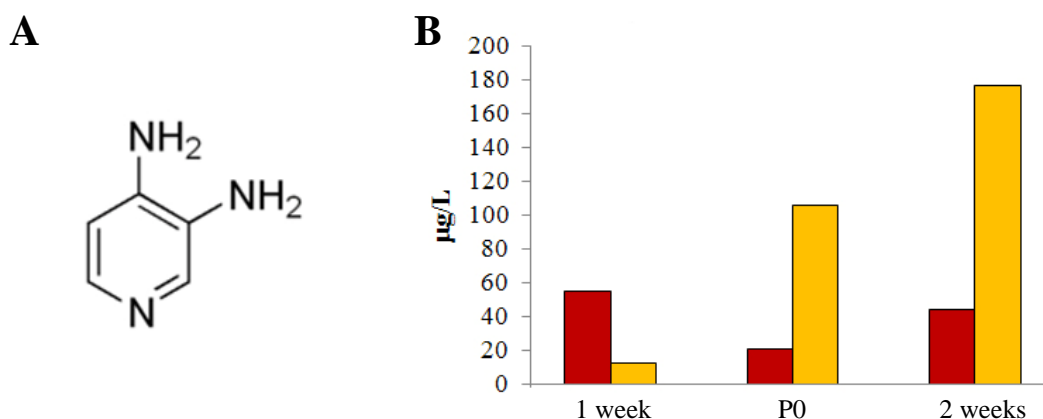
Fig. 24: Preliminary Results of Pharmacological Rescue.

(A) Structure of 3,4-DAP. (B) Preliminary results of implantation of osmotic pumps in WT pregnant females: levels of 3,4-DAP detected in the blood of mothers (red) and embryos or pups (orange) through HPLC at different time points (1 week after implantation, P0 and 2 weeks after implantation) after subcutaneous implantation of osmotic pumps filled with saturated 3,4-DAP solution.

These preliminary results suggest that 3,4-DAP crosses the placenta with difficulty, reaching steady concentrations reduced by about 80% in comparison to the drug concentration detected in the mother's bloodstream; however, newborn pups appear to assume 3,4-DAP through their mother's milk, and the drug's concentration in the bloodstream of newborn pups appears to be much higher than the levels detected in the

mother's bloodstream, suggesting that pups might be unable to dispose of the drug, perhaps due to the immaturity of their systems.

7. DISCUSSION

It is currently known that proper development of the NMJ occurs through the coordinated action of the muscle fiber membrane, the nerve terminal, the Schwann cell and the nearby glial cells. Based on the current state of knowledge, putative pathways have been proposed to describe the events leading to the establishment and maturation of a proper NMJ, but despite its status as the best studied synapse, many of the biochemical processes leading to its development are still largely unknown.

However, the NMJ's relative simplicity and the comparatively small number of molecules involved in these processes offer a great advantage in comparison to the study of other synapses. Using the NMJ as a model system, then, the elucidation of the molecular mechanisms leading to its development and maturation may offer us greater insight into the general development process of other synapses, such as brain synapses, as well.

The current paradigm of NMJ development and of the contribution on the part of individual molecules to the overall differentiation of the synapse (4.3.5) is based on insights gained from the many transgenic mouse lines created in the last decade. It is now apparent that neither nerve nor muscle are exclusively responsible for the development of the NMJ, but it is rather the interaction between nerve- and muscle-derived factors that leads to the formation of a proper synapse.

For instance, studies on mice with genetically aneural muscles revealed that the clustering and pre-patterning of AChRs along the central endplate band occurs even in the absence of innervation (Lin et al., 2001; Yang et al., 2000; Pun et al., 2002), suggesting that these events are not initiated by nerve-derived factors, although the maintenance of these clusters requires innervations. Additional studies in zebrafish also showed that aneural clusters could be incorporated into synapses through contact with the nerve terminal, and that this contact could in turn influence presynaptic development (Flanagan-Steet et al., 2005).

The analysis of animals in which neurotransmission in the NMJ was abolished by knocking out ChAT, which is the only enzyme synthetizing ACh, showed defects in postsynaptic differentiation and in presynaptic nerve growth, including abnormal nerve branching, presence of multiple endplates on the same muscle fiber, and a widened endplate band (Misgeld et al., 2002; Brandon et al., 2003). These studies also showed additional defects at late embryonic stages, such as larger endplate sizes

and irregular shapes, which suggested a modulatory role for synaptic activity in regard to postsynaptic differentiation.

Agrin knock-out mice displayed aberrations in postsynaptic differentiation (Gautam et al., 1996), but AChR cluster formation was not abolished, although AChR clusters dispersed more quickly in agrin mutant mice than in aneural muscles, suggesting that agrin might play a role in maintaining the synapse by counteracting the effect of a nerve-derived dispersal factor, later discovered to be ACh (Misgeld et al., 2005; Lin et al., 2005) through studies in agrin-ChAT knock-out animals in which it was discovered that synapse inactivity rescued the agrin phenotype.

AChR, then, plays a central role in the establishment, maintenance and maturation of the NMJ. Its presence attracts the presynaptic nerve terminal, contributes to the stabilization of nerve-muscle contacts, and its activity is important during later embryonic stages, ensuring the proper development of pre- and postsynaptic structures. Further proof of the importance of its role in the development of the NMJ is given by the observation that mutations in AChR subunits lead to defects in neuromuscular transmission which are manifested as CMSs (Müller et al., 2007; Engel et al., 2003a).

The effect of AChR activity on the maturation of the NMJ without disrupting molecular pathways can be studied in several ways. One approach would be to study the development of the NMJ during embryonic and early postnatal life in a transgenic mouse line in which receptor density is dramatically decreased; one mouse line generated in our lab, the $AChR^{\gamma\text{-GFP}}$ line, displays this feature due to highly reduced expression of the γ-GFP transgenic subunit (Yampolsky et al., 2008).

Another possibility would be to use a transgenic mouse line in which fetal-type AChR displays reduced affinity for ACh, leading to the near-absence of synaptic activity in the NMJ during embryonic development. The goal of this thesis was to characterize such a knock-in mouse line, generated in our lab and expressing structurally intact but functionally silent AChRs.

7.1   The γ/ε-fc Mouse Line

The γ/ε-fc mouse line enables the study of the effects of synaptic activity on the development of the NMJ without disrupting other molecular pathways depending on the presence of the AChR. In this line, the fetal-type γ subunit of the AChR is replaced by the transgenic γ/ε-fc subunit, which permits the assembly of structurally intact AChRs with lower conductivity.

The γ/ε-fc subunit is based on a point mutation first discovered in CMS patients (Ohno et al., 1986), in which the replacement of a single amino acid in the ε subunit (proline 121 into leucine, P121L) reduces overall channel open time.

7.1.1   Generation of the γ/ε-fc Knock-In Mouse Line

The amino acid sequence of AChR subunits is highly conserved, both among different subunits in a single species, and between the sequences for the same subunit in different species; proline 121 is conserved in all of them (Peter C., dissertation 2003). The P121L mutation is located on the extracellular domain of the ε subunit, near the binding site for ACh (Miyazawa et al., 2003) and it was shown through cell culture studies to affect channel opening rate, as well as affinity for ACh in the open channel state (Ohno et al., 1996). *Xenopus* oocytes studies in which the P121L mutation was introduced into the cDNA codifying for different subunits by changing one base (C441T), and the resulting AChRs were analyzed for their electrophysiological properties revealed that the mutation had maximum effect when localized in the ε subunit, without significantly affecting AChR expression and translocation to the membrane (Peter et al., 2005). This observation was the basis for the generation of a transgenic construct composed of a hybrid γ/ε subunit, offered by Dr. Michael Koenen and mutated with P121L, which was successfully used to generate the γ/ε-fc mouse line (Peter C., dissertation 2003).

Because of the strongly reduced activity of the AChR at physiological concentrations of ACh during embryonic life, the γ/ε-fc knock-in mouse line offers new insights in the study of NMJ development and the role played in it by AChR-mediated synaptic activity. Its advantages lie in the presence of structurally intact AChRs on the

postsynaptic membrane, which ensures that observable phenotypes are caused only by reduced activity as opposed to complete absence of the AChR and disruption of related molecular pathways, and in the possibility to study embryonic development of the NMJ lacking synaptic activity without need for toxin administration, thereby eliminating the risk of undesirable toxin-related side effects.

7.1.2 General Phenotype and Perinatal Death

Whereas heterozygous animals show no phenotypical differences in comparison to WT, homozygous γ/ε-fc animals die at birth. Presumably, strongly reduced synaptic activity inhibits diaphragm contraction, preventing the animals from breathing and leading to death by asphyxiation. Perinatal death was observed in transgenic mouse lines lacking ChAT (Brandon et al., 2003; Misgeld et al., 2002), where synthesis of ACh was prevented, thus abolishing synaptic transmission in the NMJ. Interestingly, mice in which the γ subunit has been deleted do not necessarily die at birth, but survive for two days before dying, presumably due to impaired milk intake (Takahashi et al., 2002). Taken together, these results might suggest that in the absence of γ subunit, AChRε partially compensates for the lack of AChRγ. This mechanism, however, might not work if the γ subunit is present and functionally impaired. It is worth noting that, in a complementary observation, transgenic mice in which the ε subunit is deleted display a continued presence of AChRγs in adult muscle, although this mechanism is not enough to ensure their survival for more than three months (Witzemann et al., 1996).

Macroscopical differences could be noticed in homozygous γ/ε-fc animals when compared to WT littermates; some, such as hunched posture and lack of muscle tension, are characteristics of flaccid paralysis which are shared with homozygous animals from ChAT knock-out lines, and as such probably result from neuromuscular defects. Like ChAT$^{-/-}$ embryos, γ/ε-fc embryos were never seen to move and did not respond to stimulation even at late embryonic stages. In contrast to this, animals with highly reduced expression of the γ subunit, from the γ-GFP line, survived though expression levels of γ-GFP subunit mRNA in homozygous embryos were reduced to 10% of WT levels (Yampolsky et al., 2008). This difference demonstrates that any

residual activity in the γ/ε-fc embryos has a negligible effect on NMJ maturation and embryo survival.

7.1.3 Differences in Endplate Anatomy

Although the early steps of neuromuscular synaptogenesis are independent from postsynaptic activity, later stages of NMJ stabilization and maturation are thought to be activity-dependent (Sanes and Lichtman, 1999).

The γ/ε-fc embryos display noticeable differences in endplate anatomy in comparison to the WT littermates. These differences are minor at earlier embryonic stages, but become more significant and noticeable towards later embryonic stages, presumably reflecting the increased importance of the role played by postsynaptic activity in the maturation of the NMJ. Receptor density and endplate area in the γ/ε-fc embryos are similar to those of WT littermates around E16, but are changed significantly by E18. However, correlating the observed increase in endplate area (about 20% in E18 embryos) with the 35-40% decrease in AChR density at the same embryonic age, the data suggest that lack of postsynaptic activity has no major effect on the overall number of receptors, which can be estimated to be reduced by less than 20%. In ChAT$^{-/-}$ animals of the same embryonic ages, on the other hand, the small changes in overall receptor density (<20%), if correlated with the large increase in endplate area (68-89%) suggest that overall receptor number is highly increased (Misgeld et al., 2002). The increase in endplate area in γ/ε-fc embryos is also consistent with the paradigm that ACh might act as dispersal factor through AChR-mediated postsynaptic activity, and that strongly reducing or completely blocking postsynaptic activity abolishes the dispersal and removal effect of ACh (Misgeld et al., 2005; Lin et al., 2005), leading to increased clustering of AChRs at the endplate.

Of particular interest is the possibility that endplate areas significantly differ from WT in the sternal regions of the E18 diaphragm, but not in the lumbar region, suggesting the possibility that different muscle fiber type composition or origin may have an impact on NMJ maturation and remodeling (Prakash et al., 1999; Prakash et al., 1995). Interestingly, the increase in endplate area in ChAT$^{-/-}$ animals (Misgeld et al., 2002) is about four times higher than the increase observed in γ/ε-fc animals; this

discrepancy may be explained by the fact that ChAT^{-/-} embryos completely lack ACh signaling, possibly disrupting additional signaling pathways.

The effect of lack of activity on endplate shape may be partly attributable to the increase in clustering of AChRs, leading to a more irregular shape in comparison to the smooth, ovoid shape of WT endplates. However, it has been suggested (Misgeld et al., 2002) that lack of postsynaptic activity may not only affect cluster growth, but accelerate endplate maturation as well. In light of this observation, it is possible to speculate that the more irregular shape of γ/ε-fc endplates might be at least in part due to muscle-autonomous differentiation.

7.1.4   Aberrant Endplate Distribution

The distribution of endplates along the muscle fibers is significantly affected by lack of postsynaptic activity. Endplates in the diaphragms of WT embryos are arranged along the so-called central endplate band, which corresponds to the innervation area of the phrenic nerve branches (Ackerman and Greer, 2007). This ordered distribution is severely disrupted in γ/ε-fc animals, where endplates are scattered along a much broader endplate band covering up to 35% of diaphragm width. Because the lumbar regions of the diaphragm are wider than the sternal regions, this increase in endplate band width appears as an almost-complete disruption of the endplate band organization. This aberrant distribution of endplates across the diaphragm due to lack of activity is already well-established at E16, and does not significantly change at late pregnancy stages, suggesting that this phenotype might either be independent from further maturation of the NMJ, or that a certain threshold of activity is needed before the phenotype can be rescued.

Although AChRs cluster in a central endplate band even in the absence of motor innervation (Yang et al., 2001), suggesting that the pre-patterning of the endplate band may be nerve-independent, an increase in its width in comparison to WT littermates seems to be a common phenotype in muscles where postsynaptic activity is absent (Lømo et al., 2003; Misgeld et al., 2002). This may partially depend on the presence of multiple endplates along individual muscle fibers, since activity is known to play a role in synapse establishment and in preventing the formation of additional extra-synaptic AChRs clusters on the same muscle fiber (Sanes and Lichtman, 2001).

In fact, a large percentage of muscle fibers in the γ/ε-fc embryo indeed displays the presence of multiple endplates, most or all of which appear to be contacted by neurites and display similar appearances. Individual muscle fibers have been detected in which up to five endplates could be distinguished, further supporting the implication that lack of activity might promote multiple endplate survival. In WT animals, *in vivo* studies suggest that synaptic activity leads to postsynaptic changes such as increases in transcription levels of AChR subunits in subsynaptic nuclei, downregulation of AChR subunit transcription in non-synaptic nuclei, and synaptic AChR metabolic stability; lack of activity at the NMJs of a single muscle fiber would therefore prevent these activity-dependent processes, allowing the formation of additional extrasynaptic AChR clusters.

7.1.5   Changes in the Innervation Pattern

In the diaphragms of WT embryos, the phrenic nerve enters the left hemidiaphragm, and splits into two main branches which then continue the innervation of the diaphragm in a highly ordered fashion, along the central endplate band (Ackelman and Greer, 2007; Greer et al., 1999). Neurites branch from the main phrenic nerve and contact nearby endplates, halting their progress and developing presynaptic specializations. This innervation pattern, however, is completely disrupted in γ/ε-fc animals. In the diaphragms of both E16 and E18 γ/ε-fc embryos, nerve branching is vastly increased, with γ/ε-fc diaphragms showing more than twice as many neurite branches in comparison to WT littermates, and no discernible organization or directionality can be noted. Branching appears to further increase between E16 and E18, while the average neurite length does not significantly change. In fact, an analysis of the percentage of total neurites in relation to their length shows that neurites are distributed much more evenly along the spectrum of measured lengths, and that no appreciable change occurs between E16 and E18, suggesting that no rescue occurs at late embryonic stages. Furthermore, our synaptophysin studies have shown that despite this highly aberrant pattern, individual neurites do innervate single NMJs, but rather than stopping at the innervation site, they extend further processes past the presynaptic specialization.

It has already been proposed that impaired activity at the level of the NMJ leads to increased motoneuron survival (Oppenheim et al., 2000; Oppenheim, 1991; Banks et al, 2001; Terrado et al, 2001), and *in vivo* studies on transgenic lines with reduced receptor density (Yampolsky et al., 2008) or lack of activity (Misgeld et al., 2002) have further confirmed this effect to varying degrees. The same appears to be true in the case of the γ/ε-fc animals, where motoneuron death seems to be completely abolished and the number of motoneurons remains stable during late embryogenesis, whereas it decreases dramatically in WT littermates. Furthermore, neurites in WT embryos grow past the central endplate band but, at late embryonic stages, they retract until no innervation occurs outside the central region of the diaphragm. In contrast to this, in the γ/ε-fc embryos, lack of AChR activity at the NMJ significantly affects not only neurite length, but also neurite branching. Neurites innervating NMJs and extending processes leading to further growth suggest that postsynaptic activity is not needed in order to recognize a cluster of AChRs and to stabilize it into a NMJ. However, an activity-dependent muscle-derived stop signal seems to be needed for the neurite to halt its growth. Lacking postsynaptic activity, neurites innervate the endplate properly, but extend further processes past the contact site. Interestingly, activity seems to also be needed to ensure the directionality of neurite growth, as the neurites in γ/ε-fc embryos grow randomly across the diaphragm, forming a complex and disorganized meshwork, in comparison to WT neurites which tend to grow parallel to muscle fibers.

7.1.6   Defects in Muscle Fiber Organization

The overall organization of individual muscle fibers in the diaphragms of γ/ε-fc embryos is largely abnormal in comparison to WT littermates. Many fibers, especially in the lumbar region of the diaphragm, appear to lose their directionality and cross over other fibers, or follow the inner surface of the ribcage, rather than growing perpendicularly to the central endplate band. Interestingly, however, this phenotype is restricted to a subset of the analyzed slow muscle fibers, whereas many other slow muscle fibers retain a normal phenotype and display no growth aberrations. Fast muscle fibers were not stained, and it is not possible at the moment to specify whether the phenotype is specific for slow muscle fibers, or if it affects all

muscle fibers to some extent. A similar phenotype has not been reported in denervated animals or ChAT^{-/-} mice in which ACh signaling was completely abolished, but it might well correlate with what is known about myogenesis in vertebrates.

Muscle formation in vertebrates occurs in two waves of myogenesis. Primary myogenesis occurs prior to the establishment of an innervation pattern in the muscle, and therefore it is not affected by synaptic activity; additionally, primary myotubes develop into both slow and fast muscle fibers (Zhang and McLennan, 1998). However, from about embryonic day E14 in the mouse, quiescent myoblasts begin proliferating and fusing into a wave of secondary myogenesis which correlates with the onset of innervation (Buckingham, 2001) and which leads to the formation of additional slow muscle fibers. Furthermore, zebrafish studies have demonstrated that while the inhibition of nerve activity during embryo development does not affect slow muscle fiber number or migration, it has a profound effect on myofiber organization, abolishing their directional growth and increasing their length (Brennan et al., 2005).

Taken together with our results, this suggests the possibility that the organization of secondary, slow muscle fibers in the mouse diaphragm might be affected by an activity-dependent mechanism. Disruption of AChR-mediated activity would produce aberrations in the organization of secondary muscle fibers, but no changes in the organization of primary muscle fibers due to their activity-independent development. Interestingly, the diameter of the E16 slow muscle fibers in γ/ε-fc homozygous embryos was not significantly affected by lack of AChR-mediated activity in comparison to WT embryos, suggesting that minimal or no myofiber atrophy occurs despite lack of activity. Diaphragm thickness was somewhat reduced, presumably due either to atrophy, or to a slight decrease in overall number of muscle fibers. These data seemingly contradict the data reported for the ChAT^{-/-} mice, which displayed high levels of myofiber atrophy, as well as extensive myofiber necrosis and a dramatic decrease in diaphragm thickness (Misgeld et al., 2002), already as early as E14. It was already suggested by *in vitro* studies that ACh might promote myogenesis (Entwistle et al., 1988; Krause et al., 1995), and that myotube survival might require neurotransmission (Sandri and Carraro, 1999). However, in analyzing the discrepancy between our results and the data on the ChAT-/- mouse line, it is worth noting that *in vivo* studies already presented different phenotypes of muscle fiber development and maturation between aneural and paralyzed muscles (Creazzo and Sohal, 1983; Sohal

and Holt, 1980). These studies suggested that in the absence of neurotransmission due to lack of presynaptic nerve terminals, myogenesis is severely impaired, and that in the last stages of embryonic development aneural muscles undergo massive cell death and disorganization. At the same time, paralyzed muscles displayed a milder phenotype in which the late stages of myogenesis were delayed and the number of muscle fibers was slightly reduced, but no cell death occurred and the existing muscle fibers had a normal appearance. These results are similar to those reported for the ChAT$^{-/-}$ mice in which neurotransmission is abolished (Misgeld et al., 2002) and in our results, respectively, suggesting that ACh might play a role in myotube survival and maturation, and that this role might be independent from AChR-mediated activity.

7.1.7   Differences in Gene Expression

Several additional questions during characterization of the γ/ε-fc mouse line required an analysis of mRNA transcript levels to be answered. One important point relates to the expression levels of the γ/ε-fc subunit, when compared to the expression of WT γ subunit. Another important question concerning the effects of an activity-impaired AChR during embryonic development is related to the possibility that absence of activity in muscle fibers expressing the γ/ε-fc subunit, or a very low expression level for the γ/ε-fc subunit, might lead to early expression of the ε subunit as a compensatory mechanism. Furthermore, it was important to collect additional data about the expression levels of other AChR subunits which could be affected by the presence of the mutated subunit, such as the α subunit, and the transcript levels for MuSK, which is known to be essential in initial synapse formation (DeChiara et al., 1996) and maintenance, even in adult muscle (Hesser et al., 2006), and which could therefore be affected by the abnormal development of the γ/ε-fc NMJ.

RT-PCR results at both E16 and E18 indicate that the expression levels of the the γ/ε-fc subunit are about 30-40% of WT γ subunit expression levels, suggesting that this is enough to synthesize and assemble a comparable amount of receptors as in the WT animal. The results also suggest that no overcompensation on the part of the ε subunit occurs when the functionality of the AChRγ is compromised and the activity of the

muscle fiber is impaired; this is consistent with similar observations related to lack of ε subunit overcompensation when γ subunit transcription and translation are extremely low (Yampolsky et al., 2008), and to complementary observations about the lack of stable overcompensation on the part of the γ subunit in mice whose ε subunit has been deleted (Witzemann et al., 1996), highlighting the two different roles played by AChRγ and AChRε during the animal's life.

Additionally, the expression levels of the α subunit are not significantly different from WT levels in γ/ε-fc embryos, suggesting that transcriptional regulation of the subunit does not depend on overall AChR activity nor on the transcriptional levels of other subunits, such as the γ/ε-fc subunit. Interestingly, expression levels for MuSK also appear to be unchanged between WT and γ/ε-fc embryos, confirming that transcription and activity of MuSK along the agrin pathway is not affected by the inactivity of the muscle fiber.

7.1.8 Conclusions

The role of the AChR during the embryonic development of the NMJ is a crucial point which needs to be elucidated in order to further our understanding of NMJ maturation and, by extension, of synapse formation. Thus far, however, knock-out mouse lines aimed at analyzing the effects of postsynaptic activity during embryonic development, such as the ChAT^{-/-} mouse line (Misgeld et al., 2002) or the AChRγ^{-/-} mouse line (Takahashi et al., 2002), could not properly distinguish between phenotypes caused by absence of postsynaptic transmission, and phenotypes caused by the disruption of additional molecular pathways due to the absence of crucial molecules such as ACh or the AChR itself.

In this regard, the γ/ε-fc mouse line is an extremely refined tool to study the specific contribution of postsynaptic activity to the development of the NMJ, without disturbing additional pathways which do not depend upon receptor activity, due to the presence of a structurally intact AChR. Through the characterization of this mouse line and a comparison of its phenotype with the described phenotypes for other mouse lines with abolished synaptic transmission, it is possible to estimate the extent at which synaptic transmission is important for the proper development of the NMJ.

Such a comparison unavoidably leads to an interesting question. The phenotype described in animals with abolished synaptic transmission (ChAT$^{-/-}$) is similar, but not identical, to the phenotype we describe here for the γ/ε-fc mouse line. Noteworthy differences present in the ChAT$^{-/-}$ animal include, but are not limited to an increase in endplate area at late embryonic stages that is almost four times the increase displayed in the γ/ε-fc embryos at the same age; the presence of a much thinner diaphragm leading to herniation of the liver; and extensive necrosis of muscle tissue. Previously, these phenotypes were thought to be also linked to synaptic transmission (Misgeld et al., 2002; Brandon et al., 2003), but their absence in the γ/ε-fc mouse line suggests that the picture might be more complex than it was once assumed.

The complete AChR contains two binding sites for ACh (4.2.1): one is located between one α subunit and the δ subunit (αδ binding site) and the other is located between the second α subunit and the γ subunit (during embryonic development) or the ε subunit (during adult life) (αγ binding site). The transgenic γ/ε-fc subunit impairs the binding of ACh to the αγ binding site, and this has been shown to completely impair whole-cell currents of recombinant receptors expressed in heterologous systems (Peter et al., 2005; Ohno et al., 1996). ACh binding to the αδ binding site might, however, be unaffected or only affected to a lesser extent by the mutation. It is also known that the two binding sites have different properties, so that the same mutation in the δ subunit does not reduce the affinity of the αδ binding site for ACh as strongly, but still allows generation of electrical activity in the cell (Peter et al., 2005). Furthermore, gating studies have suggested that the two binding sites play different roles during the channel opening event, and that when both sites are bound to ACh, subunits participating in the αγ binding site move first, and are followed then by subunits participating in the αδ binding site (Mitra et al., 2005). Clinical studies have also strengthened the assertion of a difference in the activity of the two binding sites and the subunits they are composed of. Data from CMS patients suggest that mutations inducing significantly shorter channel-opening events when inserted in the AChRδ may have an opposite effect when inserted in the AChRε (Shen et al., 2002).

If the two binding sites are not redundant, but have different functions to play, how could we correlate this assumption to the phenotypical differences we notice between animals in which synaptic transmission is completely abolished at both sites due to

lack of ACh (ChAT-/-) and animals in which synaptic transmission is abolished but both ACh and the WT αδ binding site are still present? Does the αδ binding site act as a modulator for channel-opening events which are triggered by the αγ binding site, and if that were true, would that be its only function?

The E381K mutation, which is located in the long cytoplasmic loop of the δ subunit, was discovered in a German patient and characterized as the cause of a novel CMS (Müller et al., 2006). *In vitro* studies have demonstrated that this mutation in the δ subunit impairs the association of AChRs with rapsyn, but that if the same mutation is inserted in the ε subunit, it has no appreciable effect on rapsyn and AChR co-clustering. It was then suggested that the δ subunit might play a special role in AChR-rapsyn interactions. Taken together with the data about the different contributions of the αδ and αγ binding sites to AChR activity, such a hypothesis could suggest that some molecular events previously thought to be activity-dependent – such as rapsyn association and ACh-mediated dispersal of AChRs – could in fact depend on activity-independent signaling on the part of AChR, perhaps through conformational changes of the receptor's cytoplasmic region, and that this signaling would be mediated by the αδ binding site, with only minor contributions from the αγ binding site.

Circumstantial evidence then suggests that the αδ binding site might play an important role apart from modulating synaptic transmission by correlating the description of this δ subunit-related CMS and its effects on the formation of synaptic clusters *in vitro*, to the differences between γ/ε-fc and ChAT^{-/-} animals.

This hypothesis could explain, for example, why the clustering of AChRs at late embryonic ages is much more pronounced in the ChAT^{-/-} animals than in γ/ε-fc animals: conformational changes triggered by binding of ACh to the αδ binding site would not trigger channel opening, but might reduce the affinity of AChR for rapsyn, preventing rapsyn and AChR co-clustering and leading to the dispersal of these receptors. Because this pathway would not necessarily require activity or binding of ACh to the αγ binding site, the γ/ε-fc mouse line would not display a large increase in receptor clustering. In the absence of ACh, however, not only would activity be abolished, but lack of ACh binding at the αδ binding site would prevent rapsyn from disassociating, and lead to vastly increased clustering of AChRs. Several phenotypes could then be assigned to either the αδ or αγ binding site (Table 3) by comparing the γ/ε-fc to the ChAT^{-/-} mouse lines.

The difference in the functionality of the two binding sites could also explain the decreased thickness of ChAT$^{-/-}$ diaphragms in comparison to γ/ε-fc diaphragms, and the presence of extensive muscle fiber necrosis which we have not observed in the γ/ε-fc mouse line.

Table 3. Phenotypes and Putative Association to the Impairment of Different AChR Binding Sites.

αγ binding site	αδ binding site
Triggers channel opening	*Modulates channel opening*
No postsynaptic current	Reduced postsynaptic current
Activity-dependent phenotypes	Conformation-dependent phenotypes
Abnormal nerve growth	Increased AChR clustering (rapsyn binding?)
Disruption of muscle fiber organization	Decreased number of muscle fibers?
Presence of multiple endplates	Muscle fiber necrosis
Flaccid paralysis, perinatal death	Impaired muscle fiber maturation
Inactivity-induced muscular atrophy	
Inactivity-dependent motoneuron survival	
Increased width of central endplate band	

Until we acquire in-depth knowledge of the mechanisms of rapsyn binding to the AChR, which are still unknown, or a mouse model is created in which the αδ, but not the αγ binding site is functionally impaired, we can only speculate on whether the two binding sites of AChR could play such different roles during embryonic development. If this were the case, though, we could speculate that AChR sits at the center of two distinct pathways: an already described, molecular pathway in which AChR interacts with rapsyn through the δ subunit (Müller et al., 2006) and, through the action of dystroglycan and utrophin, with the muscle fiber cytoskeleton (Kummer et al., 2006); and an activity-dependent pathway in which AChR activity is responsible for retrograde signaling to the nerve terminal and plays a crucial role in the establishment of nerve architecture.

7.1.9 Further Projects Involving the γ/ε-fc Mouse Line

The γ/ε-fc mouse line is an extremely powerful tool to study activity-dependent pathways in the development of the NMJ, and it has already offered interesting insights into the function of postsynaptic activity during embryonic life. An interesting question which we are currently addressing involves the possibility of rescuing γ/ε-fc newborns from perinatal death, and analyzing the presence or absence of long-lasting morphological differences in their diaphragms after the γ/ε switch has occurred. This will allow us to establish to which extent the morphological defects displayed during embryonic development are retained in postnatal life, and in particular whether muscle fiber organization defects, endplate anatomy, and the aberrant innervation pattern of γ/ε-fc animals can undergo plasticity and return to a WT-like situation, or if activity-related, embryonically acquired defects remain present throughout the animal's life.

Of further interest will also be the study of the activity threshold endplates need to reach in order for the animal to be viable, and exploiting a feature of the AChRγ-GFP line, we have begun studies of animals exhibiting strongly reduced presence of functional AChRs during embryonic development, coupled with the presence of a large majority of γ/ε-fc receptors, in order to study differences in the development of the NMJ between homozygous γ/ε-fc animals in which activity is abolished, and hemizygous animals in which activity is extremely reduced.

8. METHODS

8.1 Animals

Experiments were performed on γ/ε-fc animals derived from C57Bl/6 background. The animals were housed in the Interfakultäre Biomedizinische Forschungseinrichtung (IBF) in Heidelberg, fed *ad libitum* with commercial food pellets and chlorinated water. Temperature in the animal facility was maintained between 20-25°C with 55-65% humidity and a day-night cycle with 12-hour phases.

8.1.1 Dissection and Preparation of Muscles

In accordance with FELASA guidelines, female pregnant mice aged 2 to 12 months were anesthetized with CO_2 and sacrificed through cervical dislocation. Embryos aged E16 and E18 were extracted from the uterus, sacrificed through decapitation, and dissected. Tails were removed for genotyping purposes. Extracted diaphragm muscles were held in Sylgard®-coated Petri dishes with insect needles and fixed with 1% formaldehyde for 1h, then transferred into 24-well plates containing neural rat Ringer solution.

Muscles from embryo upper hind legs were explanted and flash-frozen in liquid nitrogen to preserve RNA integrity, then stored at -80°C until RNA extraction.

8.1.2 Preparation and Implantation of Osmotic Pumps

ALZET mini-osmotic pumps (DURECT, CA, USA) model 2002 were filled with 200 μl of a solution of 3,4-DAP (Sigma, St. Louis, MO, USA) in 0,9% saline, according to the manifacturer's guidelines.

Wild type female pregnant mice aged 2 to 6 months were anesthetized through intraperitoneal injection of anaesthetic mix (see below) and osmotic pumps were implanted subcutaneously according to manifacturer's guidelines. Anesthesia was countered through subcutaneous injection of antidote mix (see below).

Anaesthetic Mix (1,1 ml/Kg, i.p.)
22% Domitor®   PfizerAH, Exton, PA, USA
22% Dormicum®   Roche, Basel, Switzerland
56% Fentanyl®   Ratiopharm, Ulm, Germany

Antidote Mix (2,5 ml/Kg., s.c.)
14% Antisedan®   PfizerAH, Exton, PA, USA
18% Naloxone®   Ratiopharm, Ulm, Germany
68% Anexate®   Roche, Basel, Switzerland

Blood was collected from mothers and embryos or newborn animals after one or two weeks of implantation. In accordance to FELASA guidelines, implanted and control animals were anesthetized with CO_2 and sacrificed through cervical dislocation prior to blood collection. A minimum of 500 µl of blood was collected from each adult animal. Embryos and pups were killed through decapitation and the blood from each animal in the same litter was pooled together.

Whole blood was centrifugated at 5°C, at a speed of 2.000 x g, for 30 min. Plasma was collected and sent for HPLC analysis performed by Labor Limbach (Heidelberg, Germany). Statistical analyses and graphical representations of data acquired from ImageJ were performed using the IgorPro software (WaveMetrics, Lake Oswego, OR, USA).

8.2   *Confocal Microscopy*

Confocal microscopy permits an increase in microphotograph contrast, the acquisition of high-resolution optical images, and the possibility to generate a projection or a three-dimensional reconstruction of a stack of images.

Samples were analyzed using a Leica TCS NT (Leica Microsystems) microscope, using objectives with 10x, 20x, 40x and 63x magnification. An Argon-Krypton laser allowed fluorescence detection with wavelengths of 488 nm for green fluorescence, and 566 nm for red fluorescence. Fluorescence was enhanced through the use of a photomultiplier. Images were processed using Leica TCS NT software (Leica Microsystems) and ImageJ software (National Institute of Health, USA).

For muscle fiber staining, samples were analyzed using a Leica SP2 microscope (Leica Microsystems) using objectives with 10x, 20x and 63x magnification. A Helium-Neon laser allowed fluorescence detection with wavelengths of 488 nm for

green fluorescence, and 566 nm for red fluorescence, while an UV laser allowed fluorescence detection with wavelengths of 354 nm for blue fluorescence. Fluorescence was enhanced through the use of a photomultiplier. Images were processed using Leica TCS SP2 software and Leica LAS AF Lite (Leica Microsystems), and ImageJ software (National Institute of Health, USA).

8.2.1 Fluorescent Quantification

Pictures of endplates from four different diaphragm regions and from three different animals per time point were taken at 63x magnification using confocal microscopy, with the same laser intensity but different green filter settings (30%, 50% and 80%). The pictures were opened using ImageJ software (NIH, USA) using standard plug-ins and a self-made automatized macro. Signal density in the green fluorescence was analyzed, and endplate density was assigned according to the comparison of endplate areas at different filter settings.

Statistical analyses and graphical representations of data acquired from ImageJ were performed using the IgorPro software (WaveMetrics, Lake Oswego, OR, USA). The average standard deviation and standard error were calculated for each data set, and all trend lines were drawn taking into account the appropriate error bars.

8.2.2 Area Measurement

Pictures of endplates from four different diaphragm regions and from three different animals per time point were taken at 63x magnification using confocal microscopy, and opened using ImageJ software (NIH, USA) with standard plug-ins. Distinguishable endplates were selected and area measurements were collected both in pixels and in μm^2.

Statistical analyses and graphical representations of data acquired from ImageJ were performed using the IgorPro software (WaveMetrics, Lake Oswego, OR, USA). The average standard deviation and standard error were calculated for each data set, and all graphs were drawn taking into account the appropriate error bars.

8.2.3 Circularity Measurement

Pictures of endplates from four different diaphragm regions and from three different animals per time point were taken at 63x magnification using confocal microscopy, and opened using ImageJ software (NIH, USA) with standard plug-ins. Distinguishable endplates were selected and circularity measurements were collected using standard ImageJ tools.

Statistical analyses and graphical representations of data acquired from ImageJ were performed using the IgorPro software (WaveMetrics, Lake Oswego, OR, USA). The average standard deviation and standard error were calculated for each data set, and all graphs were drawn taking into account the appropriate error bars.

8.2.4 Count of Endplates per Muscle Fiber

Pictures of muscle fibers from three different diaphragm regions were taken at 63x magnification using confocal microscopy, and opened using ImageJ software (NIH, USA) with Volume Viewer plug-in (K. U. Barthel, Internationalen Medieninformatik, Berlin, Germany).

Pseudo-3D reconstructions of each section were created through the Volume Viewer plug-in and each individual muscle fiber was traced from one end to the other. Stained endplates laying over the muscle fiber were analyzed optically.

Statistical analyses and graphical representations of data acquired from ImageJ were performed using the IgorPro software (WaveMetrics, Lake Oswego, OR, USA). The average standard deviation and standard error were calculated for each data set, and all graphs were drawn taking into account the appropriate error bars.

8.2.5 Analysis of Diaphragm Thickness and Muscle Fiber Diameter

Pictures of muscle fibers from three different diaphragm regions were taken at 63x magnification using confocal microscopy, and opened using ImageJ software (NIH, USA) with Volume Viewer plug-in (K. U. Barthel, Internationalen Medieninformatik, Berlin, Germany).

Pseudo-3D reconstructions of each section were created through the Volume Viewer plug-in, and the thickness of each diaphragm section was analyzed by tracing. The minor and major diameter of each individual muscle fiber was traced at three different locations along the muscle fiber. The area of the fiber cross-section in the three different locations was calculated and the diameter of a circle with equivalent area was extracted in order to normalize the results.

Statistical analyses and graphical representations of data acquired from ImageJ were performed using the IgorPro software (WaveMetrics, Lake Oswego, OR, USA). The average standard deviation and standard error were calculated for each data set, and all graphs were drawn taking into account the appropriate error bars.

8.3   Molecular Biology Methods

8.3.1   Standard Molecular Biology Methods

Standard molecular biology methods, such as DNA cutting via restriction endonucleases, dephosphorylation of DNA endings, DNA ligation and DNA gel electrophoresis, used standard protocols from the Maniatis laboratory book (Maniatis et al., 1987). These methods are not described below.

8.3.2   Genotyping of Specimens

Genotyping of the specimens via PCR analysis was used to identify wild-type and homozygous embryos.

Extraction of genomic DNA from embryo tails was performed using Qiagen QIAamp DNA Mini Kit (Qiagen, Hilden, Germany). The final concentration of genomic DNA was not determined, and a fixed volume was used for PCR.

The analysis of transgenic embryos required two separate PCR reactions, one to detect the presence of the wild-type AChRγ gene and one to detect the presence of the γ/ε-fc transgene. The reverse primer for the identification of the γ/ε-fc transgene was

generated from a targeting vector sequence which is not present in the genomic sequence. Primers were obtained from MWG Biotech (Ebersberg, Germany).

PCR samples were analyzed by loading 20 µl on a 1% agarose gel and performing DNA gel electrophoresis.

PCR Mix

0,5 µl	genomic DNA
5 µl	10x HotStar Taq Buffer (Qiagen, Hilden, Germany)
1 µl	5' Primer (125 ng/µl)
1 µl	3' Primer (125 ng/µl)
8 µl	dNTP (1,25 mM each)
0,5 µl	HotStar Taq Polymerase (Qiagen, Hilden, Germany)
to 50 µl	ddH$_2$O

γ/ε-fc Genotyping Program

15 min	95°C	
45 s	94°C	
45 s	60°C	32x
1 min 30 s	72°C	
10 min	72°C	

8.3.3 Isolation of RNA from Muscle Tissue

RNA was isolated from embryo upper hind leg muscles according to the TRIzol protocol (Invitrogen, Carlsbad, CA, USA). Frozen muscles were homogenized in 2 ml TRIzol reagent using an Ultra-Turax T18 Polytron (IKA) power homogenizer. The isolation of RNA followed the standard protocol, with the addition of a centrifugation step at 12.000 x g for 10 minutes at 4°C in order to remove tissue remains. After drying, RNA was resuspended in 100 µl DEPC-H$_2$O, its concentration was assayed via optical density measurement, and the probes were then stored at -20°C.

8.3.4 Reverse Transcription

5 µg of RNA isolated from muscle tissue were purified of DNA remains through "DNA-free" kits (Ambion, Austin, TX, USA). The volume was brought to 50 µl, then 1/10 volume (5 µl) Na-Acetate and 2 ½ volumes (125 µl) of abs. ethanol were added. Samples were precipitated at -20°C for 10 minutes, then pelleted via centrifugation at 13.000 x g for 10 minutes at RT, on a desktop centrifuge. The pellet was then resuspended in 10 µl H_2O at 68°C.

The RNA solution was mixed with the Reverse Transcription mix, 1 µl of SuperScript II reverse transcriptase (200 U/µl; Invitrogen, Carlsbad, CA, USA) was added, and the sample was incubated at 37°C for 1 hour. Afterwards, the transcriptase was inactivated at 95°C for 5 minutes.

Reverse Transcription Mix

4 µl	5x RT Buffer (Invitrogen)	
2 µl	0,1 M DTT	
1 µl	RNA Guard (Invitrogen)	
1 µl	dNTPs	
8 µl	pd(N6) Primer	1 hour at 37°C
+1 µl	SuperScript II Reverse Transcriptase (200 U/µl; Invitrogen)	
+10 µl	RNA Solution (0,5 µg/µl)	

8.3.5 Real-Time PCR

TaqMan Assay-on-Demand Expression Products (Applied Biosystems, Darmstadt) and the standard primers within were used for Real-Time PCR. Three repetitions were performed for each PCR reaction. The housekeeping gene *glyceraldehyde-3-phosphate dehydrogenase* (GAPDH) was used as a cellular control.

Real-Time PCR Mix

8,75 µl	ddH$_2$O
12,5 µl	TaqMan Universal PCR Master Mix
1,25 µl	20x Assay-on-Demand Gene Expression Mix
2,5 µl	cDNA (125 µg/ml)

Real-Time PCR Program

95°C	10 min	
95°C	15 s	
60°C	40 s	45 cycles

An ABS 7500 RealTime System (Applied Biosystems, USA) was used for the Real-Time PCR reaction. Analysis was performed with help from 7500 System SDS Software (Applied Biosystems, USA) following the method for relative $\Delta\Delta C_t$ quantification (Livak and Schmittgen, 2001). The expression of GAPDH (Assay Mm99999915_g1) was used as an internal control.

Tissue samples from three different animals for each time point were collected. Each probe was analyzed in triplets and the analysis was repeated twice, to exclude pipetting errors. IgorPro Software (WaveMetrics, Lake Oswego, OR) was used for statistical analysis of the data. The average standard deviation was calculated for each data series, and error bars were applied to all trend lines. Since the expression of GAPDH during development is relatively stable (Mamo et al., 2007), the transcripts measured quantities as percentages of GAPDH expression. Relative quantification allows for experimental comparison of the expression levels of different genes, therefore not offering absolute gene expression data, but a trend of expression levels during development.

8.4 Histological Methods

8.4.1 Antibody – α-Bungarotoxin Staining

Antibody staining of the diaphragm using anti-neurofilament antibodies and bungarotoxin allows simultaneous detection of nerve fibers and neuromuscular synapses through confocal microscopy. In conjunction with anti-muscle fiber staining, it is possible to detect the organization of muscle fibers and aberrations in the synaptic organization of individual fibers.

Diaphragms which had previously been treated with formadehyde for fixation (see 8.1.1) were incubated overnight at 4°C with 0,1M Glycine/PBS. Afterwards, diaphragms were permeabilised with 1% Triton/PBS at RT for 3 h, and incubated overnight with primary antibody diluted in 2% BSA/PBS. Diaphragms were then washed with PBS and incubated overnight with secondary antibody in a 2% solution of BSA/PBS containing α-bgtx to enhance AChR fluorescence. Finally, diaphragms were washed with 2% BSA/PBS, mounted on glass slide with Citifluor (Agar Scientific, Stansted, England), and analyzed through confocal microscopy.

	Type, Target	Dilution
Primary Antibodies	mouse, slow skeletal myosin	1:5000
	rabbit, α-neurofilament	1:500
	rabbit, synaptophysin	1:50
Secondary Antibodies	AMCA-labeled α-mouse goat IgG	1.100
	rhodamine-labeled α-rabbit goat IgG	1:100
Toxins	FITC-labeled α-bgtx (1 mg/ml)	1:500

8.4.2 Acetylcholinesterase Staining and Endplate Distribution

AChE staining allows visualization and counting of the neuromuscular junctions in a light microscope. The staining was based on the Koelle and Friedenwald method (1949).

The diaphragm was incubated for 90 min in the staining solution, and washed with H_2O afterwards. After incubation with 5 mM potassium ferrocyanide for 30 min, synapses were stained brown. The diaphragm was washed with PBS before being mounted on a glass slide and analyzed at the microscope.

Acetate Buffer
150 mM CH_3COOH
350 mM $CH_3COO\text{-}Na$

Glycine – Copper Sulphate Solution
500 mM Glycine
100 mM $CuSO_4$

Staining Solution (fresh)
9 ml   acetate buffer
30 mg acetylthiocholine iodide
1 ml   glycine – copper sulphate solution

Pictures from sternal and lumbar sections of WT and homozygous diaphragms (2 animals per experiment) were taken using a Zeiss Axioplan2 microscope (Carl Zeiss Inc.) through conventional light microscopy, and analyzed using ImageJ software (NIH, USA) with standard plug-ins. Three lines were drawn from the inner to the outer edge of each region of the diaphragm and the distance of the first and last endplate on the line was measured from the inner edge of the diaphragm. Data were analyzed in IgorPro (WaveMetrics, Lake Oswego, OR, USA). Data were analyzed separately for each region, and an analysis of the overall hemidiaphragm was also performed. Individual percentages were generated based on the width of diaphragm for each analyzed line. The average standard deviation was calculated for each data set. Student's *t* tests were performed for statistical analysis. A probability value ≤0,05 was taken as criterion for statistical significance.

8.4.3   Paraffin Embedding of Tissue Samples

Mouse embryos were killed by decapitation. The animal was dissected to collect the torso, from the lower cervical to the upper thoracic segments of the spinal cord. The tissue was treated with a mild zinc fixative (0,05% calcium acetate, 0,5% zinc acetate, 0,5% zinc chloride, in 0,1 M Tris Buffer pH 7.4) for fixation at RT, over a period of 4 days, replacing the fixative daily. The tissue was embedded in paraffin and cut in a paraffin microtome (Zeiss) into sections 7 μm thick. The cut sections were stretched in a water bath at 42°C for 5 min, and then collected on a microscope slide and dried on a heated plate for 30 min at 45°C. The samples were stored at RT until staining.

8.4.4 Choline Acetyltransferase Staining of Paraffin Sections

ChAT staining allows visualization and quantification of motor neurons in the lateral motor column of the spinal cord.

Every fifth section taken in the region of the lateral motor column (LMC) of paraffin-embedded samples between the cervical vertebra C5 and the thoracic vertebra T1 was treated with choline acetyltransferase antibodies (α-ChAT, Chemicon). Paraffin was removed by treating sections with xylol, the sections were then rehydrated through an EtOH scale (100%, 96% and 70%, 2 minutes each) and then washed in PBS. The immunohistochemical staining with α-ChAT was performed according to the following protocol:

- Incubation in 1% H_2O_2 in ddH_2O for 20 min at RT
- Blocking with 5% BSA + 1% TritonX in PBS for 2 h
- Removal of the blocking solution, no washing
- Incubation with ChAT antibodies at 4°C o.n., diluted 1:500 in 1% BSA + 0,4% TritonX in PBS
- Washing 5x 5 minutes with PBS
- Incubation with biotinylated anti-goat secondary antibody (BA-9500, Vectorlabs) for 2 h at RT; dilution 1:200 in 1% BSA + 0,4% TritonX in PBS
- Washing in PBS for 5 min

The subsequent colorimetric quantification was performed with the help of the ABC-Elite kit (Vectorlabs) as per the manifacturer's specifications. The sections were counterstained with eosin, dehydrated in an ethanol scale, clarified with Neo-Clear® (Merck) and mounted with Neo-Mount® (Merck). Pictures were taken using a Zeiss Axioplan2 microscope (Carl Zeiss Inc.) through conventional light microscopy, and analyzed using ImageJ software (NIH, USA) with Cell Counter plug-in (K. De Vos, University of Sheffield, UK). The resulting data were analyzed in IgorPro (WaveMetrics, Lake Oswego, OR, USA).

8.4.5 Analysis of Motor Neuron Length

The innervation pattern of the diaphragm was analyzed using anti-neurofilament antibody staining. Hemidiaphragm composite images were opened with ImageJ (NIH, USA) using the NeuronJ plug-in (E. Meijering, Erasmus MC − University Medical Center Rotterdam, Netherlands). Each secondary neurite was traced starting with the primary branching away from the *nervus phrenicus* and up to its distal end. Data were analyzed in IgorPro (WaveMetrics, Lake Oswego, OR, USA). Neurites were grouped according to their absolute length, and according to their length relative to the appropriate primary neurite. Percentages were generated based on total neurite number. The average standard deviation was calculated for each data set. Student's t tests were performed for statistical analysis. A probability value $\leq 0,05$ was taken as criterion for statistical significance.

For cumulative probability distributions, Kolmogorov-Smirnov tests were performed for statistical analysis. A probability value $\leq 0,05$ was taken as criterion for statistical significance.

9. MATERIALS

9.1 Chemicals

Chemical substances used in this work were purchased from the following companies:

Aldrich, Steinheim, Germany	Pharmacia Biotech, Freiburg, Germany
Amersham, Braunschweig, Germany	PfizerAH, Exton, PA, USA
Biomol, Hamburg, Germany	Ratiopharm, Ulm, Germany
Bio-Rad, Munich, Germany	Riedel, Seelze, Germany
Biozym, Hameln, Germany	Roche, Basel, Switzerland
Fluka, Neu-Ulm, Germany	Roth GmbH, Darmstadt, Germany
GERBU, Gaiberg, Germany	Sakura, Zoeterwoude, Germany
Gibco BRL, Eggenstein, Germany	Serva, Heidelberg, Germany
IBI, New Haven, CT, USA	Sigma, St. Louis, MO, USA
MBI Fermentas, Wilna, Lithuania	Vector Laboratories, Burlingame, CA, USA
Merck, Darmstadt, Germany	

9.2 Enzymes

9.2.1 General Enzymes

DNAse I (5 U/µl)	Ambion (Austin, TX, USA)
Proteinase K (20 mg/ml)	Roche (Mannheim, DE)
RNAse A (10 mg/ml)	Roche (Mannheim, DE)
SuperScript II Reverse Transcriptase (200 U/µl)	Invitrogen (Carlsbad, CA, USA)

9.2.2 Polymerases

Hot Star Taq Polymerase	Qiagen (Hilden, DE)

9.3 Primers, Oligonucleotides and Probes

Primers and oligonucleotides used in this work were synthetized by MWG-Biotech (Ebersberg, Germany). "TaqMan Assays-on-Demand" for quantitative Real-Time PCR were purchased from Applied Biosystems (Darmstadt, Germany).

All sequences are oriented starting from the 5' end.

Genotyping Primers

	WT AChRγ
mg 187F 5' *(forward)*	5'-GAT GCG AAA CTA CGA CCC C-3'
mg 536R 3' *(reverse)*	5'-AGG AGG AGC GGA AGA TGG-3'

	γ/ε-fc
mg 187F 5' *(forward)*	5'-GAT GCG AAA CTA CGA CCC C-3'
mg 785R 3' *(reverse)*	5'-CAG AAA TGA GCA CGC AAG G-3'

9.4 Kits

ABC-Elite Kit	Vector Labs (Burlingame, CA, USA)
DNA-Free Kit	Ambion (Austin, TX, USA)
QIAAmp DNA Mini Kit	Qiagen (Hilden, DE)

9.5 DNA Ladders

Lambda DNA/EcoRI+HindIII Marker 3   MBI Fermentas (Vilnius, Lithuania)

9.6 Buffers, Solutions and Media

Citifluor	Agar Scientific (Stansted, England)
Neo-Clear	Merck (Darmstadt, Germany)
Neo-Mount	Merck (Darmstadt, Germany)
PBS	Gibco/Invitrogen (Carlsbad, CA, USA)
RT 5x Buffer	Invitrogen (Carlsbad, CA, USA)

9.7 Antibodies

α-Cholinacetyltransferase (goat)	Chemicon (Temecula, CA, USA)
α-Neurofilament (rabbit)	Chemicon (Temecula, CA, USA)
α-Slow skeletal myosin (mouse)	Sigma (St. Louis, MO, USA)
α-Synaptophysin (rabbit)	Zymed (San Francisco, CA, USA)
AMCA-conjugated goat α-mouse IgG	Molecular Probes (Eugene, CA, USA)
Biotin-conjugated horse α-goat IgG	Vector Labs (Burlingame, CA, USA)
Rhodamine-conjugated goat α-rabbit IgG	Molecular Probes (Eugene, CA, USA)

9.8 PCR and Real-Time PCR Reagents

HotStar Taq 10x Buffer	Qiagen (Hilden, DE)
dNTPs	Pharmacia (Erlangen, DE)
TaqMan Universal PCR Master Mix	Applied Biosystems (Darmstadt, DE)

9.9 Mouse Lines

C57 Bl/6J	RCC/BRL (Basel, Switzerland)

9.10   Miscellaneous Items

ALZET Mini-Osmotic Pumps 2002	Durect, CA, USA
Mounting glass slides: "Super Frost Plus"	Roth (Darmstadt, DE)
Razor Blade Holder	Dumont (Montignez, Switzerland)
Razor Blades	F.S.T. (Heidelberg, DE)
Tools for Tissue Preparation	Dumont (Montignez, Switzerland)
Tweezers	Dumont (Montignez, Switzerland)

9.11   Miscellaneous Equipment

Confocal Microscope – "TCS NT"	Leica (Heidelberg, DE)
Desktop Centrifuge – "Biofuge 13"	Heraeus (Waltham, MA, USA)
Fluorescence Microscope – "Axioplan 2"	Zeiss (Oberkochen, DE)
Light Microscope – "Axioplan 2"	Zeiss (Oberkochen, DE)
Microscope Camera – "3CCD Seescan"	Intas (Göttingen, DE)
Objectives – "Neofluar" (2,5x; 5x; 40x; 63x)	Zeiss (Oberkochen, DE)
Paraffin Microtome RM2145	Leica (Heidelberg, DE)
PCR Thermocycler – "T-Gradient"	Biometra (Göttingen, DE)
Polytron T18	Kinematic (Littau, Switzerland)
Spectral Photometer – "Heliosβ"	Unicam (Waltham, MA, USA)

10. REFERENCES

1. ACKERMAN K.G., GREER J.J. (2007) Development of the diaphragm and genetic mouse models of diaphragmatic defects. *Am J Med Genet C Semin Med Genet* **145C (2):** 109-116.

2. BANKS G.B., CHAU T.N., BARTLETT S.E., NOAKES P.G. (2001) Promotion of motoneuron survival and branching in rapsyn-deficient mice. *J Comp Neurol* **429 (1):** 156-165.

3. BRANDON E.P., LIN W., D'AMOUR K.A., PIZZO D.P., DOMINGUEZ B., SUGIURA Y., THODE S., KO C.P., THAL L.J., GAGE F.H., LEE K.F. (2003) Aberrant patterning of neuromuscular synapses in choline acetyltransferase-deficient mice. *J Neurosci* **23 (2):** 539-549.

4. BRENNAN C., MANGOLI M., DYER C.E., ASHWORTH R. (2005) Acetylcholine and calcium signalling regulates muscle fibre formation in the zebrafish embryo. *J Cell Sci* **118:** 5181-5190.

5. BROWNLOW S., WEBSTER R., CROXEN R., BRYDSON M., NEVILLE B., LIN J.P., VINCENT A., NEWSOM-DAVIS J., BEESON D. (2001) Acetylcholine receptor delta subunit mutations underlie a fast-channel myasthenic syndrome and arthrogryposis multiplex congenita. *J Clin Invest* **108 (1):** 125-130.

6. BUCKINGHAM M. (2001) Skeletal muscle formation in vertebrates. *Curr Opin Genet Dev* **11 (4):** 440-448.

7. BURGESS R.W., NGUYEN Q.T, SONY.J., LICHTMAN J.W., SANES J.R. (1999) Alternatively spliced isoforms of nerve- and muscle-derived agrin; their roles at the neuromuscular junction. *Neuron* **23 (1):** 33-44.

8. CAPECCHI M.R. (1989) The new mouse genetics: altering the genome by gene targeting. *Trends Genet* **5 (3):** 70-76.

9.   CARONI P. (1993) Activity-sensitive signaling by muscle-derived insulin-like growth factors in the developing and regenerating neuromuscular system. *Ann NY Acad Sci* **692:** 209-222.

10. COLLEDGE M., FROEHNER S.C. (1998) To muster a cluster: anchoring neurotransmitter receptors at synapses. *Proc Natl Acad Sci USA* **95 (7):** 3341-3343.

11. CREAZZO T.L., SOHAL G.S. (1983) Neural control of embryonic acetylcholine receptor and skeletal muscle. *Cell Tissue Res* **228 (1):** 1-12.

12. DECHIARA T.M., BOWEN D.C., VALENZUELA D.M., SIMMONS M.V., POUEYMIROU W.T., THOMAS S., KINETZ E., COMPTON D.L., ROJAS E., PARK J.S., SMITH C., DISTEFANO P.S., GLASS D.J., BURDEN S.J., YANCOPOULOS G.D. (1996) The receptor tyrosine kinase MuSK is required for neuromuscular junction formation in vivo. *Cell* **85 (4):** 501-512.

13. ENGEL A.G., FRANZINI-ARMSTRONG C. (1994) Myasthenic syndromes. In: Myology pp. 1798-1836.

14. ENGEL A.G., OHNO K., SINE S.M. (2003a) Congenital myasthenic syndromes: A diverse array of molecular targets. *J Neurocytol* **32 (5-8):** 1017-1037.

15. ENGEL A.G., OHNO K., SINE S.M. (2003b) Congenital myasthenic syndromes: Progress over the past decade. *Muscle Nerve* **27 (1):** 4-25.

16. ENTWISTLE A., ZALIN R.J., WARNER A.E., BEVAN S. (1988) A role for acetylcholine receptors in the fusion of chick myoblasts. *J Cell Biol* **106 (5):** 1703-1712.

17. ESCHER P., LACAZETTE E., COURTET M., BLINDENBACHER A., LANDMANN L., BEZAKOVA G., LLOYD K.C., MUELLER U., BRENNER H.R. (2005) Synapses form in skeletal muscles lacking neuregulin receptors. *Science* **308 (5730):** 1920-1923.

18. EVANS M.J., KAUFMAN M.H. (1981) Establishment in culture of pluripotential cells from mouse embryos. *Nature* **292 (5819):** 154-156.

19. FATT P., KATZ B. (1951) An analysis of the end-plate potential recorded with an intracellular electrode. *J Physiol* **115 (3):** 320-370.

20. FLANAGAN-STEET H., FOX M.A., MEYER D., SANES J.R. (2005) Neuromuscular synapses can form *in vivo* by incorporation of initially aneural postsynaptic specializations. *Development* **132 (20):** 4471-4481.

21. GAUTAM M., NOAKES P.G., MOSCOSO L., RUPP F., SCHELLER R.H., MERLIE J.P., SANES J.R. (1996) Defective muscular synaptogenesis in agrin-deficient mutant mice. *Cell* **85 (4):** 525-535.

22. GAUTAM M., NOAKES P.G., MUDD J., NICHOL M., CHU G.C., SANES J:R., MERLIE J.P. (1995) Failure of postsynaptic specialization to develop at neuromuscular junctions of rapsyn-deficient mice. *Nature* **377 (6546):** 232-236.

23. GLASS D.J., BOWEN D.C., STITT T.N., RADZIEJEWSKI C., BRUNO J., RYAN T.E., GIES D.R., SHAH S., MATTSSON K., BURDEN S.J., DISTEFANO P.S., VALENZUELA D.M., DECHIARA T.M., YANCOPOULOS G.D. (1996) Agrin acts via a MuSK receptor complex. *Cell* **85 (4):** 512-523.

24. GODA Y., DAVIS G.W. (2003) Mechanisms of synapse assembly and disassembly. *Neuron* **40 (2):** 243-264.

25. GODFREY E.W., SCHWARTE R.C. (2003) The role of nitric oxide signaling in the formation of the neuromuscular junction. *J Neurocytol* **32 (5-8):** 591-602.

26. GORDON J.W., SCANGOS G.A., PLOTKIN D.J., BARBOSA J.A., RUDDLE F.H. (1980) Genetic transformation of mouse embryos by microinjection of purified DNA. *Proc Natl Acad Sci USA* **77 (12):** 7380-7384.

27. GREER J.J., ALLAN D.W., MARTIN-CARABALLO M., LEMKE R.P. (1999) An overview of the phrenic nerve and diaphragm muscle development in the perinatal rat. *J Appl Physiol* **86 (3):** 779-786.

28. GROW W.A., GORDON H. (2000) Acetylcholine receptors are required for postsynaptic aggregation driven by the agrin signalling pathway. *Eur J Neurosci* **12 (2):** 467-472.

29. HEEROMA J.H., PLOMP J.J., ROUBOS E.W., VERHAGE M. (2003) Development of the mouse neuromuscular junction in the absence of regulated secretion. *Neuroscience* **120 (3):** 733-744.

30. HESSER B.A., HENSCHEL O., WITZEMANN V. (2006) Synapse disassembly and formation of new synapses in postnatal muscle upon conditional inactivation of MuSK. *Mol Cell Neurosci* **31 (3):** 470-480.

31. HIPPENMEYER S., HUBER R.M., LADLE D.R., MURPHY K., ARBER S. (2007) ETS transcription factor *Erm* controls subsynaptic gene expression in skeletal muscles. *Neuron* **55 (5):** 726-740.

32. IMOTO K., BUSCH C., SAKMANN B., MISHINA M., KONNO T., NAKAI J., BUJO H., MORI Y., FUKUDA K., NUMA S. (1988) Rings of negatively charged amino acids determine the acetylcholine receptor channel conductance. *Nature* **335 (6191):** 645-648.

33. KARLIN A., AKABAS M.H. (1995) Toward a structural basis for the function of nicotinic acetylcholine receptors and their cousins. *Neuron* **15 (6):** 1231-1244.

34. KATZ B., MILEDI R. (1979) Estimates of quantal content during 'chemical potentiation' of transmitter release. *Proc R Soc Lond B Biol Sci* **205 (1160):** 369-378.

35. KIM N., STIEGLER A.L., CAMERON T.O., HALLOCK P.T., GOMEZ A.M., HUANG J.H., HUBBARD S.R., DUSTIN M.L., BURDEN S.J. (2008) Lrp4 is a receptor for agrin and forms a complex with MuSK. *Cell* **135 (2):** 334-342

36. KOELLE G.B., FRIEDENWALD J.A. (1949) A histochemical method for localizing cholinesterase activity. *Proc Soc Exp Biol Med* **70 (4):** 617-622.

37.   KOENEN M., PETER C., VILLARROEL A., WITZEMANN V., SAKMANN B. (2005) Acetylcholine receptor channel subtype directs the innervation pattern of skeletal muscle. *EMBO Rep* **6 (6):** 570-576.

38.   KRAUSE R.M., HAMANN M., BADER C.R., LIU J.H., BAROFFIO A., BERNHEIM L. (1995) Activation of nicotinic acetylcholine receptors increases the rate of fusion of cultured human myoblasts. *J Physiol* **489 (Pt 3):** 779-790.

39.   KUES W.A., BRENNER H.R., SAKMANN B., WITZEMANN V. (1995a) Local neurotrophic repression of gene transcripts encoding fetal AChRs at rat neuromuscular synapses. *J Cell Biol* **130 (4):** 949-957.

40.   KUES W.A., SAKMANN B., WITZEMANN V. (1995b) Differential expression patterns of five acetylcholine receptor subunit genes in rat muscle during development. *Eur J Neurosci* **7 (6):** 1376-1385.

41.   KUMMER T.T., MISGELD T., LICHTMAN J.W., SANES J.R. (2004) Nerve-independent formation of a topologically complex postsynaptic apparatus. *J Cell Biol* **164 (7):** 1077-1087.

42.   KUMMER T.T., MISGELD T., SANES J.R. (2006) Assembly of the postsynaptic membrane at the neuromuscular junction: paradigm lost. *Curr Opin Neurobiol* **16 (1):** 74-82.

43.   LAROCHELLE W.J., FROEHNER S.C. (1986) Determination of the tissue distributions and relative concentrations of the postsynaptic 43-kDa protein and the acetylcholine receptor in Torpedo. *J Biol Chem* **261 (12):** 5270-5274.

44.   LASSAR A.B., DAVIS R.L., WRIGHT W.E., KADESCH T., MURRE C., VORONOVA A., BALTIMORE D., WEINTRAUB H. (1991) Functional activity of myogenic HLH proteins requires hetero-oligomerization with E12/E47-like proteins in vivo. *Cell* **66 (2):** 305-315.

45.   LIN W., BURGESS R.W., DOMINGUEZ B., PFAFF S.L., SANES J.R., LEE K.F. (2001) Distinct roles of nerve and muscle in postsynaptic differentiation of the neuromuscular synapse. *Nature* **410 (6832):** 1057-1064.

46. LIN W., DOMINGUEZ B., YANG J., ARYAL P., BRANDON E.P., GAGE F.H., LEE K.F. (2005) Neurotransmitter acetylcholine negatively regulates neuromuscular synapse formation by a Cdk5-dependent mechanism. *Neuron* **46 (4):** 569-579.

47. LIN W., SANCHEZ H.B., DEERINCK T., MORRIS J.K., ELLISMAN M., LEE K.F. (2000) Aberrant development of motor neurons and neuromuscular synapses in erbB2-deficient mice. *Proc Natl Acad Sci USA* **97 (3):** 1299-1304.

48. LIVAK K.J., SCHMITTGEN T.D. (2001) Analysis of relative gene expression data using real-time quantitative PCR and the 2(-Delta Delta C(T)) method. *Methods* **25 (4):** 402-408.

49. LØMO T. (2003) What controls the position, number, size, and distribution of neuromuscular junctions on rat muscle fibers? *J Neurocyt* **32 (5-8):** 835-848.

50. LUO Z.G., WANG Q., ZHOU J.Z., WANG J., LUO Z., LIU M., HE X., WYNSHAW-BORIS A., XIONG W.C., LU B., MEI L. (2002) Regulation of AChR clustering by Dishevelled interacting with MuSK and PAK1. *Neuron* **35 (3):** 489-505.

51. MAIMONE M.M., ENIGK R.E. (1999) The intracellular domain of the nicotinic acetylcholine receptor alpha subunit mediates its coclustering with rapsyn. *Mol Cell Neurosci* **14 (4-5):** 340-354.

52. MAMO S., GAL A.B., BODO S., DINNYES A. (2007) Quantitative evaluation and selection of reference genes in mouse oocytes and embryos cultured in vivo and in vitro. *BMC Dev Biol* **7:** 14.

53. MANIATIS T., FRITSCH E.F., SAMBROCK J. (1987) Molecular Cloning. A Laboratory Manual.

54. MARQUES M.J., CONCHELLO J.A., LICHTMAN J.W. (2000) From plaque to pretzel: fold formation and acetylcholine receptor loss at the developing neuromuscular junction. *J Neurosci* **20 (10):** 3663-3675.

55. MCMAHAN U.J. (1990) The agrin hypothesis. *Cold Spring Harb Symp Quant Biol* **55:** 407-418.

56.   MCMAHAN U.J., HORTON S.E., WERLE M.J., HONIG L.S., KROGER S., RUEGG M.A., ESCHER G. (1992) Agrin isoforms and their role in synaptogenesis. *Curr Opin Cell Biol* **4 (5):** 869-874.

57.   MILONE M., WANG H.L., OHNO K., PRINCE R., FUKUDOME T., SHEN X.M., BRENGMAN J.M., GRIGGS R.C., SINE S.M., ENGEL A.G. (1998) Mode switching kinetics produced by a naturally occurring mutation in the cytoplasmic loop of the human acetylcholine receptor epsilon subunit. *Neuron* **20 (3):** 575-588.

58.   MISGELD T., BURGESS R.W., LEWIS R.M., CUNNINGHAM J.M., LICHTMAN J.W., SANES J.R. (2002) Roles of neurotransmitter in synapse formation: development of neuromuscular junctions lacking choline acetyltransferase. *Neuron* **36 (4):** 635-648.

59.   MISGELD T., KUMMER T.T., LICHTMAN J.W., SANES J.R. (2005) Agrin promotes synaptic differentiation by counteracting an inhibitory effect of neurotransmitter. *Proc Natl Acad Sci USA* **102 (31):** 11088-11093.

60.   MISHINA M., TAKAI T., IMOTO K., NODA M., TAKAHASHI T., NUMA S., METHFESSEL C., SAKMANN B. (1986) Molecular distinction between fetal and adult forms of muscle acetylcholine receptor. *Nature* **321 (6068):** 406-411.

61.   MISSIAS A.C., MUDD J., CUNNINGHAM J.M., STEINBACH J.H., MERLIE J.P., SANES J.R. (1997) Deficient development and maintenance of postsynaptic specializations in mutant mice lacking an 'adult' acetylcholine receptor subunit. *Development* **124 (24):** 5075-5086.

62.   MITRA A., CYMES G.D., AUERBACH A. (2005) Dynamics of the acetylcholine receptor pore at the gating transition state. *Proc Natl Acad Sci USA* **102 (42):** 15069-15074.

63.   MIYAZAWA A., FUJIYOSHI Y., STOWELL M., UNWIN N. (1999) Nicotinic acetylcholine receptor at 4.6 A resolution: transverse tunnels in the channel wall. *J Mol Biol* **288 (4):** 765-786.

64.   MIYAZAWA A., FUJIYOSHI Y., UNWIN N. (2003) Structure and gating mechanism of the acetylcholine receptor pore. *Nature* **423 (6943):** 949-955.

65. MOHAMED A.S., RIVAS-PLATA K.A., KRAAS J.R., SALEH S.M., SWOPE S.L. (2001) Src-class kinases act within the agrin/MuSK pathway to regulate acetylcholine receptor phosphorylation, cytoskeletal anchoring, and clustering. *J Neurosci* **21 (11):** 3806-3818.

66. MÜLLER J.S., BAUMEISTER S.K., SCHARA U., COSSINS J., KRAUSE S., VON DER HAGEN M., HUEBNER A., WEBSTER R., BEESON D., LOCHMÜLLER H., ABICHT A. (2006) CHRND mutation causes a congenital myasthenic syndrome by impairing co-clustering of the acetylcholine receptor with rapsyn. *Brain* **129 (Pt 10):** 2784-2793.

67. MÜLLER J.S., MIHAYLOVA V., ABICHT A., LOCHMÜLLER H. (2007) Congenital myasthenic syndromes: spotlight on genetic defects of neuromuscular transmission. *Expert Rev Mol Med* **9 (22):** 1-20.

68. NOAKES P.G., PHILLIPS W.D., HANLEY T.A., SANES J.R., MERLIE J.P. (1993) 43K protein and acetylcholine receptors colocalize during the initial stages of neuromuscular synapse formation in vivo. *Dev Biol* **155 (1):** 275-280.

69. OHNO K., WANG H.L., MILONE M., BREN N., BRENGMAN J.M., NAKANO S., QUIRAM P., PRUITT J.N., SINE S.M., ENGEL A.G. (1996) Congenital myasthenic syndrome caused by decreased agonist binding affinity due to a mutation in the acetylcholine receptor epsilon subunit. *Neuron* **17 (1):** 157-170.

70. OKADA K., INOUE A., OKADA M., MURATA Y., KAKUTA S., JIGAMI T., KUBO S., SHIRAISHI H., EGUCHI K., MOTOMURA M., AKIYAMA T., IWAKURA Y., HIGUCHI O., YAMANASHI Y. (2006) The muscle protein Dok7 is essential for neuromuscular synaptogenesis. *Science* **312 (5781):** 1802-1805.

71. OPPENHEIM R.W. (1991) Cell death during development of the nervous system. *Annu Rev Neurosci* **14:** 453-501.

72. OPPENHEIM R.W., PREVETTE D., D'COSTA A., WANG S., HOUENOU L.J., MCINTOSH J.M. (2000) Reduction of neuromuscular activity is required for the rescue of motoneurons from naturally occurring cell death by nicotinic-blocking agents. *J Neurosci* **20 (16):** 6117-6124.

73. PARR J.R., JAYAWANT S. (2007) Childhood myasthenia: clinical subtypes and practical management. *Dev Med Child Neurol* **49 (8):** 629-635.

74. PELUFO-PELLICER A., MONTE-BOQUET E., ROMÁ-SÁNCHEZ E., CASANOVA-SORNÍ C., POVEDA-ANDRÉS J. L. (2006) Fetal exposure to 3,4-diaminopyridine in a pregnant woman with congenital myasthenia syndrome. *Ann Pharmacoter* **40 (4):** 762-766.

75. PETER C. Modulation der Aktivität des nikotinischen Acetylcholinrezeptors in transgenen Tiermodellen. *Dissertation* Universität Heidelberg. 2003. http://www.ub.uni-heidelberg.de/archiv/4296/

76. PETER C., KORNGREEN A., WITZEMANN V. (2005) Mutation of single murine acetylcholine receptor subunits reveals differential contribution of P121 to acetylcholine binding and channel opening. *Pflugers Arch* **450 (3):** 178-184.

77. PRAKASH Y.S., MIYATA H., ZHAN W.Z., SIECK G.C. (1999) Inactivity-induced remodeling of neuromuscular junctions in rat diaphragmatic muscle. *Muscle Nerve* **22 (3):** 307-319.

78. PRAKASH Y.S., SMITHSON K.G., SIECK G.C. (1995) Growth-related alterations in motor endplates of type-identified diaphragm muscle fibers. *J Neurocytol* **24 (3):** 225-235.

79. PUN S., SIGRIST M., SANTOS A.F., RUEGG M.A., SANES J.R., JESSELL T.M., ARBER S., CARONI P. (2002) An intrinsic distinction in neuromuscular junction assembly and maintenance in different skeletal muscles. *Neuron* **34 (3):** 357-370.

80. RAFTERY M.A., HUNKAPILLER M.W., STRADER C.D., HOOD L.E. (1980) Acetylcholine receptor: complex of homologous subunits. *Science* **208 (4451):** 1454-1456.

81. SAKMANN B., BRENNER H.R. (1978) Change in synaptic channel gating during neuromuscular development. *Nature* **276 (5686):** 401-402.

82. SANDERS D.B. (1998) 3,4-diaminopyridine (DAP) in the treatment of Lambert-Eaton myasthenic syndrome (LEMS). *Ann NY Acad Sci* **841:** 811-816.

83. SANDRI M., CARRARO U. (1999) Apoptosis of skeletal muscles during development and disease. *Int J Biochem Cell Biol* **31 (12):** 1373-1390.

84. SANES J.R., LICHTMAN J.W. (2001) Induction, assembly, maturation and maintenance of a postsynaptic apparatus. *Nat Rev Neurosci* **2 (11):** 791-805.

85. SANES J.R., LICHTMAN J.W. (1999) Development of the vertebrate neuromuscular junction. *Annu Rev Neurosci* **22:** 389-442.

86. SHEN X.-M., OHNO K., FUKUDOME T., TSUJINO A., BRENGMAN J.M., DE VIVO D.C., PACKER R.J., ENGEL A.G. (2002) Congenital myasthenic syndrome caused by low-expressor fast-channel AChR δ subunit mutation. *Neurology* **59 (12):** 1881-1888.

87. SOHAL G.S., HOLT R.K. (1980) Role of innervations on the embryonic development of skeletal muscle. *Cell Tissue Res* **210 (3):** 383-393.

88. TAKAHASHI M., KUBO T., MIZOGUCHI A., CARLSON C.G., ENDO K., OHNISHI K. (2002) Spontaneous muscle action potentials fail to develop without fetal-type acetylcholine receptors. *EMBO Rep* **3 (7):** 674-681.

89. TERRADO J., BURGESS R.W., DECHIARA T., YANCOPOULOS G., SANES J.R., KATO A.C. (2001) Motoneuron survival is enhanced in the absence of neuromuscular junction formation in embryos. *J Neurosci* **21 (9):** 3144-3150.

90. THOMPSON S., CLARKE A.R., POW A.M., HOOPER M.L., MELTON D.W. (1989) Germ line transmission and expression of a corrected HPRT gene produced by gene targeting in embryonic stem cells. *Cell* **56 (2):** 313-321.

91. UCHITEL O., ENGEL A.G., WALLS T.J., NAGEL A., ATASSI M.Z., BRIL V. (1993) Congenital myasthenic syndromes: II. Syndrome attributed to abnormal interaction of acetylcholine with its receptor. *Muscle Nerve* **16 (12):** 1293-1301.

92. VILLARROEL A., SAKMANN B. (1996) Calcium permeability increase of endplate channels in rat muscle during postnatal development. *J Physiol* **496 (Pt 2):** 331-338.

93. WANG H.L., OHNO K., MILONE M., BRENGMAN J.M., EVOLI A., BATOCCHI A.P., MIDDLETON L.T., CHRISTODOULOU K., ENGEL A.G., SINE S.M. (2000) Fundamental gating mechanism of nicotinic receptor channel revealed by mutation causing a congenital myasthenic syndrome. *J Gen Physiol* **116:** 449-462.

94. WANG H.L., MILONE M., OHNO K., SHEN X.M., TSUJINO A., BATOCCHI A.P., TONALI P., BRENGMAN J., ENGEL A.G., SINE S.M. (1999) Acetylcholine receptor M3 domain: stereochemical and volume contributions to channel gating. *Nature Neurosci* **2 (3):** 226-233.

95. WESTON C., YEE B., HOD E., PRIVES J. (2000) Agrin-induced acetylcholine receptor clustering is mediated by the small guanosine triphosphatases Rac and Cdc42. *J Cell Biol* **150 (1):** 205-212.

96. WITZEMANN V. (2006) Development of the neuromuscular junction. *Cell Tissue Res* **326 (2):** 263-271.

97. WITZEMANN V., BARG B., CRIADO M., STEIN E., SAKMANN B. (1989) Developmental regulation of five subunit-specific mRNAs encoding acetylcholine receptor subtypes in rat muscle. *FEBS Lett* **242 (2):** 419-424.

98. WITZEMANN V., BARG B., NISHIKAWA Y., SAKMANN B., NUMA S. (1987) Differential regulation of muscle acetylcholine receptor gamma- and epsilon-subunit mRNAs. *FEBS Lett* **223 (1):** 104-112.

99. WITZEMANN V., BRENNER H.R., SAKMANN B. (1991) Neural factors regulate AChR subunit mRNAs at rat neuromuscular synapses. *J Cell Biol* **114 (1):** 125-141.

100. WITZEMANN V., SCHWARZ H., KOENEN M., BERBERICH C., VILLARROEL A., WERNIG A., BRENNER H.R., SAKMANN B. (1996) Acetylcholine receptor

epsilon-subunit deletion causes muscle weakness and atrophy in juvenile and adult mice. *Proc Natl Acad Sci USA* **93 (23):** 13286-13291.

101. WYATT R.M., BALICE-GORDON R.J. (2003) Activity-dependent elimination of neuromuscular synapses. *J Neurocytol* **32 (5-8):** 777-794.

102. YANG X., ARBER S., WILLIAM C., LI L., TANABE Y., JESSELL T.M., BIRCHMEIER C., BURDEN S.J. (2001) Patterning of muscle acetylcholine receptor gene expression in the absence of motor innervation. *Neuron* **30 (2):** 399-410.

103. YAMPOLSKY P., GENSLER S., MCARDLE J., WITZEMANN V. (2008) AChR channel conversion and AChR-adjusted neuronal survival during embryonic development. *Mol Cell Neurosci* **37 (3):** 634-645.

104. ZHANG B., LUO S., WANG Q., SUZUKI T., XIONG W.C., MEI L. (2008) LRP4 serves as a coreceptor of agrin. *Neuron* **60 (2):** 285-297.

105. ZHANG M., MCLENNAN I.S. (1998) Primary myotubes preferentially mature into either the fastest or slowest muscle fibers. *Dev Dyn* **213 (1):** 147-157.

11. INDEX OF FIGURES AND TABLES

FIGURES

TABLES